THE UNIVERSITY OF MANITOBA

POSITRON ANNIHILATION IN CONDENSED HYDROCARBONS

by

GARRY R. A. De BLONDE

A THESIS

SUBMITTED TO THE FACULTY OF GRADUATE STUDIES

IN PARTIAL FULFILMENT OF THE REQUIREMENTS FOR THE DEGREE

OF DOCTOR OF PHILOSOPHY

DEPARTMENT OF PHYSICS

WINNIPEG, MANITOBA

October, 1972

TABLE OF CONTENTS

LIST OF FIGURES

LIST OF TABLES

ACKNOWLEDGEMENTS

The author wishes expressly to offer his sincere thanks to Dr. B. G. Hogg for the assistance and encouragement given by him throughout the course of this work.

Thanks are due to Dr. D. P. Kerr of the University of Winnipeg for his aid in the angular correlation and three photon experiments. The author is also indebted to Mr. A. G. Gould, Dr. A. M. Cooper and Dr. S. Y. Chuang for their assistance during the experimental work and for many helpful discussions.

The financial aid of the National Research Council of Canada and the American Chemical Society is gratefully acknowledged.

ABSTRACT

Methane, butane, cyclohexane and benzene are used as the media in which a study of positron annihilation takes place. The decay process is studied over a range of temperatures and with the three standard techniques normally employed.

In previous experiments with positrons annihilating in liquid organic materials the measurements of I_N (intensity of the low momentum component from angular correlation data)and I_2 (intensity of the long lived component from lifetime measurements) have resulted in $I_N = I_2/3$ within experimental error.

For samples of methane, butane, cyclohexane and benzene measurements in the liquid state yield the expected equality between I_N and $I_2/3$. However, in the solid state for these substances there is marked disagreement between I_N and $I_2/3$. The value of I_N, in all cases, is essentially zero suggesting that no positronium is formed, but the value of I_2 remains large.

In addition, the experimental high momentum distributions compare well with a modified Chuang calculated distribution and the lifetime versus temperature results are consistent with the Free Volume Model.

CHAPTER I

INTRODUCTION

In the subject of annihilation of positrons in matter, the annihilation process itself can be considered to be well understood on the basis of quantum electrodynamics. The predictions of quantum electrodynamics in regard to the properties of positronium have been strikingly verified in dilute gases, where the positronium atom can be treated as an isolated two body system with little interference from the other atoms of the gas. Such information has given one considerable confidence in the use of the annihilation process as a tool for the investigation of the interaction of positrons with matter under varying circumstances. Recently positron annihilation techniques have been used widely in chemical and solid state investigations.

The physical behaviour of positrons after slowing down and before annihilation in condensed matter is of interest for obtaining information about the dynamical properties of the annihilating partner which is the electron. The high energy γ-rays which emerge from the annihilation process escape without appreciable attenuation or scattering, from reasonably small samples. Moreover, the positron annihilation takes place deep inside the material. Thus the annihilation γ-rays can give information about the structure of matter in the condensed state. In practice, however, a theoretical analysis of these processes is only possible with the help of models which are used to understand the matter in condensed state.

1.1 Annihilation Characteristics of Positrons

The positron is an elementary particle belonging to the class known as leptons. The positron is the antiparticle of the

electron and the two particles can be annihilated as a pair with the emission of gamma quanta. Both particles have the same mass and have equal charge, although opposite in sign. The spin of the positron is such that $S = \frac{1}{2}$ and like the electron it obeys Fermi-Dirac statistics.

Annihilation of positrons upon interaction with electrons occurs with the emission of photons. The most probable modes of decay lead to two and three photons being emitted. In solids the annihilation could take place without the emission of a photon, provided the total energy could be transferred to the lattice in the form of phonons. However, the probability of such a process occurring is extremely small. Annihilation accompanied by the emission of a single photon requires the presence of a third body to absorb the recoil momentum but at thermal energies the probability of this process is also negligible. In condensed material, about 98 per cent of fast positrons are slowed down to nearly thermal energies and, therefore, the single quantum annihilation mode is of little importance.

To understand 2γ and 3γ annihilation we consider the interaction of slow positrons and electrons when orbital momentum is $\ell = 0$. Higher orbital angular momentum states are not of interest since in these states the wave functions of the positron and electron do not overlap sufficiently for appreciable annihilation to occur. We need to consider only two states, the singlet state $^1S_0$ with positron and electron spins antiparallel and total momentum $J = 0$, and the triplet state $^3S_1$ with $J = 1$ and spins parallel. According to Yang (1950) the appearance of two photons upon annihilation is only possible from the singlet state. Annihilation of a singlet state with the emission of three γ-quanta would mean that charge parity was not conserved,

whereas 2γ annihilation of a triplet state would be impossible even if charge parity were conserved because it would violate conservation of angular momentum.

This feature of positron-electron annihilation has led to a search for charge non-conservation through the study of three photon decay of the singlet state (A. P. Mills and S. Berko 1967).

Ore and Powell (1949) have shown that the ratio of cross-sections for 3γ and 2γ annihilation is $\frac{1}{372}$ and Goldanskii (1968) has shown that the one photon rate will be more than two orders of magnitude less than the three photon rate. These are calculated values.

1.2 Bound State Formation - Positronium

The possibility of bound electron-positron states was first postulated by Mohorovicic (1934), but the name positronium (P_S) for the electron-positron atom was first suggested by Ruark (1945). Experimental evidence for the existence of the atom of positronium was not found until the work of Deutsch (1951), on the slowing down of positrons in gases. His experiments showed the bound state to be a reality.

Since positronium is a complete structural analogue of the hydrogen atom many of its characteristics, such as binding energy, radius, quasi-classical velocity of the atomic electron and so forth, are well described by the simple Bohr theory - the reduced mass being one-half of the electron mass. One thus obtains a "Bohr radius" of a positronium atom $a_p = \frac{\hbar^2}{\mu_e^2} = \frac{2\hbar^2}{me^2} = 2a_0 = 1.06$ Å, with a ground state energy $E = \frac{e^2}{2a_p} = \frac{e^2}{4a_0} = 6.77$ ev.

There are two ground (n = 1, 1S) states of positronium: the triplet state, or orthopositronium, ($^3S_1$) with parallel spins of elec-

tron and positron, and the singlet state, or parapositronium, ($^1S_0$) in which the electron and positron have antiparallel spin. The angular momentum of orthopositronium is J = 1, and here three sub-states can occur with different magnetic quantum numbers: m = +1, 0, 1. For parapositronium J = 0 and m = 0. Therefore, the statistical weight of the triplet state is three times as large as that of the singlet state, with formation of orthopositronium in 75% of cases and parapositronium in 25%. Following the argument presented before, orthopositronium undergoes 3γ annihilation and parapositronium 2γ annihilation. The lifetimes of triplet and singlet positronium annihilating in vacuum have been calculated as 1.4×10^{-7} seconds and 1.25×10^{-10} seconds (Ore and Powell 1949).

In the formation of positronium, high energy positrons are degraded in energy by various processes such as ionizing and excitation collisions until they reach an energy at which positronium formation becomes favourable. This lies in a very narrow kinetic energy interval of positrons, called the "Ore gap", first proposed by A. Ore in 1949. The width of the gap is controlled by the properties of the medium under investigation. This will be discussed more fully later with some emphasis placed on the effect of phase changes.

Apart from the positronium atom there are several other possible bound states of positrons, each of which gives a different lifetime against annihilation. In this connection it is useful to investigate theoretically all possible bound states to which the positron may give rise, with the aim of comparing the results with experimental data. Experimental data from Bell (1960), Stewart (1961), and Bisi (1963) could be interpreted on the basis of the assumption

that positron bound states besides the well-known positronium are formed, such as H^-e^+, $C\ell^-e^+$, Lie^+, $e^-e^+e^-$, and so on. A number of theoretical papers by Neamtan (1962, 1964), Goldanskii (1964), and Brandt (1966) have been devoted to this topic.

1.3 Experimental Methods

Among the basic experimental techniques are (1) measurements of positron lifetime; (2) investigations of the angular correlation of annihilation γ-quanta; and (3) determination of the probability of 3γ annihilation.

In positron lifetime experiments,measurements are made on the delayed coincidences between the emission of a positron and its subsequent annihilation. This method was used by Deutsch in 1951 when he first showed the existence of positronium in gases. This experimental method measures the decay rates of the various modes of positron annihilation and also determines the percentage of positrons decaying by each process. Much experimental data have indicated that the long lifetime component in condensed media is a direct measure of the amount of positronium formed. Thus by use of the lifetime method one is able to study the effect changes in a given system have on both decay rates and the relative abundance of positrons decaying by the different decay modes.

The second experimental method is the measurement of the angular correlation of the two photon annihilation radiation. The 2γ annihilation of a positron-electron pair at rest in a laboratory system results in two photons of energy m_0c^2 at a relative emission angle of π radians. If the annihilating pair has a finite momentum and energy, then the two photons must carry away this additional

momentum and energy. In the case of a random distribution of the momentum direction, momentum conservation leads to photon pair emission at relative angles differing from π, and energy conservation to a broadening of the m_0c^2 gamma line. The observation of either of these two phenomena yields information about the state of the electron just prior to annihilation. The angular distribution has been studied extensively by a number of workers.

The third experimental method of positron annihilation studies is the measurement of the triplet annihilation rate by a triple coincidence experiment. Since theory predicts that the ratio of 3γ to 2γ annihilation for free positrons will be $\frac{1}{372}$, whenever a rate larger than this is found we have proof of positronium formation. However, a reduction in the number of triple coincidences could be due both to a decrease in positronium formation and to quenching of ortho-positronium. This experiment cannot isolate the separate contributions of these two processes.

1.4 Quenching of Positronium

Processes which alter the lifetime of singlet and triplet positronium can be classified as follows:

(1) Pick-off annihilation, i.e. annihilation with electrons of other molecules during collisions;

(2) Ortho-para conversion resulting from the interaction with paramagnetic particles;

(3) Chemical quenching which involves various chemical reactions of positronium, such as oxidation, addition, and substitution.

Foremost among the quenching processes is the "pick-off" process since in condensed media this governs the triplet positronium

lifetime. Due to the continual scattering of positronium by the surrounding molecules, the positron in orthopositronium may annihilate with an electron from a molecule whose spin relative to the positron in positronium is anti-parallel. This process accounts for the long lived lifetime of positronium of about 10^{-9} seconds in condensed media rather than the lifetime of 1.4×10^{-7} seconds predicted for positronium in free space.

Ortho-para conversion can occur when positronium interacts with any paramagnetic particle having a total electron spin of $J \geq \frac{1}{2}$. Here we are not dealing with the mixing of triplet and singlet states, produced by a magnetic field set up near the paramagnetic particles (this effect is quite weak), but with direct interaction between the spins of these particles and positronium. The simplest form which this interaction can take is direct spin exchange, when ortho-para conversion is accompanied by reversal of spin of the paramagnetic particle.

Temperature and pressure changes have pronounced effects on the lifetime of quenched positronium since these changes alter the electron densities in the media under consideration. The degree of crystallinity in molecular substances, phase changes in materials, and changes in crystalline structure can all affect the long lifetime to a considerable degree.

1.5 Application of Positron Techniques

Observations of the formation and annihilation of positronium are of particular interest for many problems in contemporary physics. The probability of positronium formation is related to several factors such as the mode of thermalizing positrons in various media, the com-

peting processes of ionization, electron excitation and capture of electrons by positrons, and the ratio of cross-sections for elastic scattering, excitation of vibrational and rotational molecular levels, and attachment of slow positrons. A knowledge of these relationships could provide a new method for studying many elementary processes in high energy chemistry - processes which have scarcely been touched on in condensed media.

Positronium is a unique labelled atom whose properties, lifetime and annihilation mechanism depend to a great extent on the nature of the surrounding medium. The short intrinsic lifetime of positronium could provide a useful standard for investigations of rapid chemical reactions.

The application of positrons in solid state physics has become a fruitful area of research. In metallic solids much information has been gained on Fermi surfaces and electron structure of solids. In ferromagnetic solids the momentum distributions of spin aligned electrons has been studied, yielding important information in the study of ferromagnetism. A large variety of non-metallic samples have also been investigated using angular correlation and lifetime measurements.

In this work studies are conducted to ascertain the effect on positronium lifetimes and intensities due to temperature variations and phase changes in specific organic materials. This provides information to test the validity of models used to explain positron decay processes. Angular correlation measurements have also been carried out on the same organic substances. The angular distribution of the photons yields important information about the momentum distributions

of electrons involved in the chemical binding of molecular systems. Therefore, one is able to use these data to check the calculated atomic and molecular orbital wave functions.

CHAPTER II

LIFETIME MEASUREMENTS

2.1 General Description

The apparatus used in measuring positron lifetimes has been described in detail previously by Cooper (1969) and therefore only the general description will be discussed here.

A block diagram of the time sorting system used in this work is shown in Fig. 2-1. Most of the actual circuitry was designed and built at the University of Manitoba. The system consists of three separate parts; the fast side, the slow side, and the calibration section. A general description of each of these parts will be given to present an overall view of how the apparatus functions.

The function of the apparatus is to determine the relative delay between the appearance of the positron in the sample and the subsequent appearance of one of the gamma rays which appears upon the annihilation of the positron. This is done by detecting in one photo-tube the 1.28 Mev gamma ray which is emitted coincident with the positron's formation (coincident in the sense that the time difference is much smaller than the resolving time of the apparatus), and by detecting in the second phototube one of the .511 Mev gamma rays which signifies annihilation of the positron. The two phototube signals thus produced are transformed to fast-rising flat topped pulses by their respective limiters after which they are routed to the Time to Amplitude Converter (T.A.C.). In this circuit the pulses are clipped to 40 nsec in length and are then overlapped in such a way that the T.A.C. circuit output is proportional to the amount of overlap, that is, proportional to the time difference between the two events. Output pulses from the

Figure 2-1

Block Diagram of the Time Sorting System

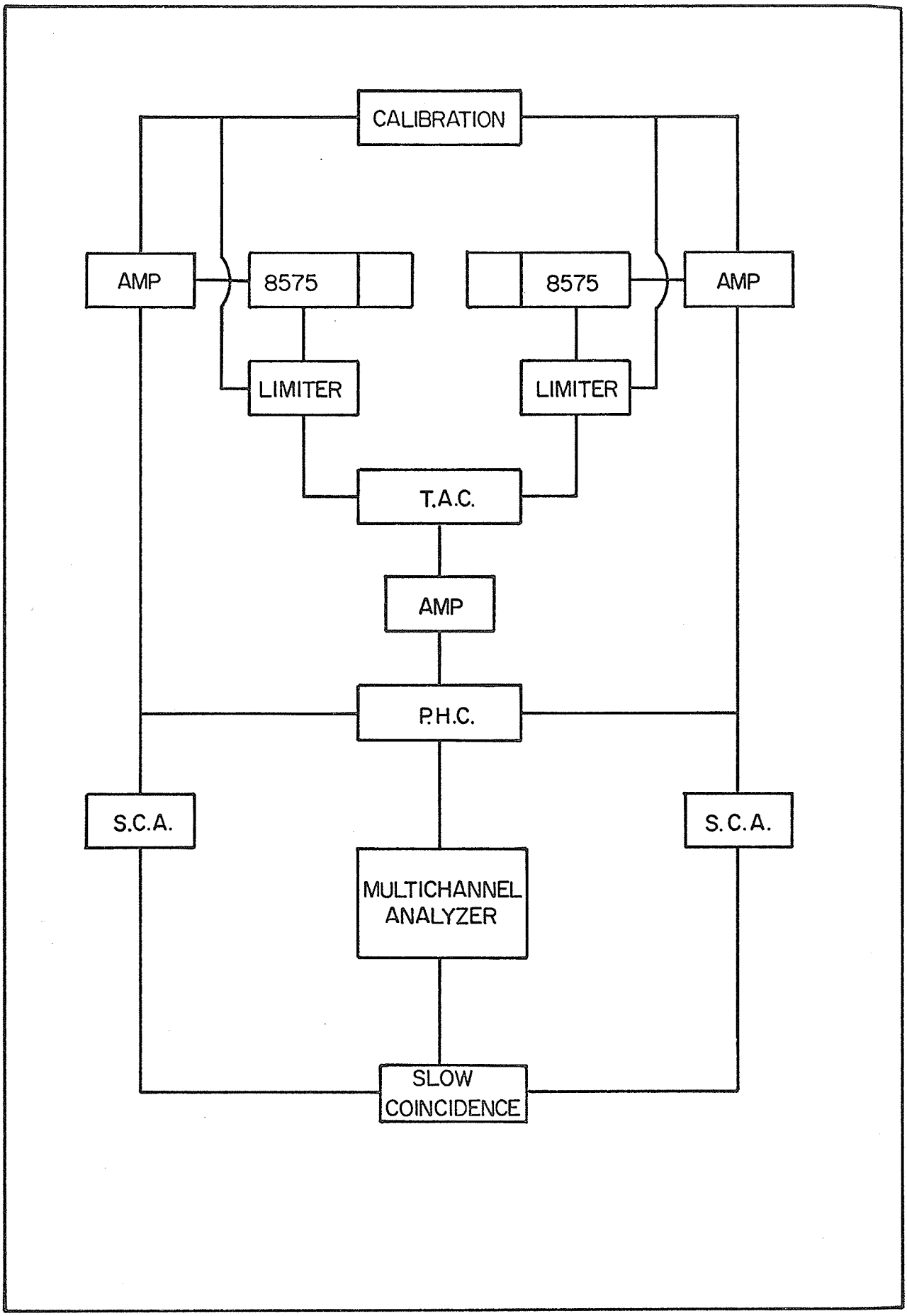
CALIBRATION
AMP
8575
8575
AMP
LIMITER
LIMITER
T.A.C.
AMP
P.H.C.
S.C.A.
S.C.A.
MULTICHANNEL ANALYZER
SLOW COINCIDENCE

T.A.C. are then sent through a linear amplifier to the Pulse Height Compensator (P.H.C.). The P.H.C. serves to correct T.A.C. signals for errors which arise because of the various pulse sizes originating from the phototubes. The output from the P.H.C. is fed into a multichannel analyzer where it will be recorded if the slow side has opened the gate.

The slow side of the system consists of emitter followers which take linear signals from the tenth dynode of each phototube and feed these through amplifiers to each of the single channel analyzers and to the P.H.C. In the P.H.C. the linear amplifier signals are added to the T.A.C. output to give corrected signals. If the input signals to the single channel analyzers are in the appropriate part of the phototube spectrum then the single channel analyzers will send output pulses to the slow coincidence unit. If signals from each of the single channel analyzers arrive within the slow coincidence unit's resolving time a gating signal is produced which activates the multichannel analyzer and lets it accept a count.

Calibration of the timing apparatus is achieved by use of an air-cored helical delay line, fed by a mercury pulser, which allows one to place accurately known delays of different values between the two limiters. This allows an integral linearity curve to be produced on the multichannel analyzer and from this curve the sensitivity per channel of the apparatus can be deduced.

2.2 Electronics

The type of phototube used was the R.C.A. 8575 which is a 12 stage, head on, flat faced photomultiplier containing an extremely high photon conversion efficiency photocathode. The high cathode quantum efficiency and the very good timing characteristics of the

phototube (anode pulse rise time 2.1 nsec, electron transit time 31 nsec) coupled with low dark current and high amplification all combine to make this tube ideal for fast time work. The scintillators used for the majority of this work consisted of highly polished plastic crystals of NE 102A, 1 inch diameter by 1 inch long, which were coated with white reflecting paint. Some data was also obtained using NE 111 crystals but it was found that these deteriorated with time.

The limiter circuit employed produced fast rising (1 nsec rise time) flat topped pulses of .5 μsec duration. The fast rising negative pulses from the photomultiplier arriving at the grid of a E810F pentode caused a sharp cutting off of the tube which produced the fast rising pulse.

The T.A.C. circuit used is similar to that outlined by Bell (1966) and is of the pulse overlap type. Fig. 2-2 is a schematic diagram illustrating the principle of operation. Pulses arriving from the limiters are clipped to a length of 40 nsec by a clipping cable. A and B of Fig. 2-2 illustrate coincident pulses arriving at the T.A.C. input. Both pulses are of equal amplitude and length and are offset from one another by 10 nsec due to different lengths of limiter cable. Section C shows the amount of overlap corresponding to the coincident input pulses. The equipment is arranged so that the pulses arriving from limiter #1 are the prompt pulses, as selected by the side channels, and those from limiter #2 are from the delayed radiation. Thus coincident pulses give maximum overlap and therefore maximum T.A.C. output and as the delay time between the prompt radiation and the delayed radiation increases, the T.A.C. output decreases.

Figure 2-2

T.A.C. Input Pulses

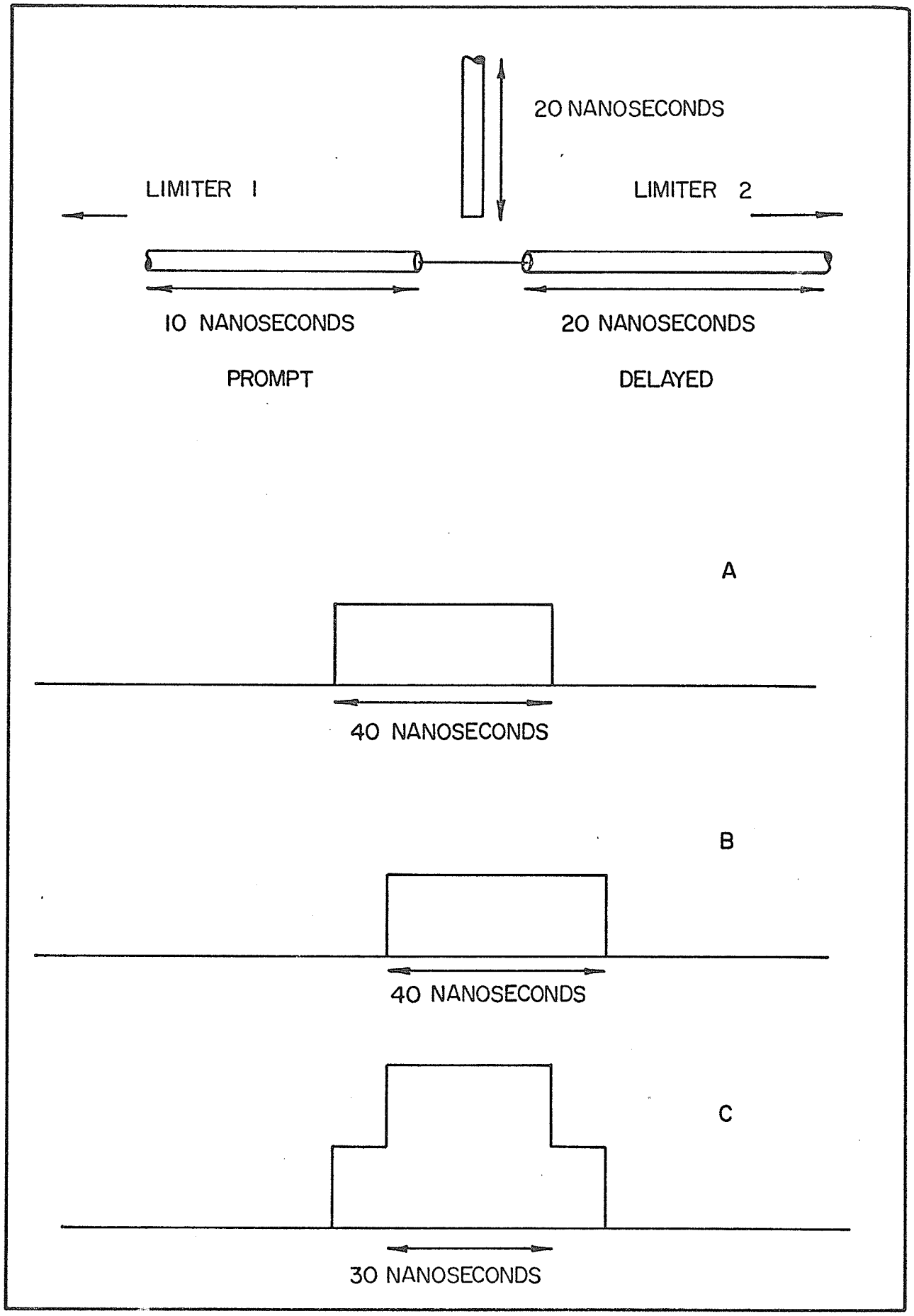
20 NANOSECONDS
LIMITER 1
LIMITER 2
10 NANOSECONDS
PROMPT
20 NANOSECONDS
DELAYED
A
40 NANOSECONDS
B
40 NANOSECONDS
C
30 NANOSECONDS

The slow coincidence system operates as follows. The discriminator in the prompt side is set to pass pulses to the slow coincidence unit corresponding to energies greater than .75 Mev. The pulse height analyzer in the second slow channel is set to pass pulses corresponding to energies between .3 and .5 Mev. Thus, the side channels accept the Compton distributions of the 1.28 Mev and .511 Mev gamma spectra. If the two events occur within the time resolution of the slow coincidence unit (200 nsec) a gating pulse is sent to the multichannel analyzer.

The P.H.C. used in this apparatus is functionally the same as the one first described by Bell and Jorgensen (1960) in which some fraction of the signals from each of the slow side amplifiers is added to the T.A.C. pulse. Fig. 2-3 illustrates the time jitter introduced by varying pulse heights arriving at the limiters. Since on the delayed side a larger pulse gives a larger T.A.C. pulse the signal must be phase inverted so that the actual process in the P.H.C. is a subtraction.

The method of calibration used with the time sorting system is based on that described by Graham et al. (1962). In this procedure an air-cored helical delay line is used to provide spaced markers of constant time differences over the range to be studied. A schematic showing the basic features of the calibration circuitry is shown in Fig. 2-4. Pulses from a mercury pulser arriving at the delay line are split and travel to opposite ends of the drum. Thus by varying the position of the carriage along the drum one changes the relative time of arrival of the two signals at the limiters. Calibration of the drum was achieved by marking equally spaced reference points along the

Figure 2-3

Schematic of Photomultiplier Anode Pulses

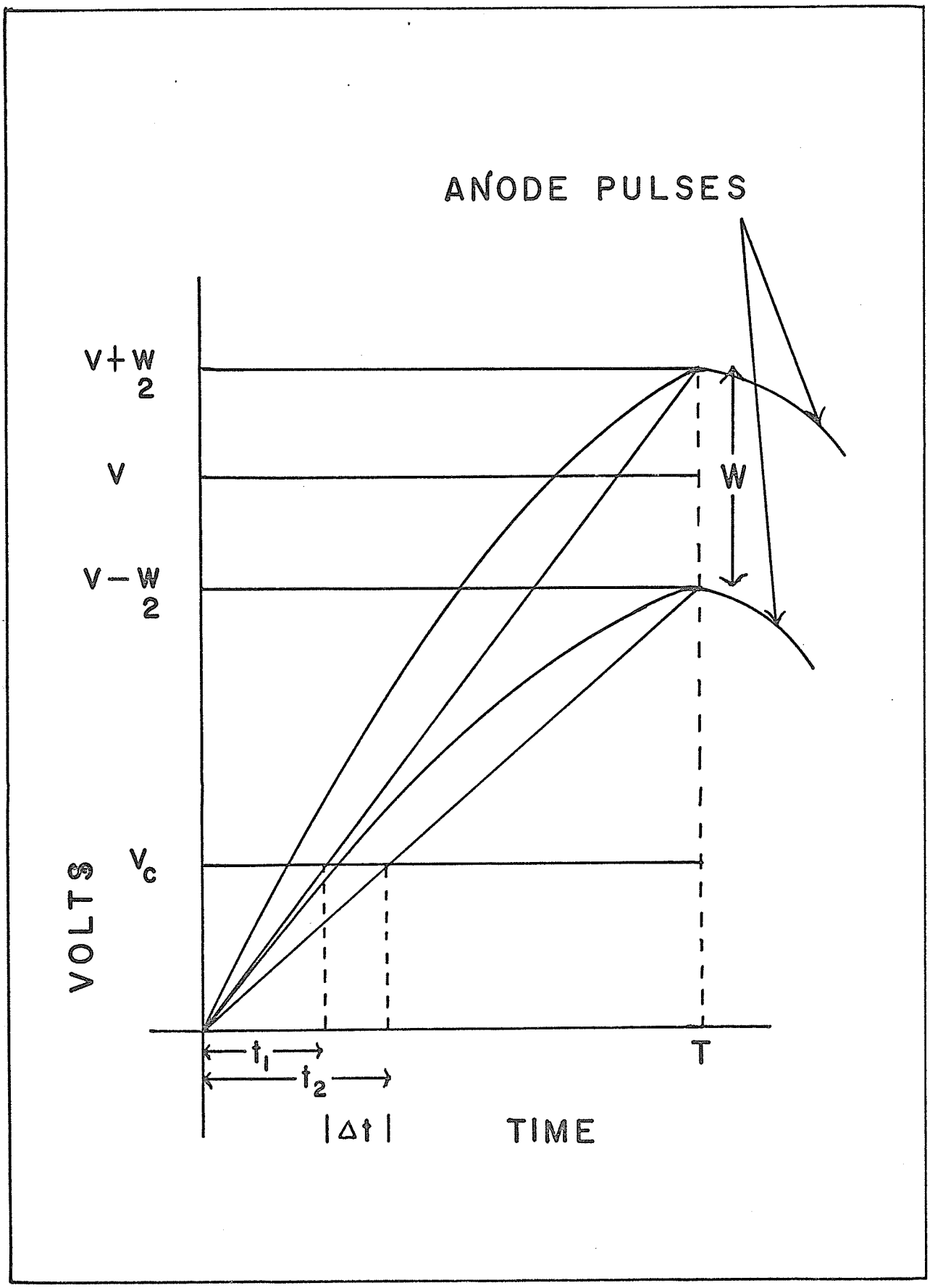
ANODE PULSES
V + W/2
V
V − W/2
W
VOLTS
Vc
t1
t2
T
|Δt|
TIME

Figure 2-4

Schematic of Calibration Circuitry

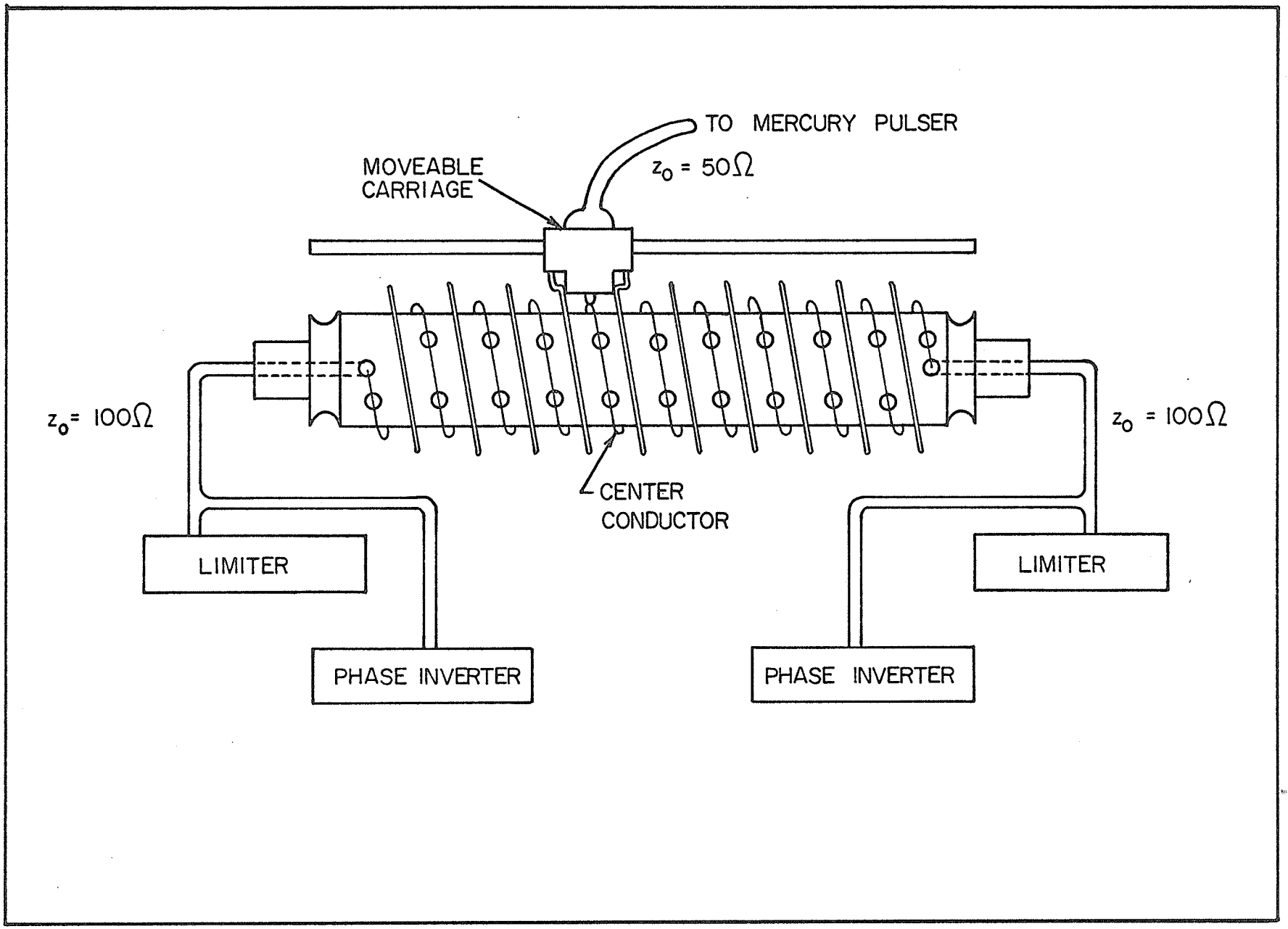
TO MERCURY PULSER
$z_0 = 50\Omega$
MOVEABLE CARRIAGE
$z_0 = 100\Omega$
$z_0 = 100\Omega$
CENTER CONDUCTOR
LIMITER
LIMITER
PHASE INVERTER
PHASE INVERTER

length of the delay line and then calibrating these points by comparison with cables whose delay times were accurately known.

2.3 Calibration and System Performance

The system parameters of prime concern in a time sorting apparatus are the resolution and the linearity. Fig. 2.5 shows an integral linearity curve obtained by use of the helical delay line. In this curve time zero occurs at channel 202 and the sensitivity as found from the curve is .175 nsec per channel. The total linear range obtained was approximately 20 nsec which was quite sufficient for the experiments conducted. A second curve which plots the differential linearity of the system under the same conditions is shown in Fig. 2-6. This curve was obtained by isolating the two photomultipliers and then activating them with uncorrelated γ-ray sources. Any detailed non-linearities which the system may possess will become evident upon analysis of the differential linearity curve. As can be seen in Fig. 2-6, the curve is essentially flat over the usable region.

The resolution obtainable with the apparatus which has been described was approximately 300 psec. Fig. 2-7 shows a Co^{60} spectrum using fairly wide windows and employing the P.H.C. As can be seen the curve falls almost linearly on the right hand side but the left hand side shows some tailing. However, since lifetimes and intensities were measured on the right side of this curve this tailing had no significant effects on our results. Fig. 2-8 shows the effect of the P.H.C. on the resolution.

The stability against drifts which the apparatus exhibited over periods of time was found to be very good if the ambient temperature was constant to three or four degrees. Under normal operating

Figure 2-5

Integral Linearity Curve

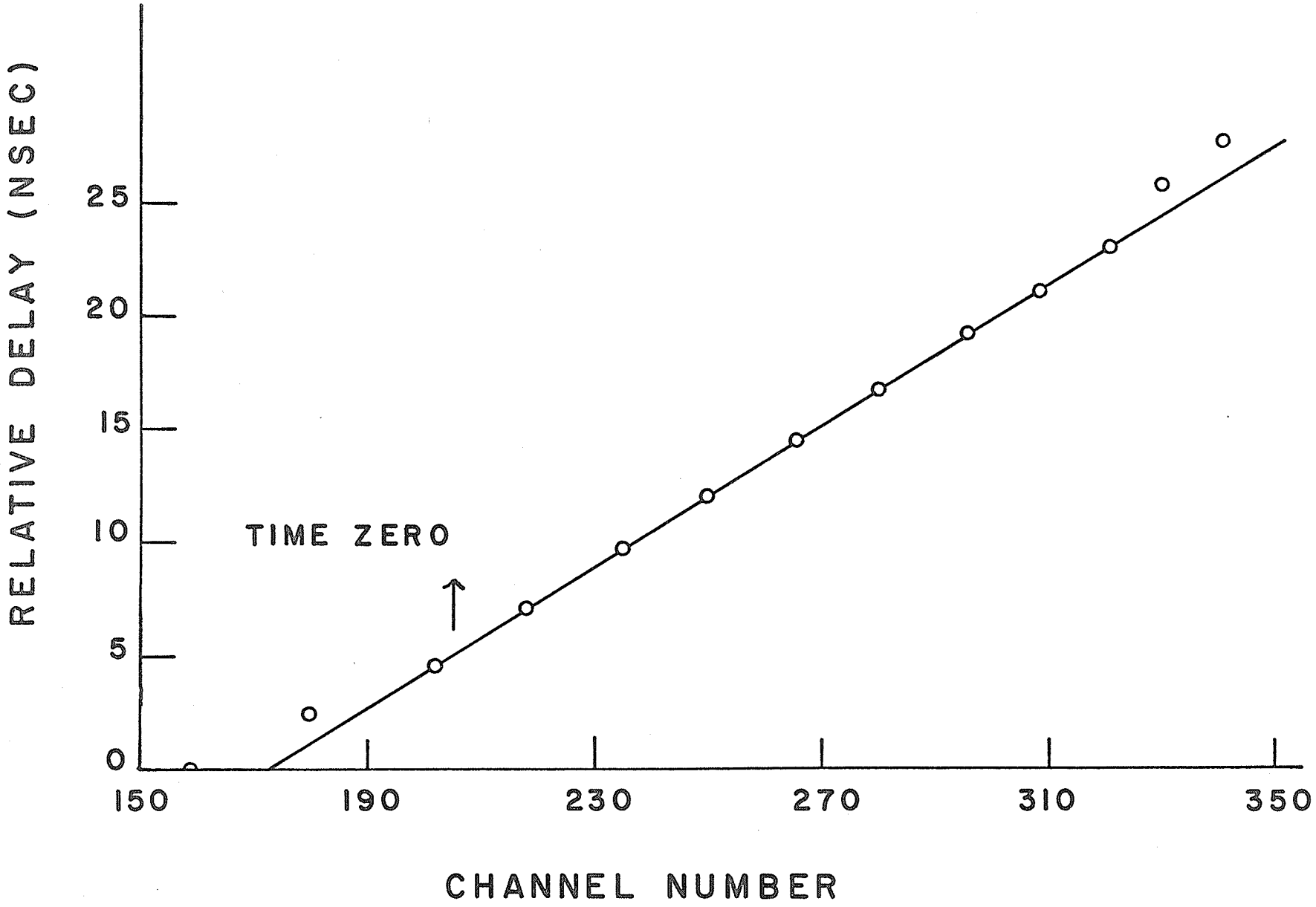
RELATIVE DELAY (NSEC)
25
20
15
10
5
0
TIME ZERO
150
190
230
270
310
350
CHANNEL NUMBER

Figure 2-6

Differential Linearity Curve

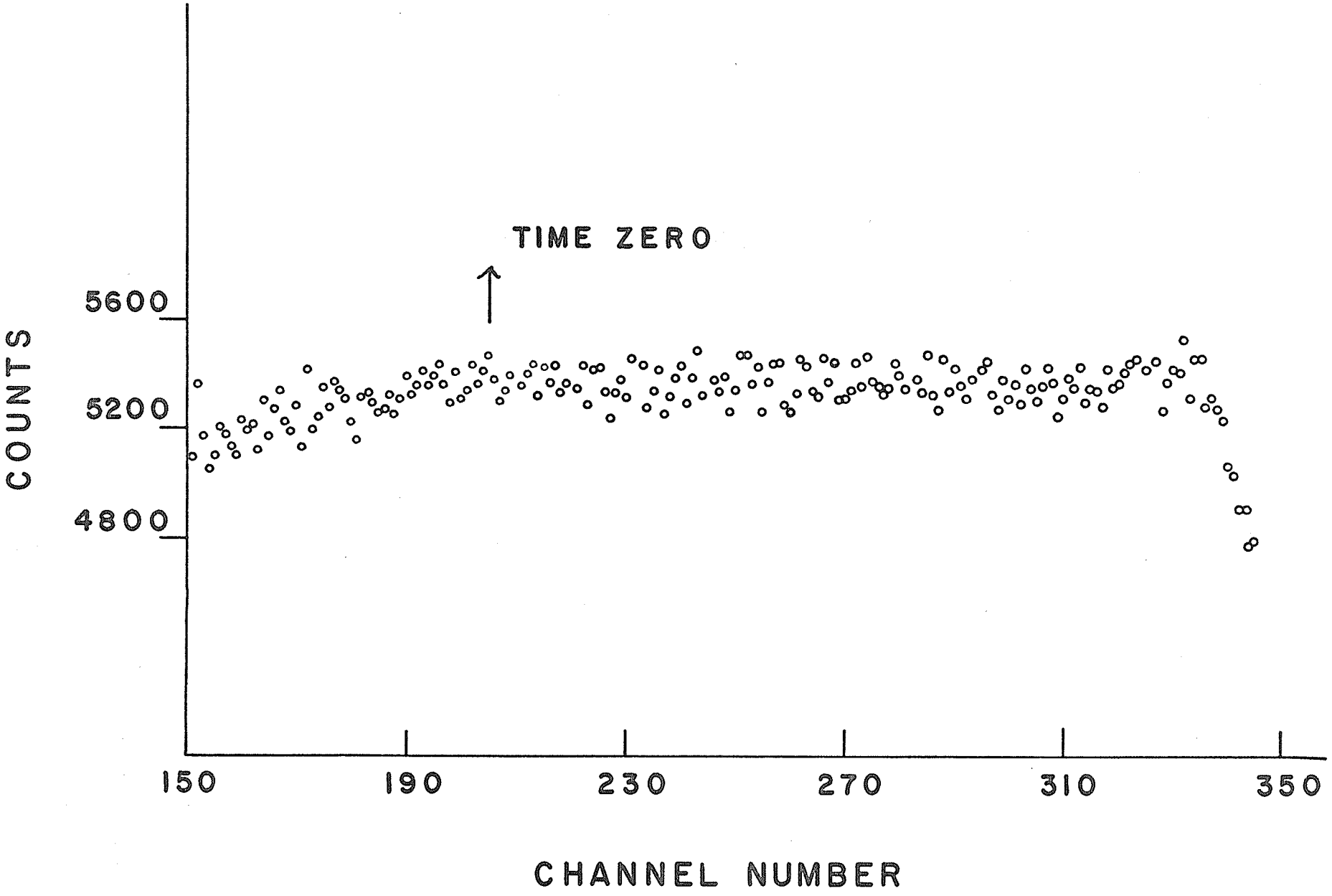
TIME ZERO
5600
5200
4800
COUNTS
150
190
230
270
310
350
CHANNEL NUMBER

Figure 2-7

Co^{60} Resolution Curve

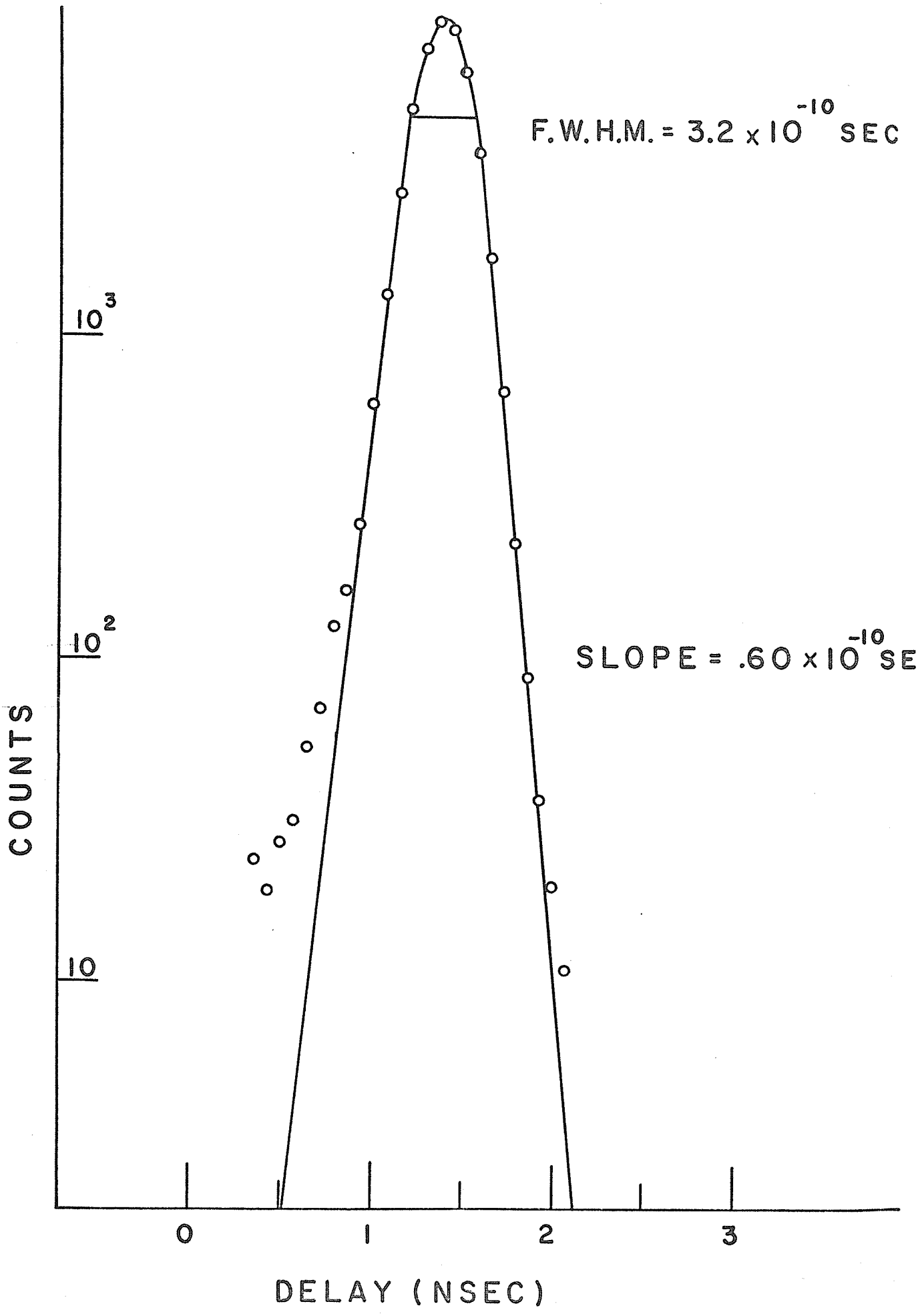
F.W.H.M. = 3.2 x 10^-10 SEC
SLOPE = .60 x 10^-10 SE
10^3
10^2
10
COUNTS
0
1
2
3
DELAY (NSEC)

Figure 2-8

Co^{60} Resolution Curve Showing Effect

of Pulse Height Compensation

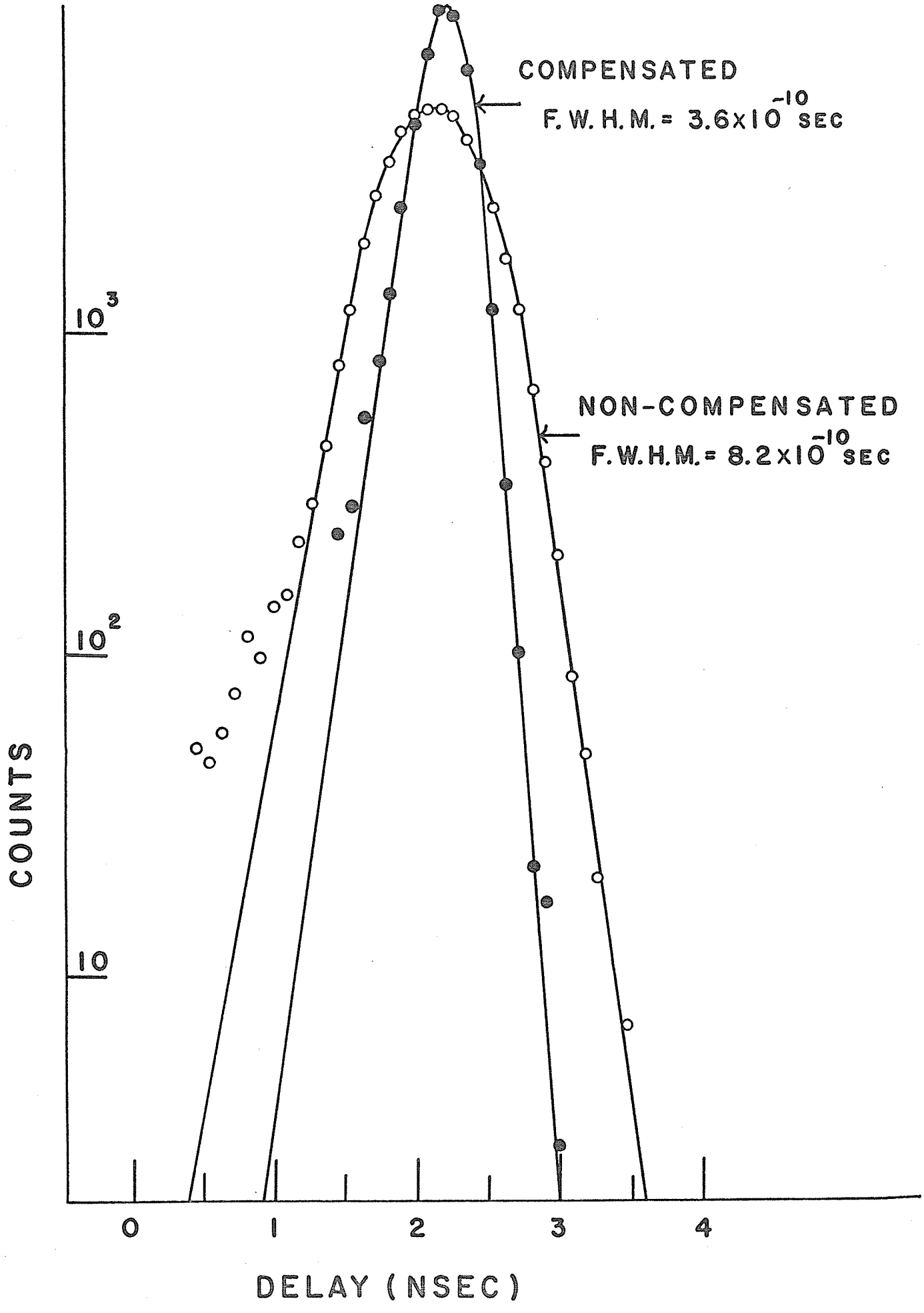
COMPENSATED
F.W.H.M. = 3.6x10^-10 SEC
NON-COMPENSATED
F.W.H.M. = 8.2x10^-10 SEC
10^3
10^2
10
COUNTS
0
1
2
3
4
DELAY (NSEC)

conditions typical centroid shifts during given runs were found to be of the order of 50 psec or less.

2.4 Temperature Regulation Apparatus

During the course of the experiments performed runs were taken at temperatures ranging from approximately +50°C to -196°C. To achieve temperature regulation over this range various methods were used.

For temperatures above 20°C the samples used were immersed in a water bath which was kept at the desired temperature by warm water passing through heat exchange coils in the bath. Temperature regulation of within 2 or 3 degrees centigrade was easily maintained.

The arrangement shown schematically in Fig. 2-9 was used to obtain sample temperatures between 20°C and -30°C. Two 1FB-12-015-B1 frigistor cooling modules were used. These are solid state thermoelectric cooling devices which cool using the Peltier effect which is the absorption or generation of heat at the junction of two dissimilar conductors. Electric current is passed through the frigistor modules in such a way that the sides touching the brass block enclosing the test tube absorb energy and thus cool the brass block. At the outer surface of the modules energy is generated and as a result the surrounding brass jacket rises in temperature. This outer jacket is kept at approximately room temperature by passing a stream of water through it. Since the relative temperature difference between the surfaces of the frigistor modules depends on the input current, sample temperatures can be preset and maintained very accurately.

For temperature regulation between -20°C and -140°C the liquid nitrogen system shown in Fig. 2-10 was used. This consisted

Figure 2-9

Frigistor Temperature Regulation Device

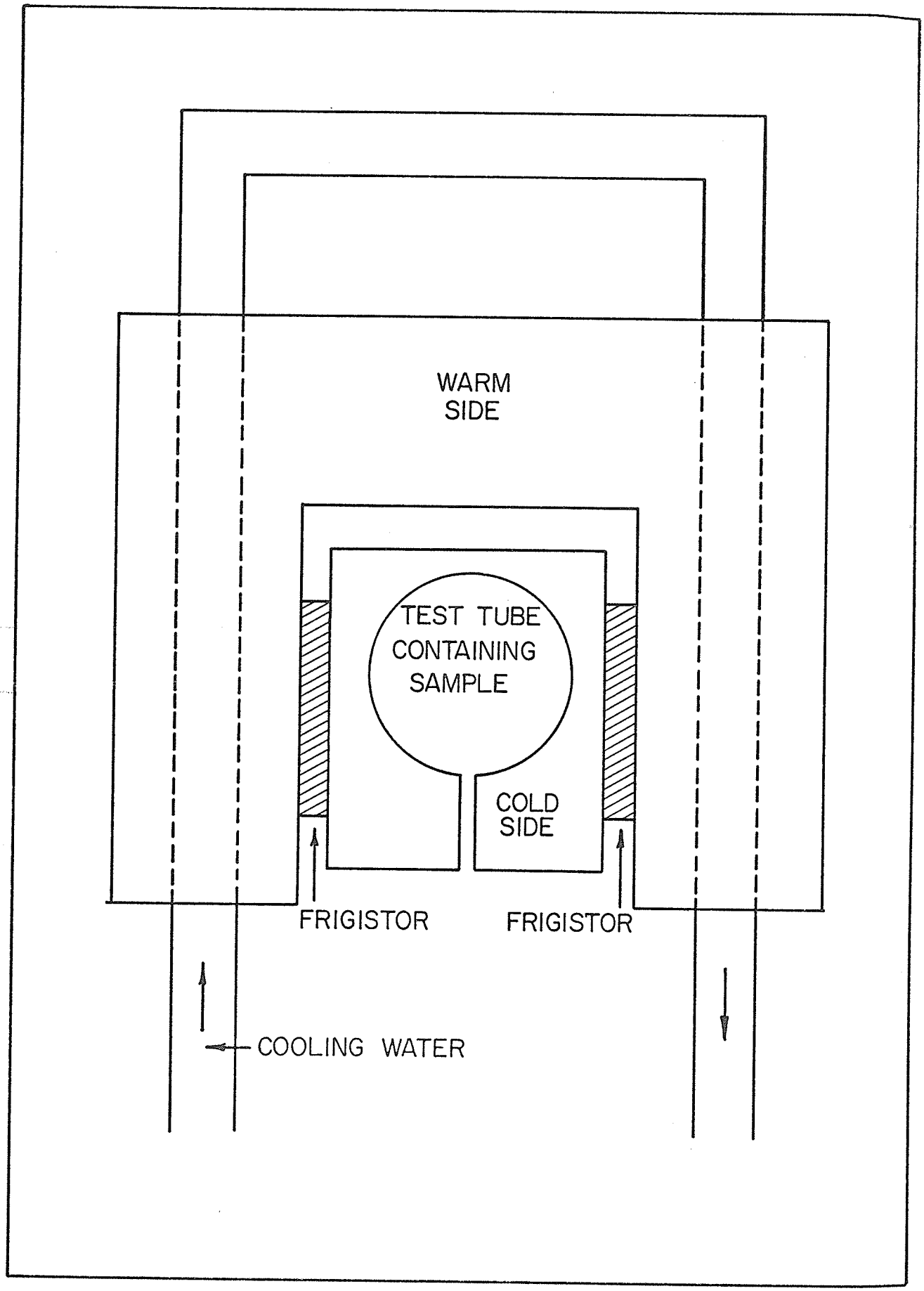
WARM
SIDE
TEST TUBE
CONTAINING
SAMPLE
COLD
SIDE
FRIGISTOR
FRIGISTOR
COOLING WATER

Figure 2-10

Temperature Regulation Apparatus

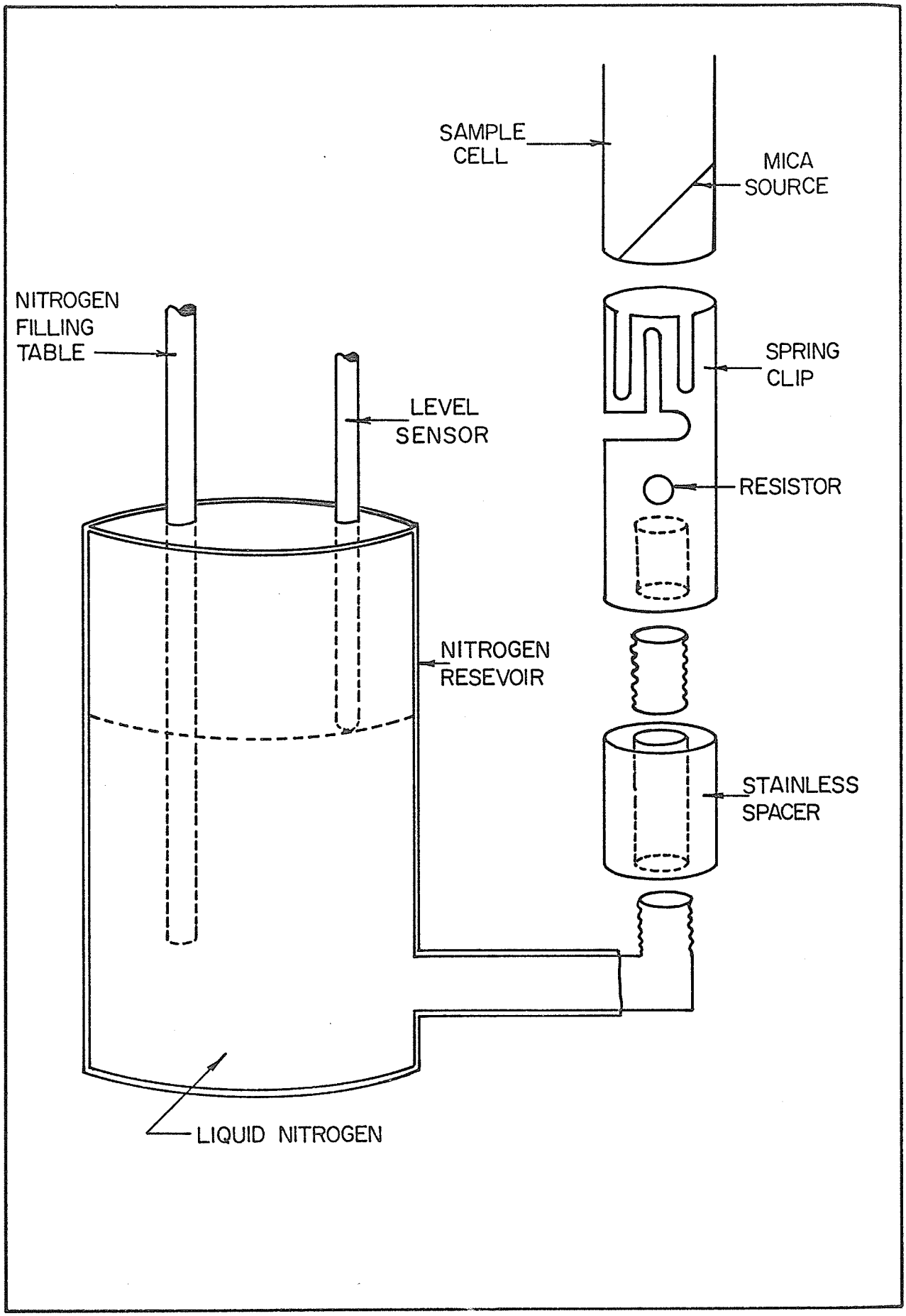
SAMPLE CELL
MICA SOURCE
NITROGEN FILLING TABLE
SPRING CLIP
LEVEL SENSOR
RESISTOR
NITROGEN RESEVOIR
STAINLESS SPACER
LIQUID NITROGEN

of a liquid nitrogen reservoir which cooled, through a series of spacers, a spring clip made of aluminum. The glass sample cell fitted tightly into the spring clip and thus cooled to the desired temperature. By altering the size of the spacers variations in temperature were achieved and fine variations were obtained by heating a resistor in the spring clip. Using this method temperature variations during a run were typically less than $1^{o}C$. The filling device for the nitrogen reservoir consisted of a level sensing mechanism (Fig. 2-11), which opened and closed a solenoid valve on the transfer line, allowing nitrogen to transfer from a 25 litre dewar whenever the level dropped below a predetermined point. Nitrogen consumption varied with the various configerations employed but was typically of the order of 1 litre per hour.

The method used to achieve temperatures lower than $-150^{o}C$ consisted of inserting an aluminum rod into the spring clip and then immersing the rod into a dewar of liquid nitrogen to the depth necessary to obtain the required temperature. The nitrogen level was then held constant by use of the level controller and filling system. With this arrangement temperatures down to liquid nitrogen could be achieved. The temperature regulation was good to only $\pm 4^{o}C$ but this was sufficient as the experimental parameters being measured were found to be fairly insensitive at these temperatures.

In each of the temperature regulation systems used temperature readings were made from a thermocouple attached to the outside of the glass cell. If a sufficient cooling period was allowed it was found that the outside and inside temperature of the sample cell were identical.

Figure 2-11

Liquid Nitrogen Control Circuit

Transistors: PNP 2N3702
Diodes: Ge 1N3121

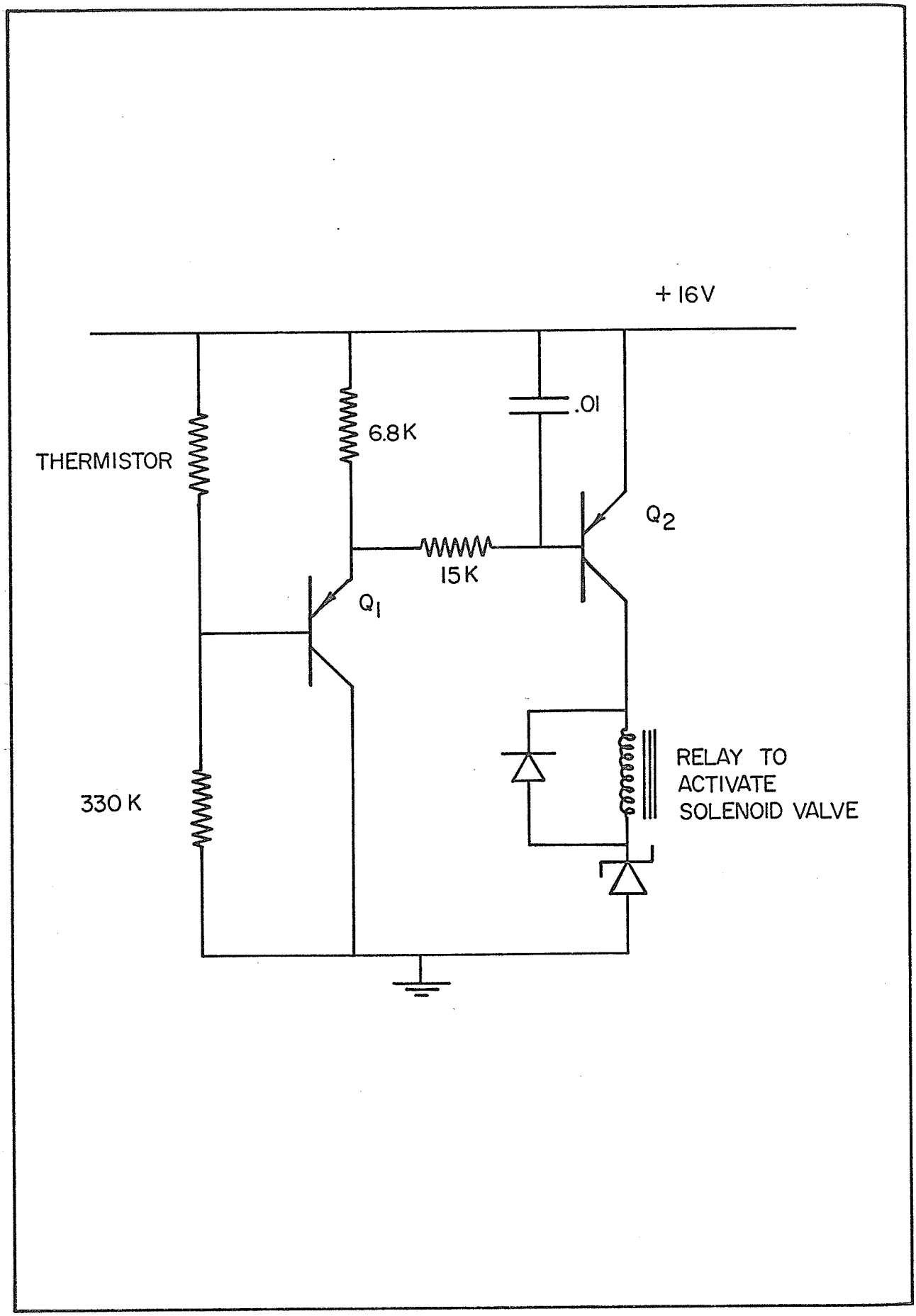
+16V
.01
6.8K
THERMISTOR
Q_2
15K
Q_1
330 K
RELAY TO
ACTIVATE
SOLENOID VALVE

2.5 Source and Sample Preparation

The radioactive source used throughout these experiments consisted of Na^{22}, which has a half-life of 2.58 years and emits positrons of maximum energy 0.54 Mev. Apart from its comparatively long half-life the greatest advantage of Na^{22} is that it gives a time indication marking the instant of positron emission. This indication is the emission of a 1.28 Mev γ quantum, separated by less than 10^{-11} seconds from the moment of positron formation.

The sources were prepared by evaporating aqueous $Na^{22}Cl$ solution onto thin sheets of mica (2 mg/cm^2) over an area of approximately 1 cm^2. Open sources were used in all cases as the $Na^{22}Cl$ was not soluble in the substances studied. The source material had a sufficiently high specific activity so that the problem of self-absorption could be discounted. Mica was chosen for source backings since it does not exhibit any long lifetime in its time spectrum and also since if thin backings are used it absorbs only a small fraction of the positrons emitted. Bertolaccini and Zappa (1967) conducted experiments to ascertain the fraction of positrons decaying in a mica source and found that for a sandwich source employing mica of the thickness which we used, approximately 6% of the positrons decay in the source backings. Therefore in an open source of the type we employed probably not more than three or four percent of the positrons annihilated in the mica. Since these events all register in the prompt peak the lifetimes obtained are not affected but a small uncertainty of the order of .5% is introduced into the intensity measurements taken.

The major part of the experimental work performed using the lifetime apparatus was on the organic material cyclohexane which

is liquid at room temperature. In the experiments performed on these samples, runs were taken on degassed as well as normal air-saturated ones. The degassing was achieved by use of the vacuum freeze-thaw technique in which the sample was repeatedly frozen and then pumped on. By employing this technique a low concentration of oxygen in the sample was achieved. After degassing some samples were analyzed mass spectroscopically and were found to contain less than 1% of the oxygen present in the air-saturated samples.

Information on lifetimes and intensities were also obtained using liquid and solid methane samples. Since methane boils at $-161.6^{o}C$ a different technique was employed to obtain the samples. Methane gas was introduced to an evacuated system and condensed into a sample cell which was cooled to liquid nitrogen temperature. The sample thus obtained was at all times contained in a closed vacuum system and kept cool.

2.6 Data Accumulation and Analysis

During the course of the experiments performed, runs lasting anywhere from a few hours to a few days were recorded. During these times the peak channel of the spectrum accumulated from a few thousand to one hundred thousand counts. After each run a background was noted from a portion of the spectrum not affected by true coincidences. Also after almost all runs a time calibration curve for the system was recorded.

When analyzing the data produced by the system the important parameters are the lifetimes and intensities of the various decay modes. In cases where no positronium is formed generally only one mode of decay is exhibited. However, when positronium is formed at least

three different modes of decay should be operative. These are decay due to pick-off of triplet positronium, decay of free positrons and decay of singlet positronium. The problem in analyzing the experimental spectra is then one of finding the parameters of the various exponential terms which make up the spectra.

To analyze the data use was made of an I.B.M. 360-65 computer and a multi-exponential curve fitting program developed by W. R. Wall (1968). The program assumes that the experimental spectra can be represented by a sum of exponential terms such that

$$y = \Sigma A_K e^{-t/\tau_K}$$

where k = 1....n and n is the number of components in the spectra. The program determines the lifetime τ for each mode and also the amplitude A from which the intensity is computed. Also produced were least-squares standard deviations for each of the parameters and a chi-squared variance which was a test of the goodness of fit of the data. The errors quoted throughout the work are either standard deviations produced by the computer program or in cases where a number of runs were taken for the same quantity the standard deviations of the various runs.

In the actual analysis two component fits were applied to the data since it was found impossible to separate the shortest lived component from the system response function meaningfully. The long-lived pickoff lifetime of triplet positronium was designated as τ_2 with a corresponding intensity of I_2, while the parameters of the second component were given as τ_1 and I_1.

CHAPTER III

ANGULAR CORRELATION MEASUREMENTS

3.1 General Description

A standard parallel slit angular correlation apparatus has been used to measure the angular distribution of annihilation photons. This apparatus has been described in detail previously by Kerr (1964) and therefore only the general description will be discussed here.

A. Mechanical Construction

A diagram of the mechanical parts of the angular correlation apparatus is shown in Figure 3.1. The apparatus consisted of a source and sample housing located halfway between two gamma-ray detectors. These components were mounted on two parallel 3" by 6" aluminum I-beams approximately 20 feet long.

The two gamma-ray detectors were mounted on either end of the I-beam structure. One detector was fixed and the other movable. The fixed detector and its collimating slits were mounted on a brass plate 265 cm from the source. The movable detector was mounted on a steel plate 265 cm on the other side from the source. The steel plate was moved along a set of rails by means of a worm screw driven by a 600 ounce-inch "Slo-Syn" motor. The collimating slits of the detectors were made from 3" thick lead blocks and were .15 cm wide. The detectors were heavily shielded to cut down the accidental background rate from scattered gamma-rays and from other sources in the laboratory.

The sample housing consisted of an insulating polystyrene box and two collimating slits. The width of the slits were .15 cm and 1.5 cm facing the fixed and movable detectors respectively. The

Figure 3-1

Angular Correlation Apparatus

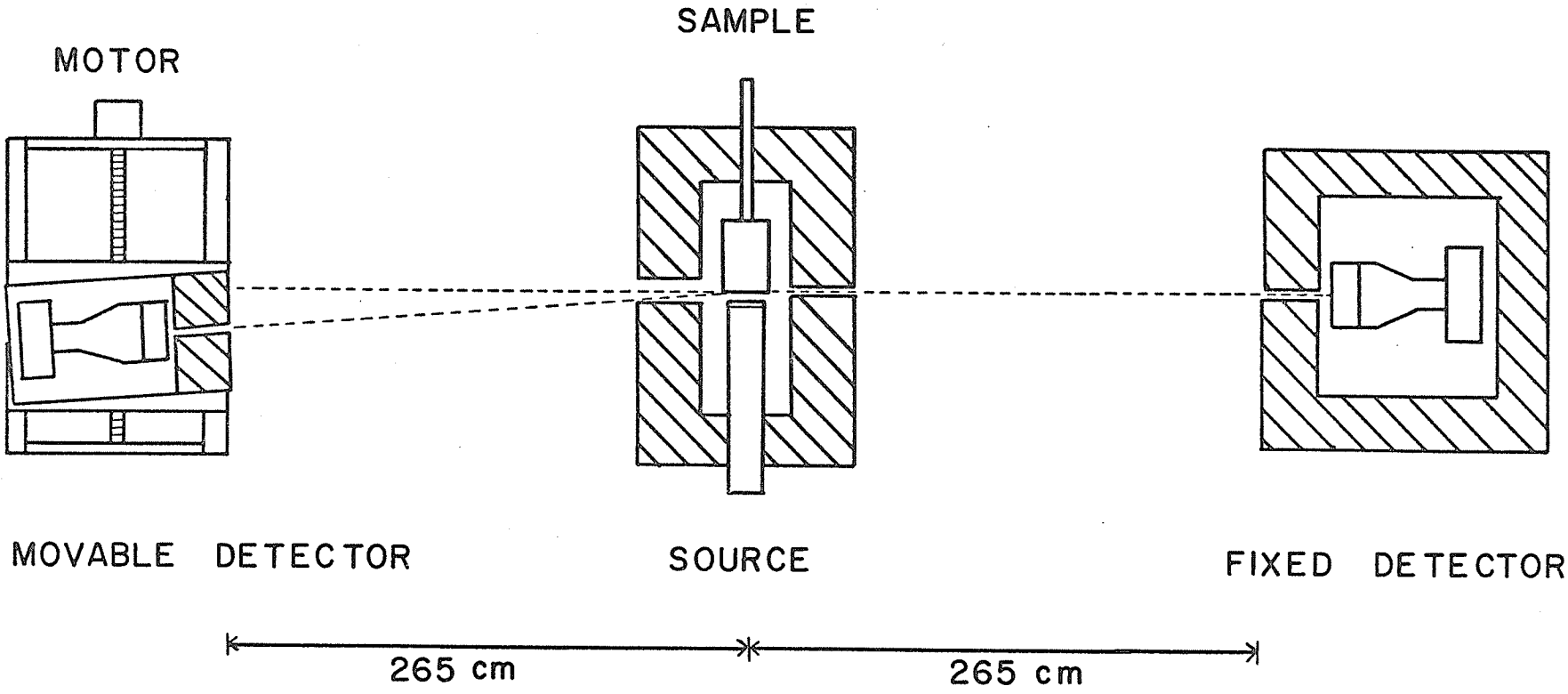
SAMPLE
MOTOR
MOVABLE DETECTOR
SOURCE
FIXED DETECTOR
265 cm
265 cm

larger slit facing the movable detector was necessary in order that gamma-rays from the sample could reach the detectors for the whole range of momenta studied.

An aluminum beam was used to keep the collimating slit of the movable detector aligned towards the sample as the detector moved through different positions.

B. Electronics

A block diagram of electronics is shown in Figure 3.2. The detectors were Integral Assembly model 16MB4/A-X and consisted of 4" diameter, 1" thick NaI(Tℓ) crystals mounted on 5018 HB photomultipliers with mu-metal shields. A positive potential of 1050 volts was applied to the photomultipliers by a Hamner N401 high voltage supply. Negative pulses (approximately 1 volt) were fed from the cathode followers in the detector heads to amplifiers, and were amplified about five times and shortened to approximately one microsecond.

Pulses from the amplifiers were sent to a pair of single channel analyzers set to select gamma-rays in the energy range between 0.1 and 0.6 Mev. This allowed through the Doppler shifted .511 Mev photons from the annihilations but blocked out the low energy noise and the 1.27 Mev gamma-rays from the source. The fast rising, narrow pulses from the single channel analyzers were sent to a coincidence unit which has a resolving time of about 150 nanoseconds. The resolution time of the coincidence unit was determined by providing a random source of gamma-rays for each detector, and measuring the chance coincidence counting rate and single counting rates, N_1 and N_2, for the two detectors. The resolution time, T, was then determined from the relation:

$$\text{chance coincidence counting rate} = 2TN_1N_2.$$

Figure 3-2

Block Diagram of Angular Correlation System Electronics

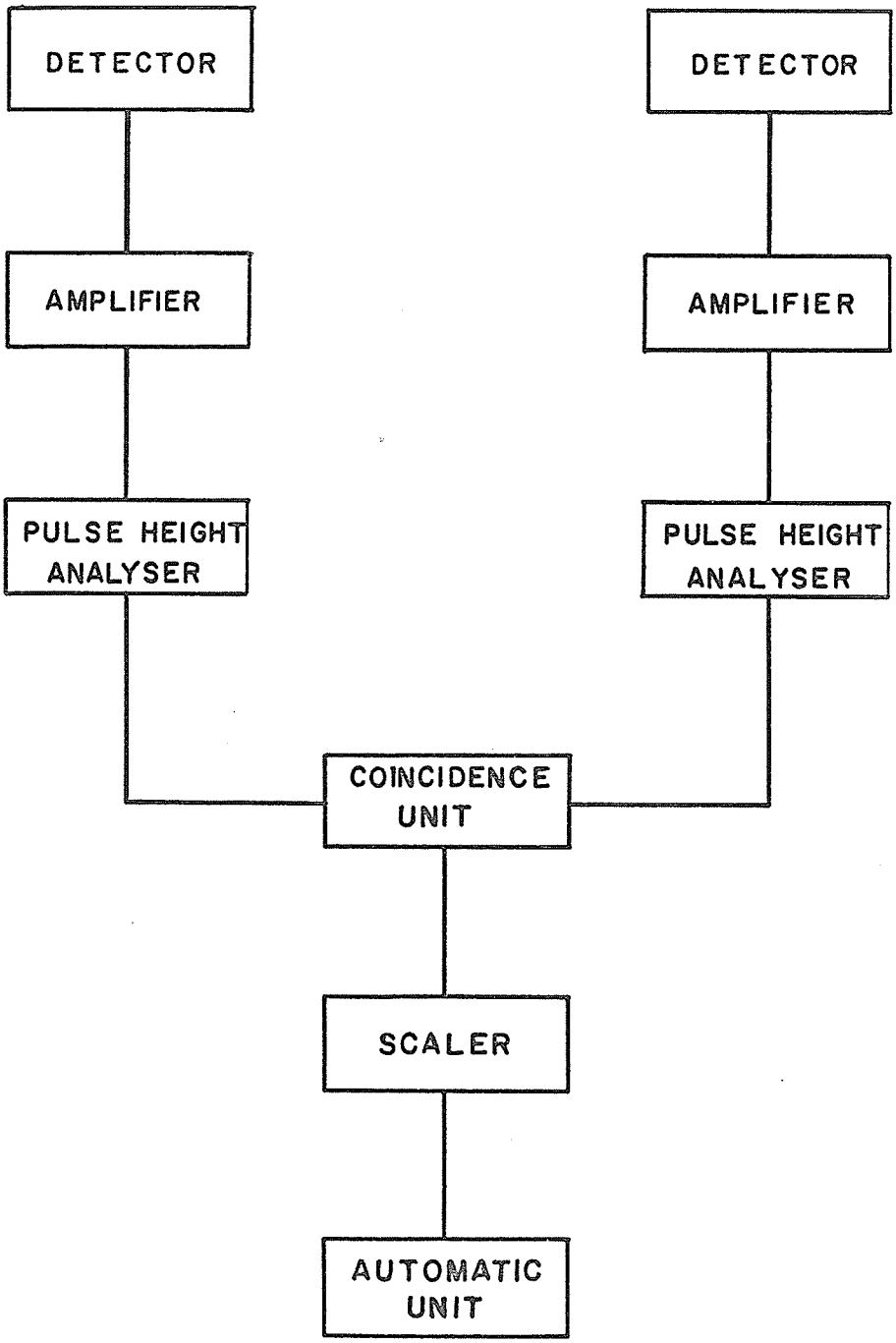
DETECTOR
DETECTOR
AMPLIFIER
AMPLIFIER
PULSE HEIGHT ANALYSER
PULSE HEIGHT ANALYSER
COINCIDENCE UNIT
SCALER
AUTOMATIC UNIT

A Technical Measurement Corporation Model SG-3A scaler was used to record the number of coincidences.

When 400 counts had been accumulated on the scaler, the "automatic unit" described previously by Kerr (1964) started the track motor and moved the movable detector to its next position. The scaler stops counting while the detector is being driven to its new position and starts again when the detector stops. At a predetermined position the direction of motion of the detector is reversed by a micro switch.

A Simplex ET-100 interval timer was used to record the time spent at each position to accumulate the required 400 counts. All the electronics was powered by a Sorenson model 2000 S A.C. voltage regulator.

3.2 Positron Sources

The source of positrons used in these experiments was a $Na^{22}C\ell$ source purchased from N. V. Phillips-Duphar Isotopes Division. The source consisted of $Na^{22}C\ell$ deposited in concentric grooves milled in the end of a Perspex rod 19.1 mm in diameter as shown in Figure 3.3. The end was covered with a round nylonfoil disk of thickness 2 mg/cm^2. The perspex rod was connected to a lucite rod of the same diameter to allow manipulation in the source castle. The strength of the Na^{22} source was approximately 4 millicuries.

Some experimental work was done by Chuang (1968)[1] on methane using Cu^{64} positron sources. Ordinary Cu foils measuring $\frac{3}{4} \times \frac{1}{2} \times 0.005$ inches were prepared and sent to Pinawa, Atomic Energy of Canada Ltd. for pile irradiation. Since Cu^{64} has a half-life of 12.9 hours, some haste was necessary in making use of a foil after irradiation. The activity when used in the experiment was greater than 250 millicuries.

Figure 3-3

Positron Source

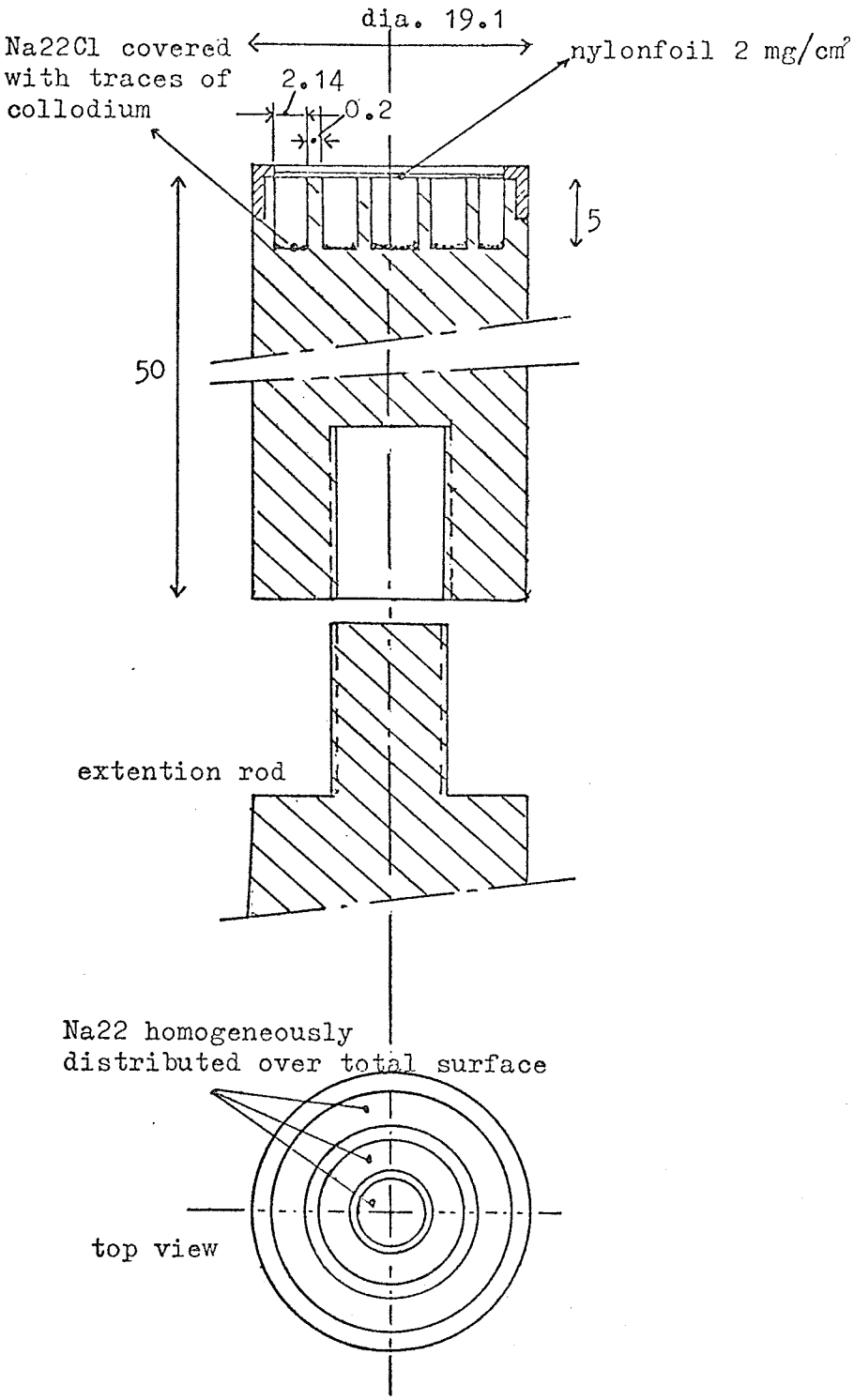

Measures in mm.

3.3 Sample Preparation and Mounting

The sample cell was constructed of $\frac{1}{32}$ inch aluminum. A window of .001" aluminum foil across one end of the cell permitted positrons to enter the sample. It was necessary to have the window this thick in order that the sample cell should be capable of holding a vacuum better than 10^{-3} torr. The volume of the sample cell was approximately 7 mℓ.

During the experiment, the sample cell was positioned so that only annihilations in a region just inside the window were recorded. Due to this and the fact that very few positrons penetrate through the sample and reach the walls of the cell, no correction was needed for annihilations in the aluminum.

For this experiment, research grade cyclohexane, No. C-556, was obtained from the Fisher Scientific Co. The cyclohexane used was the same as that from which the lifetime data was obtained. To remove the air dissolved in the sample it was subjected to the standard freeze-thaw technique. The cyclohexane was then transferred to the sample cell where it remained under vacuum for the duration of the experiment.

To keep the cyclohexane at the correct temperature a cold finger arrangement was utilized as illustrated in Figure 3.4. To maintain the level of the liquid nitrogen in the dewar and thus keep the temperature within prescribed limits, an electronically controlled valve was employed. A description of the operation of the circuit has been described by Chuang (1968). The boil-off from the liquid nitrogen in the storage dewar was used to force the liquid nitrogen through the transfer tube into the dewar surrounding the cold finger. With

Figure 3-4

Sample Cell and Cold Finger Arrangement

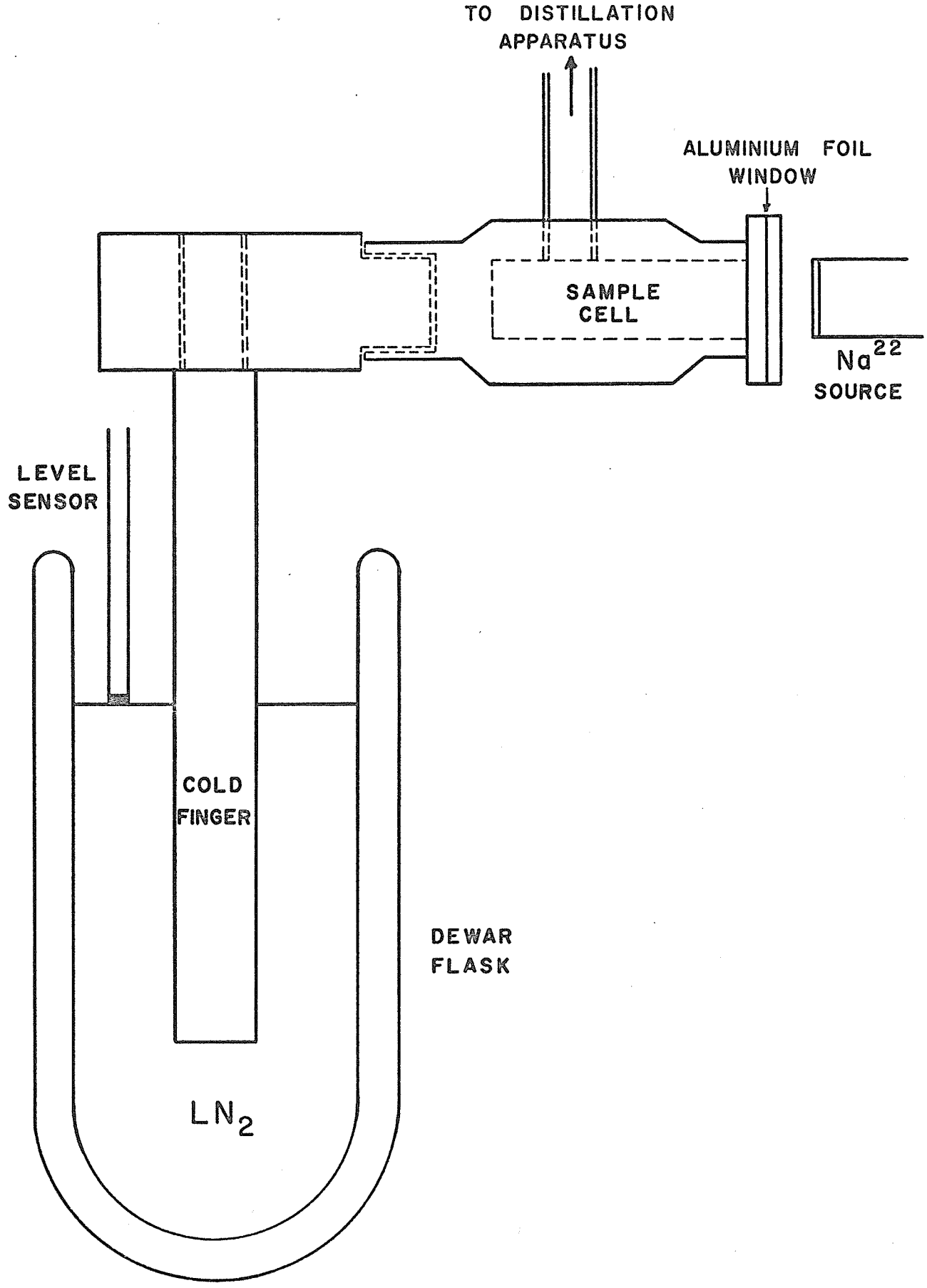
TO DISTILLATION APPARATUS
ALUMINIUM FOIL WINDOW
SAMPLE CELL
Na^{22} SOURCE
LEVEL SENSOR
COLD FINGER
DEWAR FLASK
LN_2

this arrangement the transfer time was between 5 and 10 minutes and the temperature variation was about plus or minus five degrees centigrade. Since the temperature was not critical except very close to the phase changes, this was considered to be satisfactory temperature control. Temperature measurement was achieved by use of a copper-constantan thermocouple cemented to the side of the sample cell.

Angular correlation information was also obtained using research grade benzene, No. B-245, from the Fisher Scientific Company. The freeze-thaw technique was again used to obtain a degassed sample which was subsequently transferred to the sample cell where it remained under vacuum. Temperature control was maintained by the same method as that used for the cyclohexane.

In subsequent chapters of this work angular correlation data obtained by Chuang (1968)[1] on solid and liquid methane and data obtained by Gould (1969) on solid and liquid butane will be used. For this experimental work butane and methane gas were research grade obtained from Matheson of Canada Ltd., Whitby, Ontario. The sample cell arrangement and temperature control method again were very similar to those used in obtaining data on the cyclohexane samples.

3.4 Data Accumulation and Analysis

To accumulate data the movable detector was set to examine the region between -11 to +11 milliradians. In the region from 0 to 7.5 milliradians approximately 50 runs consisting of 400 counts per point were taken on a sample. From 7.5 to 11 milliradians 5 runs of 1000 counts per point were accumulated. The points were .907 milliradians apart. Approximately a month was required to complete the investigation of a sample at a given temperature.

Each run was examined for any obvious irregularities which might be caused by electronic drifts. After a complete set of data had been obtained, the count rate was determined by dividing the total accumulated counts at each point by the total time required for the accumulation. All the data taken were corrected for the exponential decay of the source itself. Each angular distribution was plotted as counting rate vs. angle and in all cases was found to be symmetric within the experimental uncertainty.

Because of the finite angular resolution of the apparatus, the corrected angular distribution, $C'(\theta)$ is related to the true angular distribution, $C(\theta)$, by the following relation,

$$(3\text{-}1) \qquad C'(\theta_0) = \int_{-\infty}^{\infty} C(\theta)R(\theta_0-\theta)d\theta = \int_{-\infty}^{\infty} C(\theta_0-\theta)R(\theta)d\theta,$$

where $R(\theta)$ is the angular resolution function as calculated by Chuang (1968).

In the solid sample studied, the observed angular distributions are quite broad, and since the samples are more dense, this results in a small positron penetration depth and a narrow resolution function. Therefore $R(\theta)$ can be treated as a delta function and substitution into equation (3-1), yields $C'(\theta_0) = C(\theta_0)$. Therefore no correction is needed for the broad distribution curves.

For the liquid samples, the angular distributions are narrower. Equation (3-1) must be solved for $C(\theta)$ to give the desired correction, and to do this, an iterative numeric technique was used. Each iteration generated an approximate solution $C_n(\theta_0)$ where n is the iteration number. This approximate solution was obtained from that of the preceding iteration by the relation:

$$(3\text{-}2) \qquad C_n(\theta_o) = C_{n-1}(\theta_o) + \left[C'(\theta_o) - \frac{\int_{-\infty}^{\infty} R(\theta_o - \theta) C_{n-1}(\theta) d\theta}{\int_{-\infty}^{\infty} R(\theta) d\theta} \right]$$

For the zeroth approximation, i.e., the initial estimate of $C(\theta_o)$, we used $C_o(\theta_o) = C'(\theta_o)$. The iteration was continued until some arbitrary degree of convergence was attained, i.e. $C_n(\theta_o) \approx C_{n-1}(\theta_o)$. The resulting correction to the angular distributions for liquid cyclohexane and liquid benzene are shown in Figures 5-19 and 5-21.

A method has been described by Stewart (1957) whereby the momentum distribution of the annihilating positron-electron pairs may be derived from the angular correlation data obtained with an apparatus having parallel slit geometry. The following is based on Stewart's derivation.

Take $\rho(\underline{p})$ to be the density in momentum space of the annihilating pairs. Choose a set of Cartesian axes such that the x-axis lies along the line joining the fixed detector to the sample cells, the y-axis lies along the axis of the detector slit, and the z-axis is perpendicular to the x and y axes. Assuming that the number of annihilating pairs having a y-component of momentum large enough that the resulting gamma-rays would subtend an angle larger than that subtended by the slit is negligible, then the coincidence count rate is given by

$$c(p_z) = A \int_{-\infty}^{\infty} \int_{-\infty}^{\infty} \rho(p_x, p_y, p_z) dp_x \, dp_y$$

where $p_z = mc\theta$ as long as $p_z << mc$ and A is a constant.

If the variables of integration are changed to $P = (p_x^2 + p_y^2)^{1/2}$ and it is assumed that $\rho(\underline{p})$ is isotropic, then

$$c(p_z) = 2\pi A \int_o^\infty \rho(P,p_z)PdP$$

Using the substitution $p^2 = P^2 + p_z^2$, this becomes

$$c(p_z) = 2\pi A \int_{p_z}^\infty \rho(p)pdp$$

Differentiating with respect to p_z yields

$$\frac{dc(p_z)}{dp_z} = -2\pi A p_z \rho(p_z)$$

and it follows that

$$\rho(p_z) = -\frac{1}{2\pi A p_z} \frac{dc(p_z)}{dp_z}$$

Since $p_z = mc\theta$

$$\rho(p_z) = -B \cdot \frac{1}{\theta} \frac{dc(\theta)}{d\theta}$$

where B is a positive constant.

$\rho(p_z)$ is the density in momentum space of annihilating pairs having momentum of magnitude p_z. The area of a sphere in momentum space of radius p_z is $4\pi p_z^2$. Therefore, $N(p_z)$, the number of annihilating pairs having momentum of magnitude p_z is given by

$$N(p_z) = -4\pi B m^2 c^2 \theta \frac{dc(\theta)}{d\theta}$$

In the following sections the data will be presented in the form of $N(p)$ and $c(\theta)$. Since the constant B is not known the term $\frac{dc(\theta)}{d\theta}$ is simply multiplied by a normalizing factor.

A computer program developed by Gould (1969) was used for the actual analysis of the data. Input data was in the form of time

intervals required to accumulate 400 counts. The program first corrected the times for source decay and calculated the count rate $c(\theta)$ for each point. Next the program calculated the derivative at each point by means of a five point least squares fit to a parabola. For the 2nd and n-1th points a three point least squares fit to a parabola was used and for the end points a straight difference was used. Two other methods also were utilized to find the derivatives. The first fitted the data to a cubic function and the second simply used the slope between two successive data points. All methods of analysis gave equivalent results. The program then calculated $N(p)$ and $\rho(p)$ and the error in $N(p)$. Finally $c(\theta)$, the error in $c(\theta)$, $c'(\theta)$, $\rho(p)$, $N(p)$ and the error in $N(p)$ were outputed for each point in tabular form.

Upon analyzing the observed data, we must also consider any necessary corrections for the background distribution. The chance coincidence rate contributed a flat background well less than 1 count per minute. This was determined by moving the movable detector 20 milliradians off the 180-degree line so that coincidences from annihilations in the sample or any parts near the source would not be registered. A second source was the radiation resulting from annihilation in any part of the source castle or sample cell visible to both detectors. This background was determined by counting with no sample cell in place. The resulting distribution was almost flat with a peak counting rate of less than 1 count per minute. Since the analysis of the data involves taking the slope of the count rate curves to produce a momentum distribution, these background contributions have no significance. A third source was due to annihilations

in the sample cell window and in the walls of the sample cell itself. However, as explained earlier, this contribution could be neglected due to the positioning of the sample cell.

CHAPTER IV

THREE-PHOTON COINCIDENCE MEASUREMENTS

4.1 General Description

Rich (1951) was the first to use 3γ-coincidence counting for direct observation of three-photon positron-annihilation; the method was subsequently developed by de Benedetti and Siegel (1952).

An inherent difficulty in the case of 3γ annihilation is that energy-momentum conservation does not provide a unique determination of the momenta of the photons. The requirement is that the photons should be emitted in the same plane and that no more than two are emitted in the same half-plane. Since the three coincident photons are only coplanar and the two coincident photons are collinear, 3γ annihilation is more difficult to detect than 2γ annihilation. In practice, a source of relatively high strength must be used to provide reasonable statistics in a short time. However, the random triple coincidence rate will increase with larger source strengths and also with longer resolving times. Obviously, in order to maintain a high signal to noise ratio (true to random coincidences), with a high counting rate, the resolving time must be kept as low as possible.

Three scintillation counters were arranged symmetrically about the source of positrons and coplanar with it (fig. 4-1). This arrangement simplifies the problem of coincidence detection since all three annihilation photons must now have approximately the same energy, i.e. $\frac{2}{3}\,mc^2$. The scintillators were 3" by 3" NaI(Tℓ) crystals. The photomultiplier and scintillator assemblies (model no. 12512) were obtained from the Harshaw Chemical Company.

Figure 4-1

Counter Arrangement for Detection of Three-Photon Annihilations

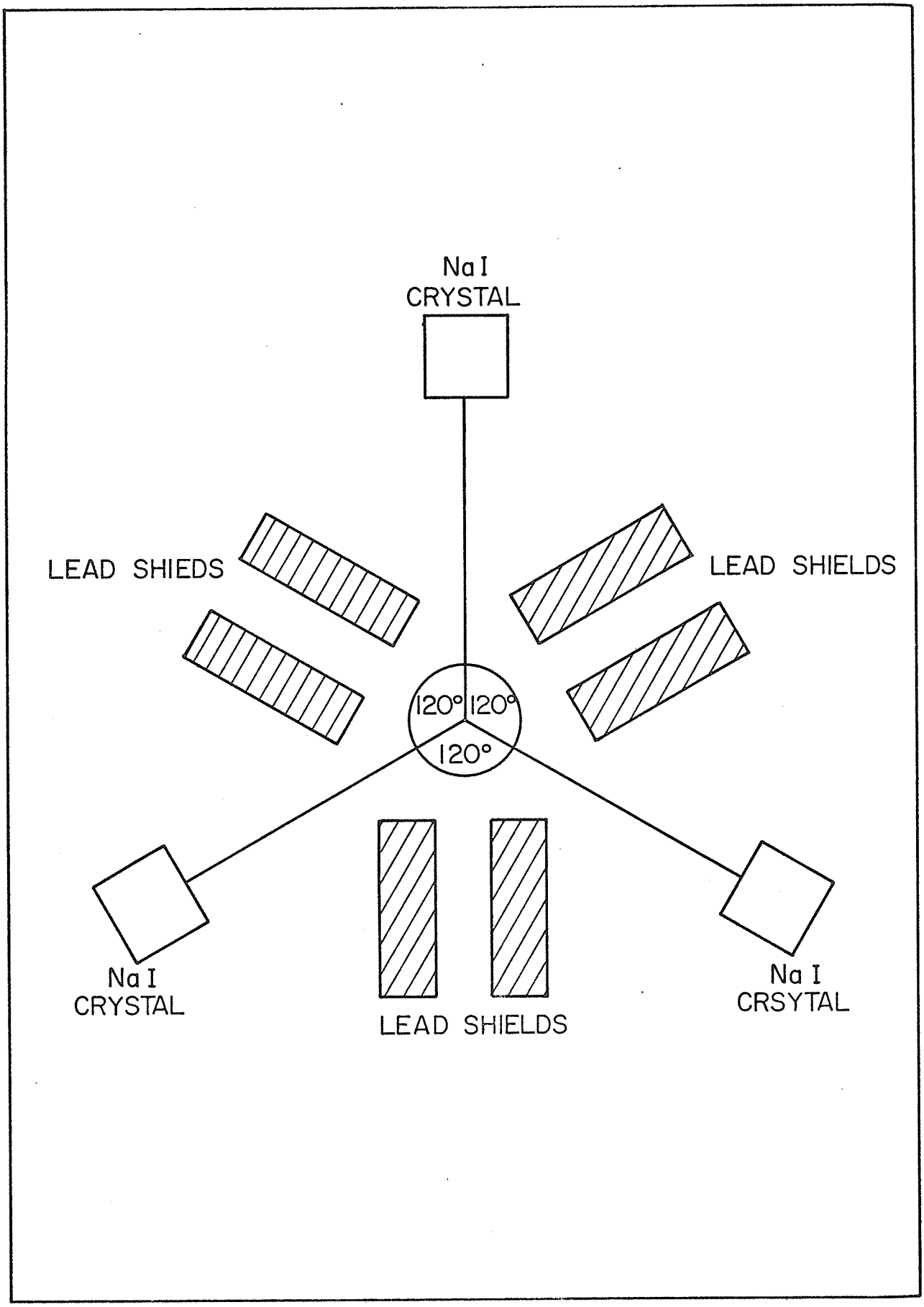
Na I
CRYSTAL
LEAD SHIEDS
LEAD SHIELDS
120°
120°
120°
Na I
CRYSTAL
LEAD SHIELDS
Na I
CRSYTAL

The apparatus is shown in block diagram in Fig. 4-2. The pulses from each of the photomultipliers were amplified so that 511 kev gamma-rays produced output signals of 5.1 volts. These were routed to timing single channel analyzers which selected photons in the energy range 100 kev to 500 kev. This energy selection was necessary to reduce background coincidences. Delays in the timing single channel analyzers were set so that output pulses originating from coincident events in the three photomultipliers arrived simultaneously at the triple coincidence unit. This was done by selecting pairs of photomultipliers and adjusting their respective single channel analyzer delays to maximize the double coincidence rates from the two counters. The resolving time of the triple coincidence unit was set at 100 nanoseconds to minimize random background counts and still maintain a reasonably high count rate.

The source of positrons was identical to that used in the lifetime experiments, i.e. approximately 50 microcuries of Na^{22} deposited on a thin sheet of mica. Although the 1.28 Mev gamma-ray from the daughter Ne^{22} released almost simultaneously with the positron was necessary for the timing work, it tends only to contribute to the background of the three photon intensity measurements. As seen in Fig. 4-1 the crystal detectors were shielded from each other with blocks of lead in order to reduce spurious coincidences. For the measurement of the background coincidences, one of the counters was removed from the plane defined by the source and by the other two counters, without altering its distance from the source.

The methods of temperature regulation of the samples has been described earlier. Samples of cyclohexane were maintained at the

Figure 4-2

Block Diagram of Triple Coincidence System

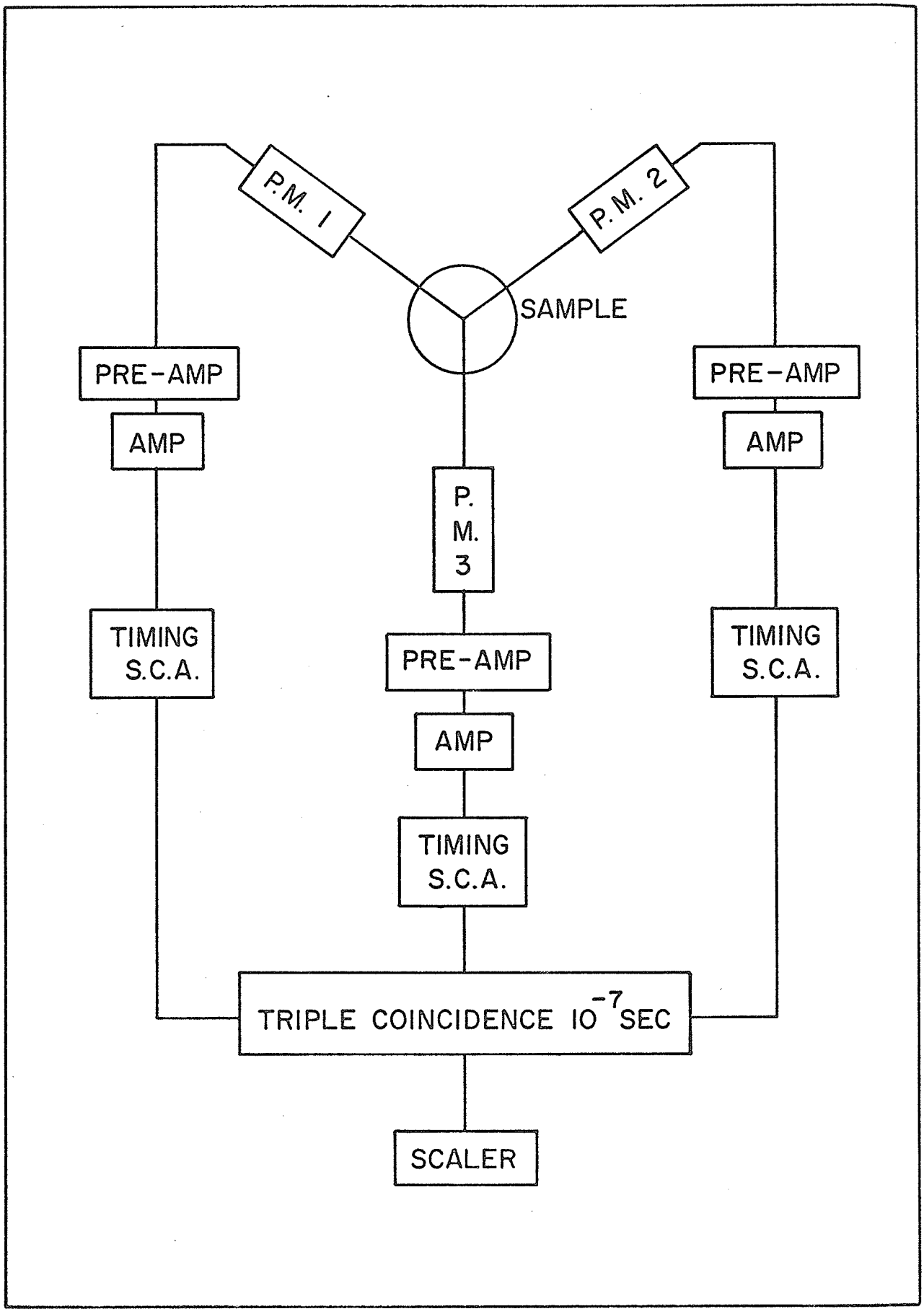
P.M. 1
P.M. 2
SAMPLE
PRE-AMP
AMP
P.
M.
3
PRE-AMP
AMP
TIMING
S.C.A.
PRE-AMP
AMP
TIMING
S.C.A.
TIMING
S.C.A.
TRIPLE COINCIDENCE 10^{-7} SEC
SCALER

required temperatures by the liquid nitrogen system shown in Fig. 2-10. Control of liquid and solid methane samples was effected by immersion of a metal cold finger into a dewar of liquid nitrogen.

4.2 Data Accumulation and Analysis

Experimental runs consisted of accumulating from 5,000 to 15,000 counts. For each sample at the required temperature the data were taken first with all counters and the source in a plane as shown in Fig. 4-1. To determine the background rate, data were next accumulated with one of the counters placed 45^{o} out of the plane. The position of this counter was adjusted so that the singles counting rate remained exactly as it was. This ensured that the counter to source distance remained constant.

Because of the relatively low count rate in these experiments and the high background coincidence rates, checks were made to ensure that a high degree of stability was maintained by the electronic components. The output spectrum of each photomultiplier as well as the singles count rate from each pulse height analyzer were monitored several times during each experimental run. Also, several independent runs were made on each sample to determine if the results thus accumulated were within statistical error.

Any direct determination from experimental data of absolute magnitudes for the probability of 3γ annihilation would require measurements of counter efficiency, of the solid viewing angle with respect to the source, and of several other characteristics of the equipment; it would also entail rather cumbersome calculations based on the spectrum of 3γ annihilation quanta. However, all these procedures are unnecessary if we can compare experimental data for

materials in which we wish to determine the 3γ probability with data for materials in which this probability is known.

In a simple model of positron decay as outlined by Goldanskii (1968) the probability of three gamma annihilation can be expressed in the following form:

$$P_{3\gamma} = \frac{3}{4} P \frac{\tau_2}{\tau_3} + \frac{1}{372} (1-P)$$

where P is the probability of positronium formation, $\tau_3(1.4 \times 10^{-7}$ sec) is the lifetime of orthopositronium in free space and τ_2 is the actual lifetime of orthopositronium as reduced by the various quenching processes. The above relation assumes (a) the three quantum production of orthopositronium arises solely from annihilation of the positron with its bound electron and occurs with a probability equal to $\frac{\tau_2}{\tau_3}$; (b) the nonpositronium part of annihilation is attributable to positrons which all have the same fate and which behave as free: their three quantum annihilation probability is $\frac{1}{372}$; (c) the parapositronium does not contribute to three quantum events through any interaction with matter.

Experimental data were obtained for methane and cyclohexane in their liquid and solid phases. By comparing the number of three gamma events in the liquid phase, where the amount of positronium formation is known, with the corresponding number in the solid phase the percentage of positronium formation in the solid can be determined.

CHAPTER V

EXPERIMENTAL RESULTS

5.1 Lifetime Results - Cyclohexane

The lifetime experimental work was done using samples of 99 mole % pure cyclohexane obtained from the Fisher Scientific Company. Time runs were taken at various temperatures using both normal air-saturated samples and samples which had been degassed. A mica source as described previously was used and after preparation the cyclohexane was placed in the temperature regulating apparatus.

Figures 5-1 to 5-6 illustrate typical lifetime decay curves for cyclohexane at various temperatures for both air-saturated and degassed samples. These curves have been plotted directly from the experimental points after subtraction of background. The straight lines drawn through the points are visual fits to the data. From the plotted curves initial estimates for the computer analysis could be calculated. Computer analysis for each of the curves obtained was then carried out and Tables 5-1 to 5-2 give a complete list of the decay parameters found for cyclohexane at the various temperatures.

Figures 5-7 to 5-10 illustrate the temperature dependence of the decay parameters for both the air-saturated and degassed cases. The solid lines drawn through the experimental points are simply best fits and the arrows indicate the liquid-solid phase transition and the solid-solid phase transition found in cyclohexane.

TABLE 5-1

Cyclohexane (Degassed)

Temp (^{o}C)	τ_2 (nsec)	τ_1 (nsec)	I_2 (%)	I_1 (%)
-196	1.04 ± .02	.31 ± .01	26 ± 1	76 ± 3
-160	1.08 ± .03	.35 ± .03	22 ± 2	80 ± 4
-128	1.17 ± .03	.34 ± .03	17 ± 1	80 ± 6
-118	1.21 ± .02	.33 ± .03	20 ± 2	79 ± 6
- 90	1.28 ± .03	.33 ± .02	17 ± 1	80 ± 4
- 88	1.28 ± .03	.38 ± .02	18 ± 2	89 ± 3
- 83	1.53 ± .03	.33 ± .02	16 ± 1	80 ± 3
- 78	1.14 ± .06	.35 ± .04	20 ± 3	82 ± 15
- 75	1.32 ± .03	.34 ± .02	17 ± 2	82 ± 3
- 73	2.05 ± .04	.36 ± .02	19 ± 1	76 ± 3
- 68	1.90 ± .04	.36 ± .03	19 ± 2	76 ± 8
- 65	2.26 ± .04	.39 ± .02	21 ± 1	77 ± 3
- 45	2.28 ± .05	.37 ± .02	21 ± 1	75 ± 5
- 32	2.41 ± .04	.40 ± .02	23 ± 2	78 ± 3
0	2.60 ± .04	.37 ± .03	25 ± 1	74 ± 7
+ 5	2.66 ± .04	.35 ± .02	22 ± 1	72 ± 3
+ 9	3.00 ± .04	.37 ± .02	31 ± 1	70 ± 3
+ 20	3.08 ± .04	.39 ± .03	34 ± 2	58 ± 4
+ 32	3.15 ± .07	.36 ± .02	31 ± 1	65 ± 5
+ 44	3.26 ± .05	.36 ± .02	31 ± 1	67 ± 5

TABLE 5-2

Cyclohexane (Non-Degassed)

Temp (^{o}C)	τ_2 (nsec)	τ_1 (nsec)	I_2 (%)	I_1 (%)
-196	1.07 ± .02	.35 ± .02	19 ± 1	69 ± 5
-174	1.07 ± .02	.31 ± .03	15 ± 3	76 ± 10
-114	1.18 ± .04	.37 ± .04	17 ± 2	73 ± 11
-102	1.25 ± .04	.39 ± .04	18 ± 2	67 ± 10
- 86	1.26 ± .04	.33 ± .03	18 ± 2	81 ± 8
- 84	1.12 ± .02	.30 ± .02	19 ± 1	84 ± 4
- 80	1.71 ± .02	.35 ± .02	19 ± 1	75 ± 3
- 79	1.18 ± .03	.31 ± .02	21 ± 2	73 ± 4
- 78	1.96 ± .04	.39 ± .02	20 ± 1	71 ± 3
- 77	1.88 ± .04	.38 ± .02	20 ± 1	77 ± 5
- 76	1.98 ± .04	.38 ± .03	20 ± 1	75 ± 3
- 75	2.12 ± .02	.37 ± .02	18 ± 1	77 ± 4
- 52	2.11 ± .02	.36 ± .02	20 ± 1	71 ± 3
- 39	2.22 ± .04	.37 ± .01	20 ± 1	69 ± 3
- 7	2.24 ± .04	.34 ± .02	19 ± 2	74 ± 5
0	2.28 ± .04	.35 ± .03	21 ± 1	62 ± 6
+ 6	2.44 ± .04	.37 ± .01	22 ± 1	75 ± 3
+ 12	2.35 ± .02	.34 ± .02	28 ± 1	72 ± 4
+ 20	2.50 ± .04	.38 ± .03	34 ± 1	60 ± 6
+ 33	2.37 ± .02	.33 ± .02	30 ± 1	62 ± 3
+ 49	2.51 ± .02	.34 ± .02	31 ± 1	71 ± 4

Figure 5-1

Time Spectra of Cyclohexane

Degassed Sample at $+44^{o}C$

Non-Degassed Sample at $+49^{o}C$

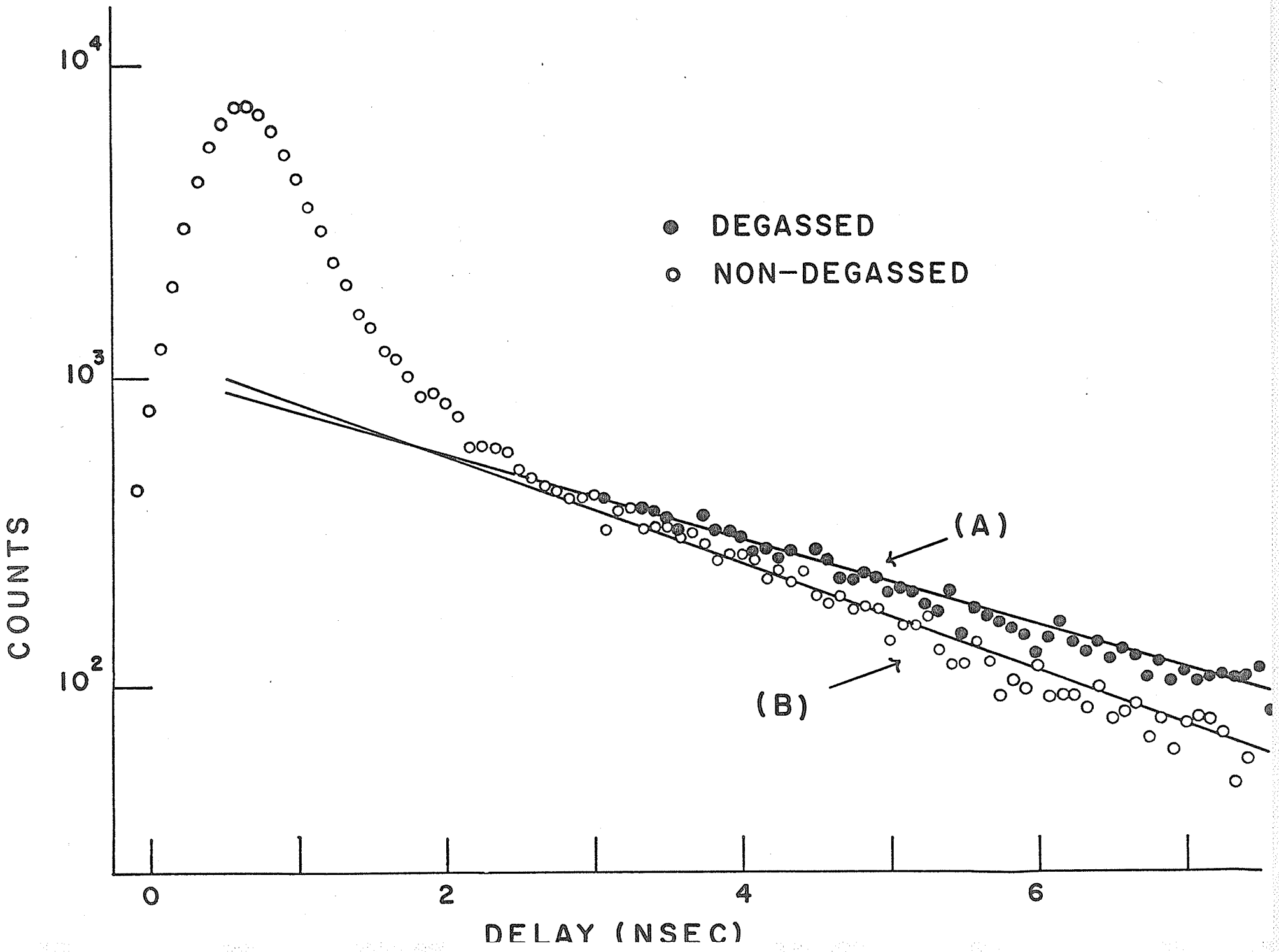
DEGASSED
NON-DEGASSED
(A)
(B)
COUNTS
10^4
10^3
10^2
0
2
4
6
DELAY (NSEC)

Figure 5-2

Time Spectra of Degassed Cyclohexane at +20^{o}C

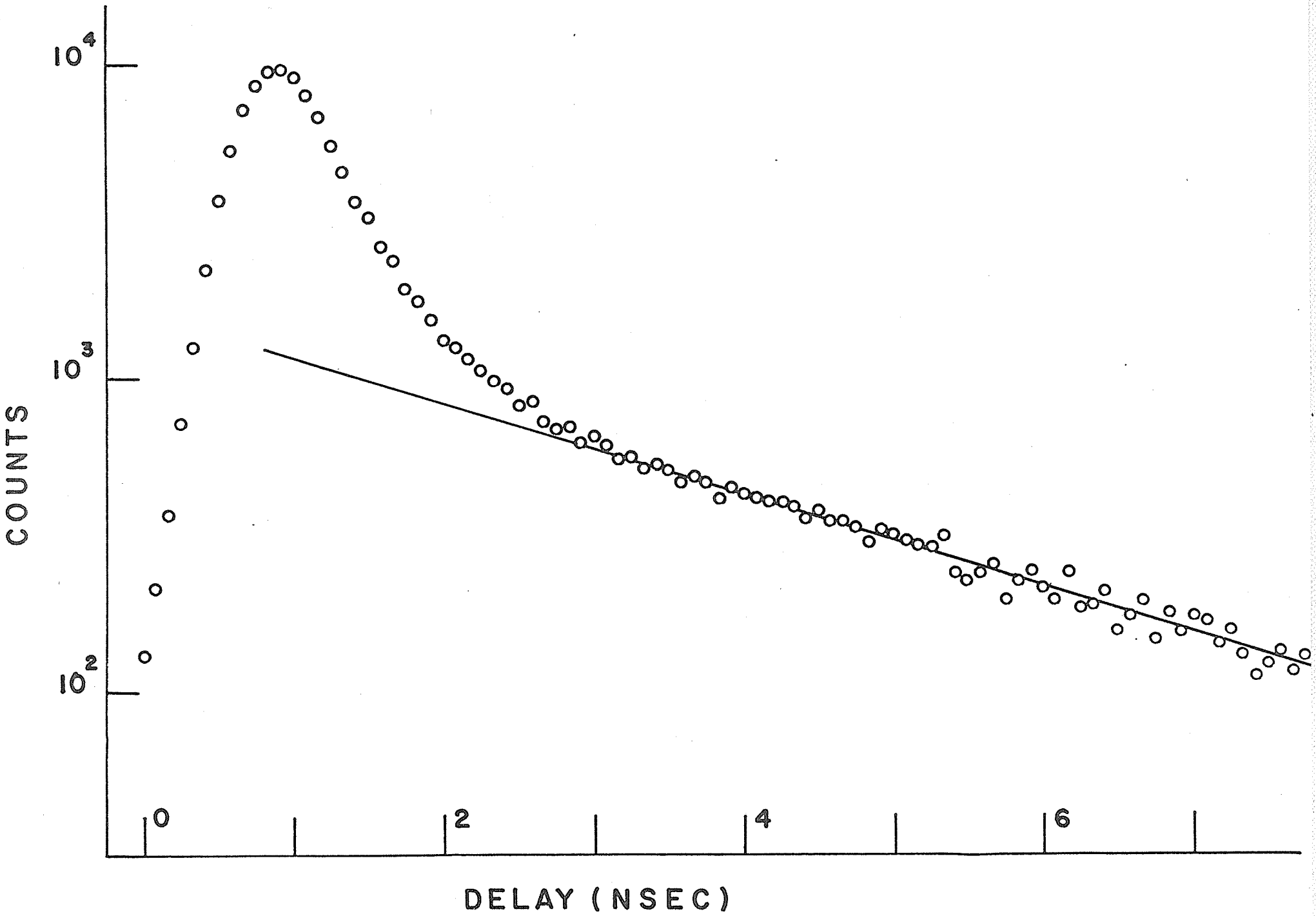
10^4
10^3
10^2
COUNTS
0
2
4
6
DELAY (NSEC)

Figure 5-3

Time Spectra of Cyclohexane

Degassed Sample at +4.7^{o}C

Non-Degassed Sample at 0^{o}C

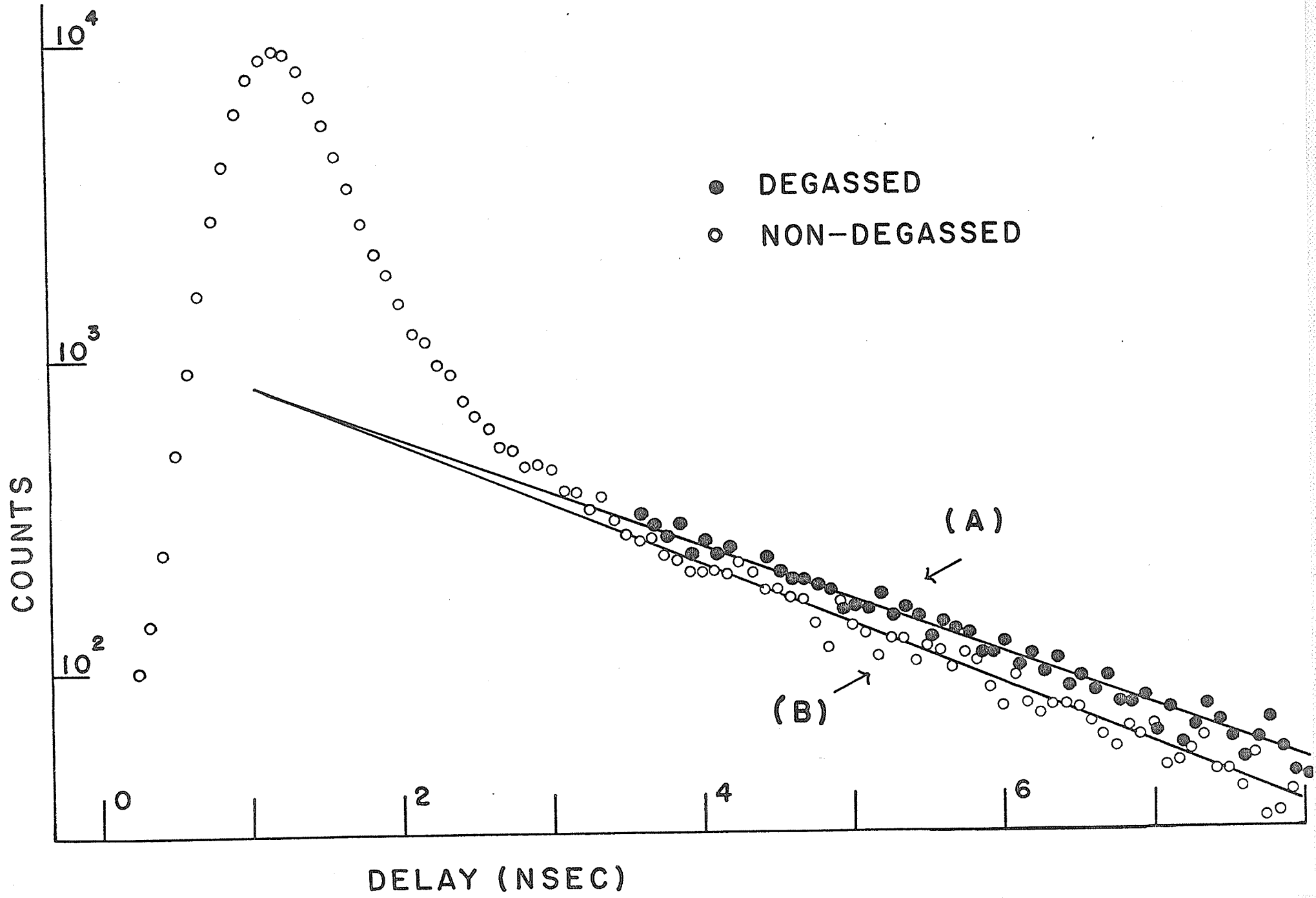
10^4
10^3
10^2
COUNTS
DEGASSED
NON-DEGASSED
(A)
(B)
0
2
4
6
DELAY (NSEC)

Figure 5-4

Time Spectra of Cyclohexane

Degassed Sample at -45^{o}C

Non-Degassed Sample at -39^{o}C

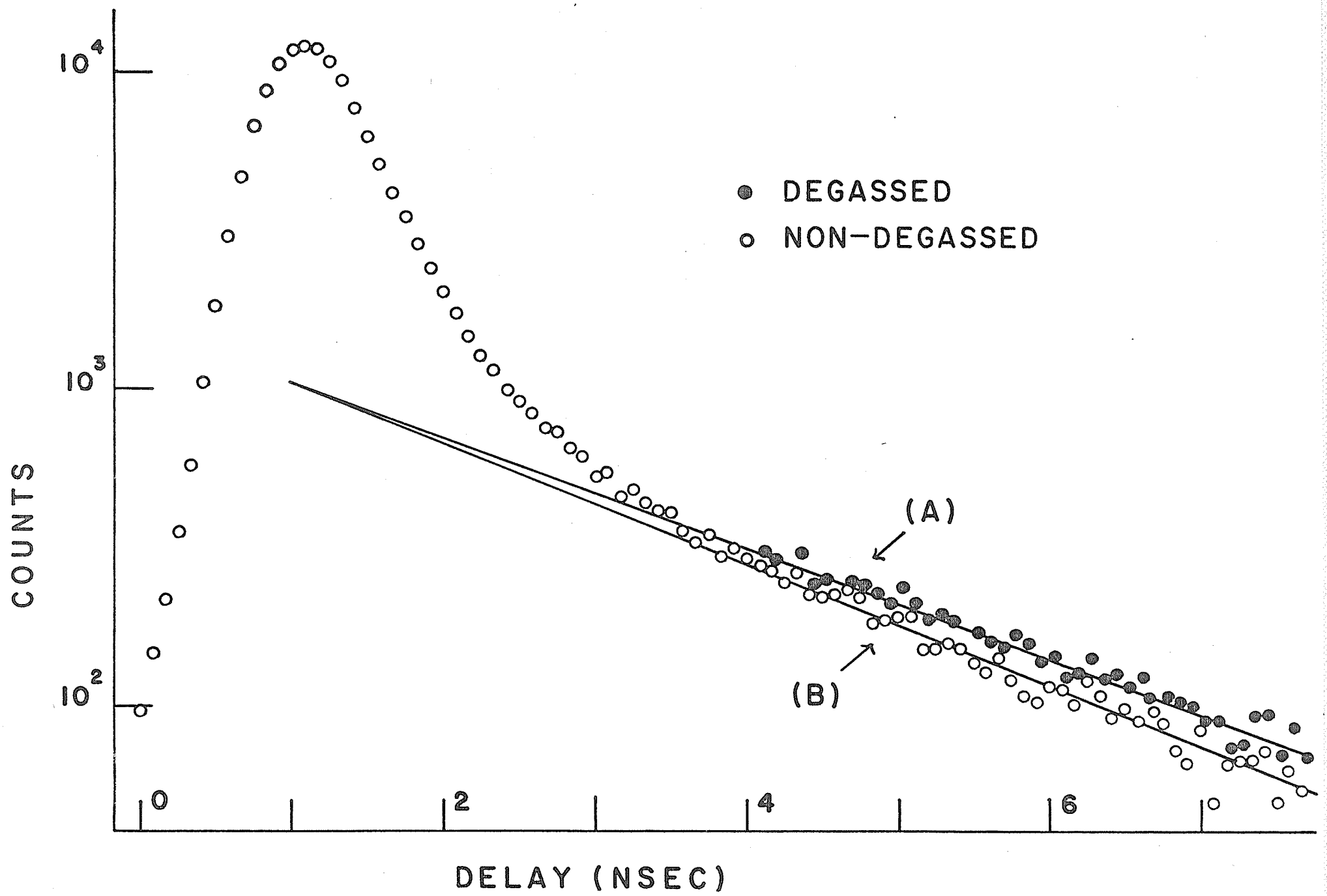
10^4
10^3
10^2
COUNTS
DEGASSED
NON-DEGASSED
(A)
(B)
0
2
4
6
DELAY (NSEC)

Figure 5-5

Time Spectra of Non-Degassed Cyclohexane at -74^{o}C

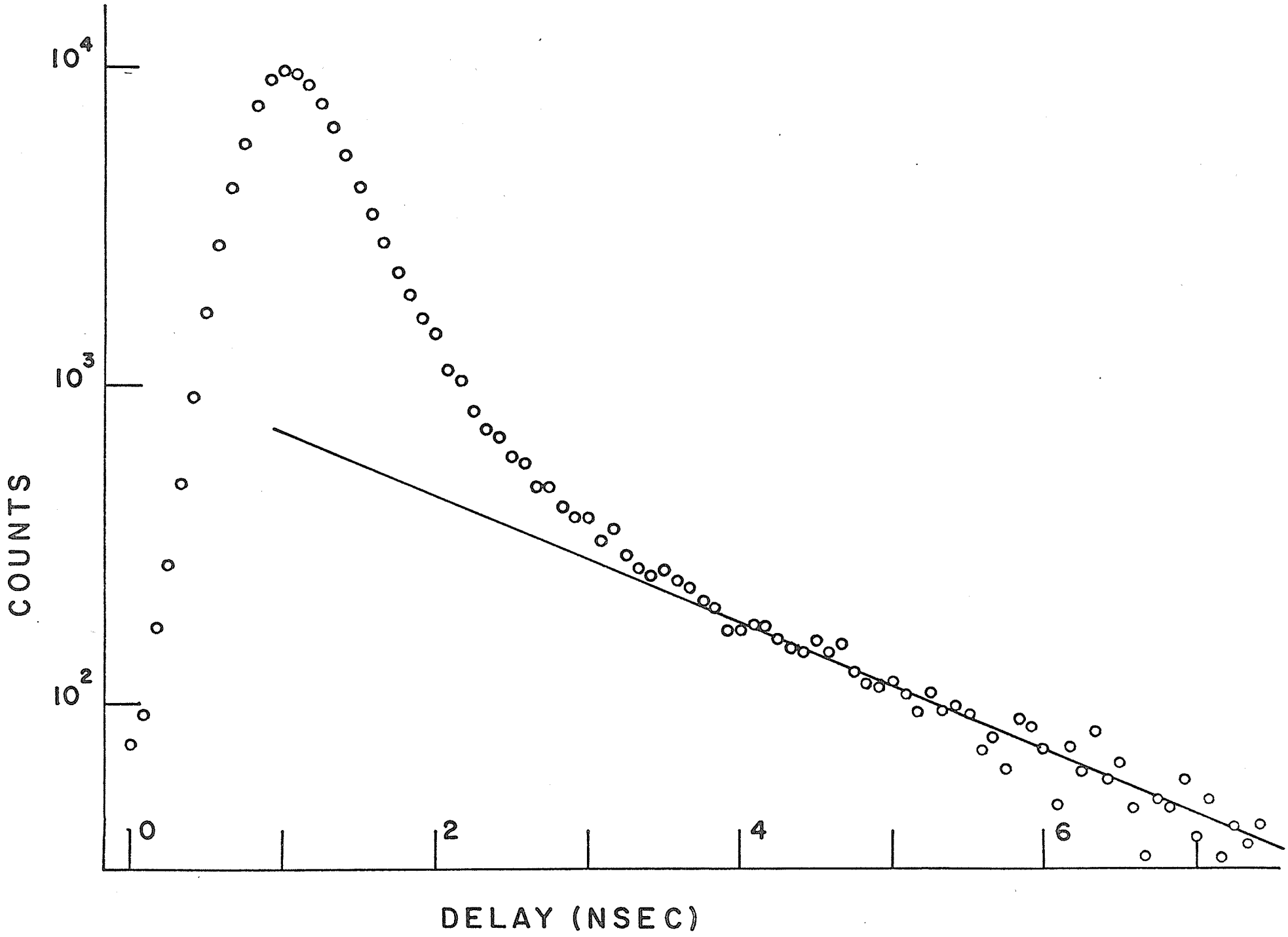
10^4
10^3
10^2
COUNTS
0
2
4
6
DELAY (NSEC)

Figure 5-6

Time Spectra of Degassed Cyclohexane at -118^{o}C

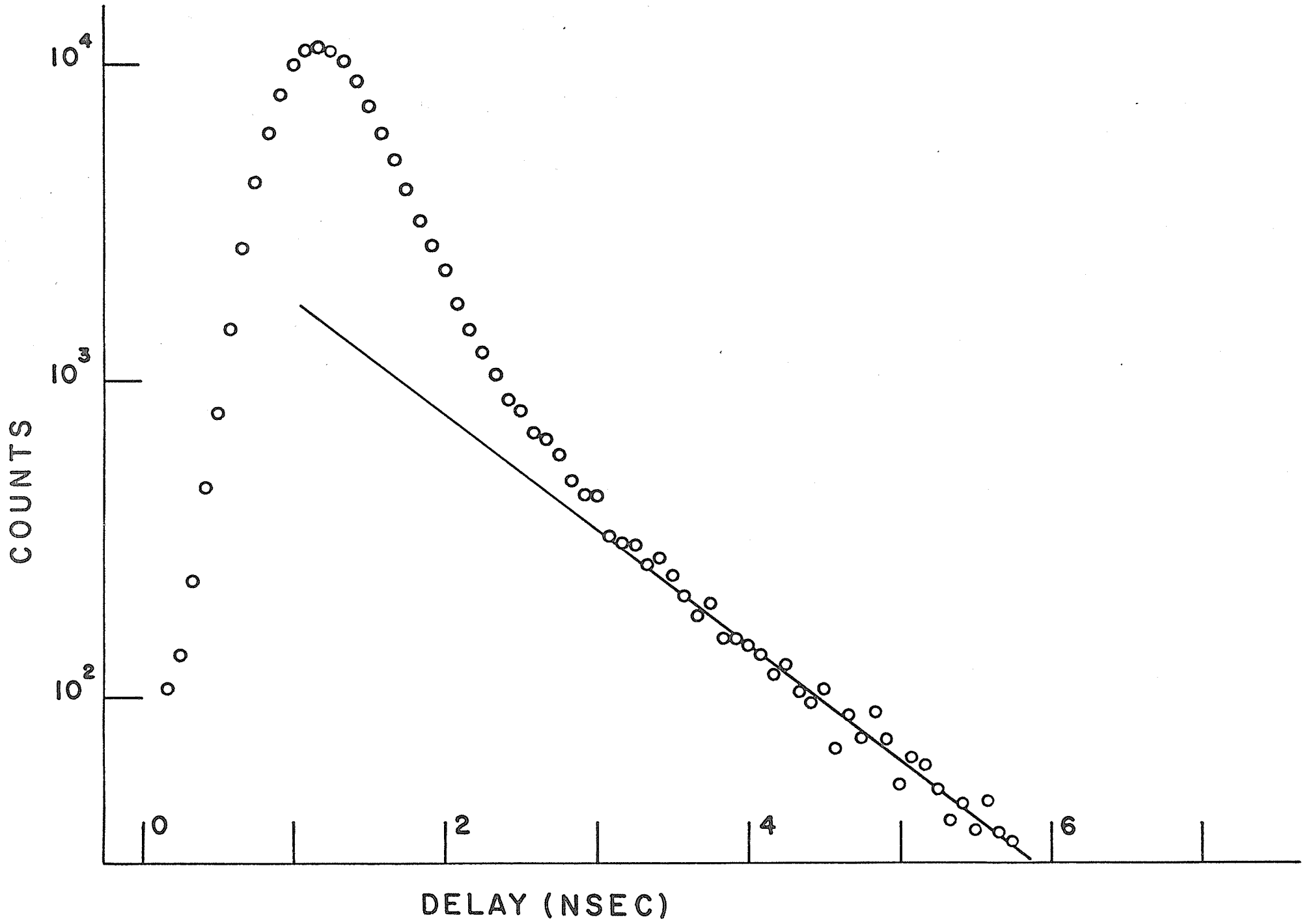
10^4
10^3
10^2
COUNTS
0
2
4
6
DELAY (NSEC)

Figure 5-7

Temperature Dependence of τ_2 for Cyclohexane

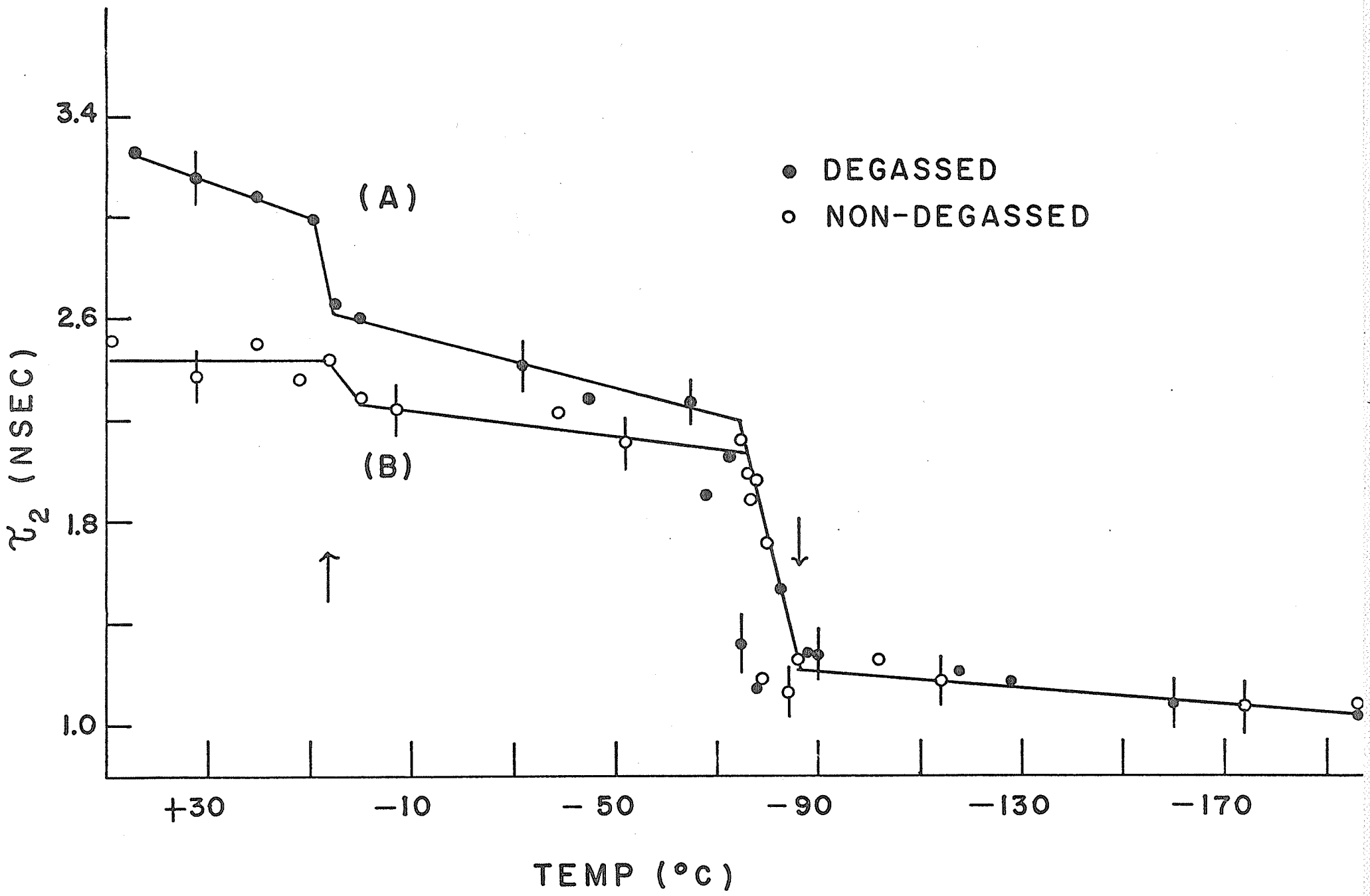
3.4
2.6
1.8
1.0
τ_2 (NSEC)
(A)
(B)
DEGASSED
NON-DEGASSED
+30
−10
− 50
−90
−130
−170
TEMP (°C)

Figure 5-8

Temperature Dependence of τ_1 for Cyclohexane

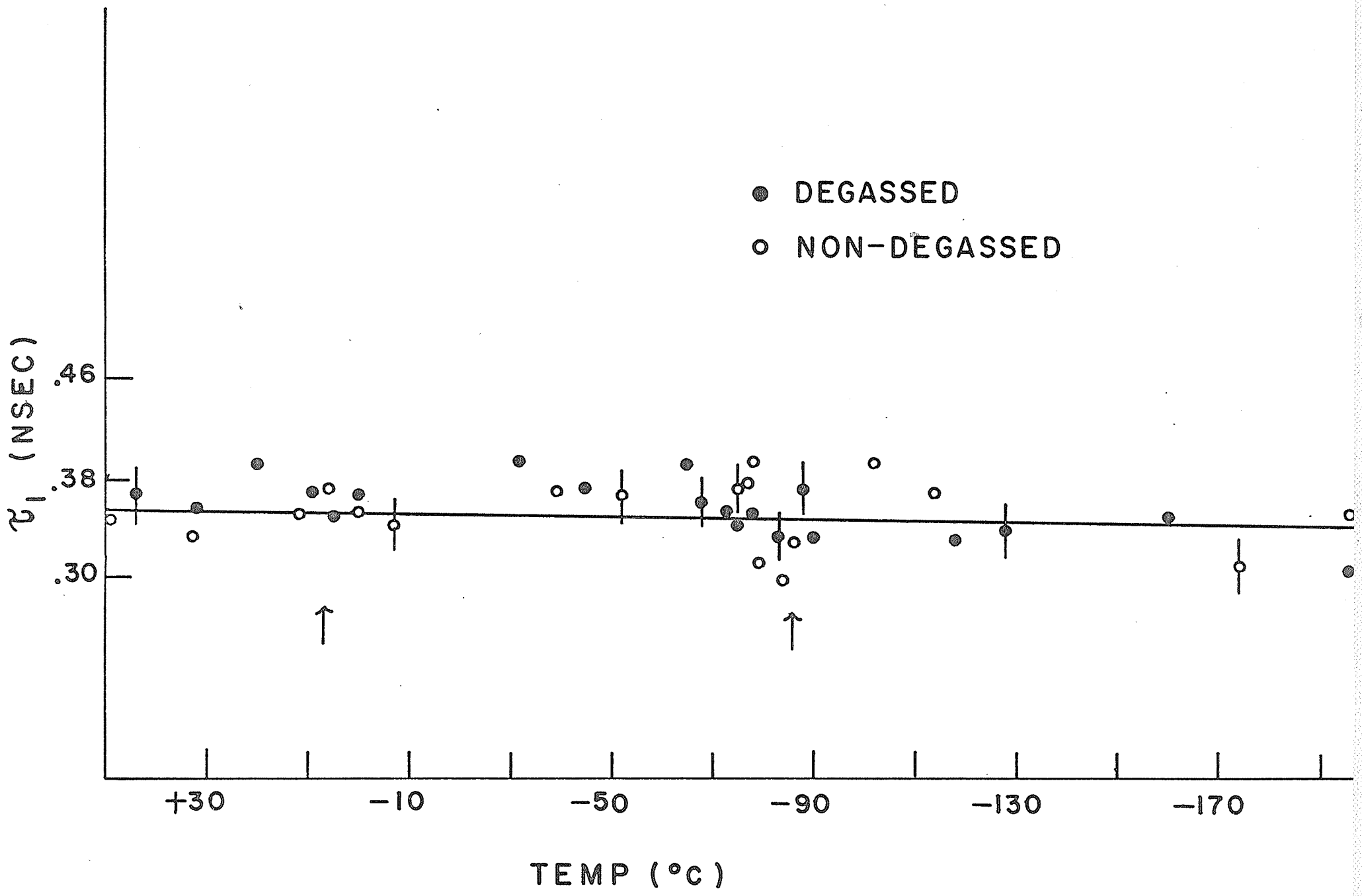
DEGASSED
NON-DEGASSED
τ_1 (NSEC)
.46
.38
.30
+30
−10
−50
−90
−130
−170
TEMP (°C)

Figure 5-9

Temperature Dependence of I_2 for Cyclohexane

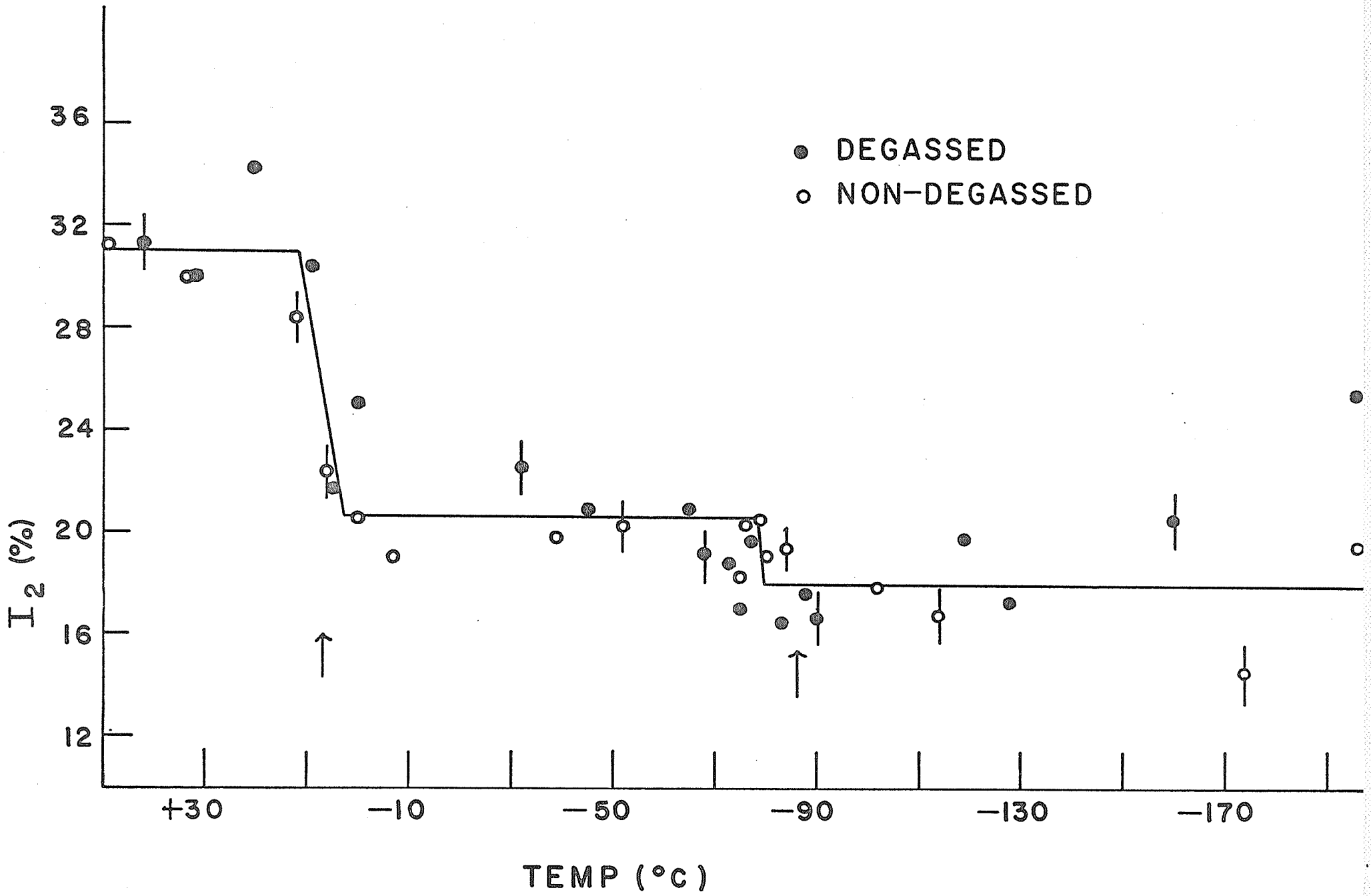
DEGASSED
NON-DEGASSED
36
32
28
24
20
16
12
I_2 (%)
+30
−10
−50
−90
−130
−170
TEMP (°C)

Figure 5-10

Temperature Dependence of I_1 for Cyclohexane

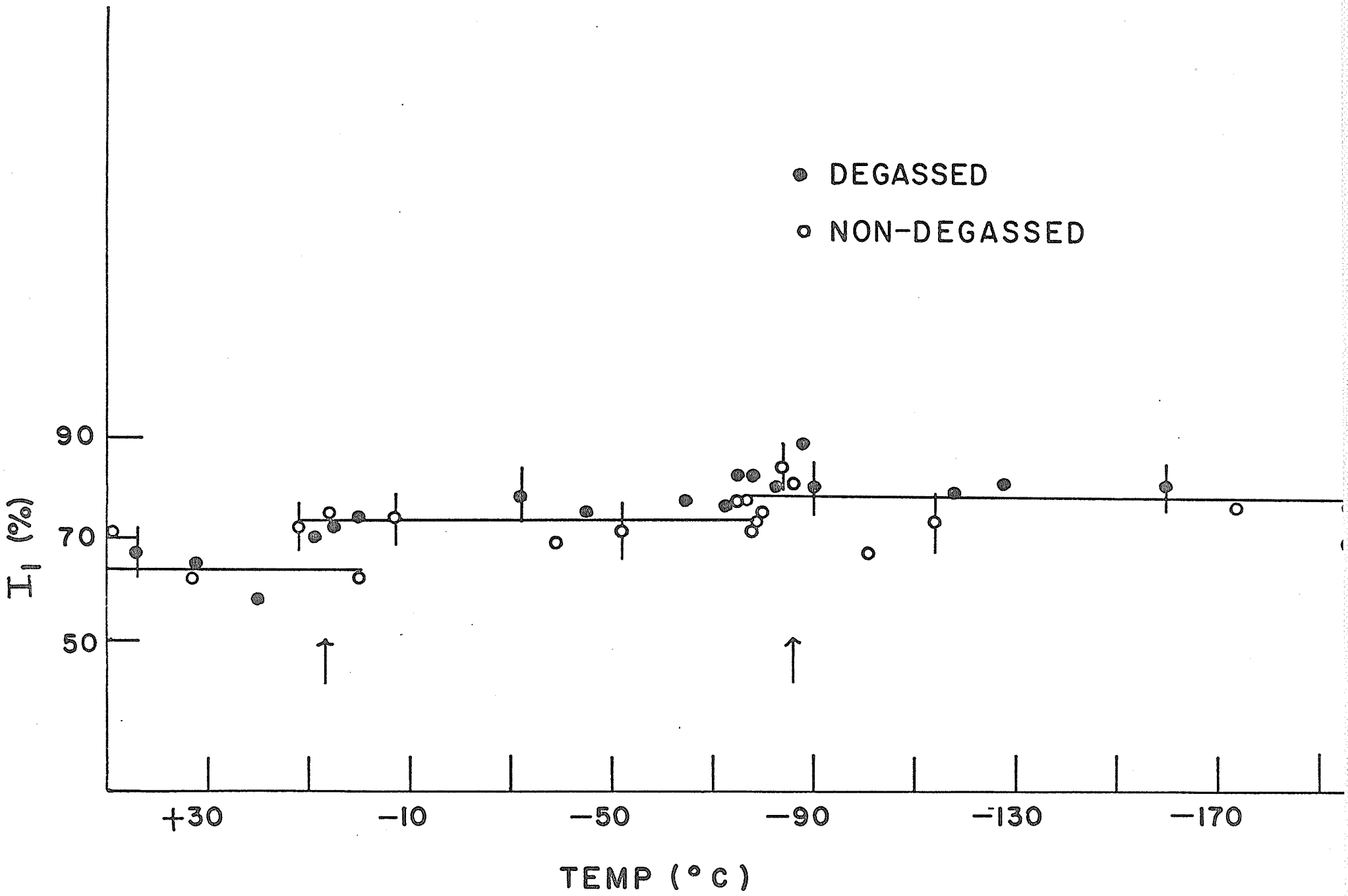
DEGASSED
NON-DEGASSED
90
70
50
I_1 (%)
+30
-10
-50
-90
-130
-170
TEMP (°C)

5.2 Lifetime Results - Methane, Butane, Benzene

As will be seen in a further portion of this chapter angular correlation results were obtained using samples of benzene and triple coincident experiments were performed on methane samples. To facilitate discussion in the following chapter it is necessary to include here lifetime data obtained by other researchers on benzene and methane. As pertinent information was obtained from butane results these will also be included here. The experimental work on methane and butane was done by Cooper (1969) and that on benzene by Germagnoli, Poletti, and Randone (1966).

Table 5-3 lists the decay parameters found for methane. Since methane boils at -161.6^{o}C only a limited range of temperature data was acquired. Figures 5-11 to 5-14 illustrate the temperature dependence of the decay parameters. Again the arrows indicate the liquid-solid phase transition.

In Table 5-4 are listed the decay parameters found for butane. The temperature dependence of the decay parameters is shown in Figures 5-15 to 5-18 with the arrows indicating the liquid-solid transition.

Table 5-5 lists the available data on benzene. The melting point of this substance is 5.5^{o}C.

TABLE 5-3

Methane

Temp (^{o}C)	τ_2 (nsec)	τ_1 (nsec)	I_2 (%)	I_1 (%)
-196	2.81 ± .05	.40 ± .01	32 ± 1	57 ± 3
-188	3.25 ± .07	.36 ± .04	31 ± 2	65 ± 11
-183	4.43 ± .06	.41 ± .04	32 ± 2	65 ± 10
-176	5.43 ± .08	.35 ± .03	33 ± 2	59 ± 8
-174	5.72 ± .07	.37 ± .04	34 ± 1	56 ± 7

Figure 5-11

Temperature Dependence of τ_2 for Methane

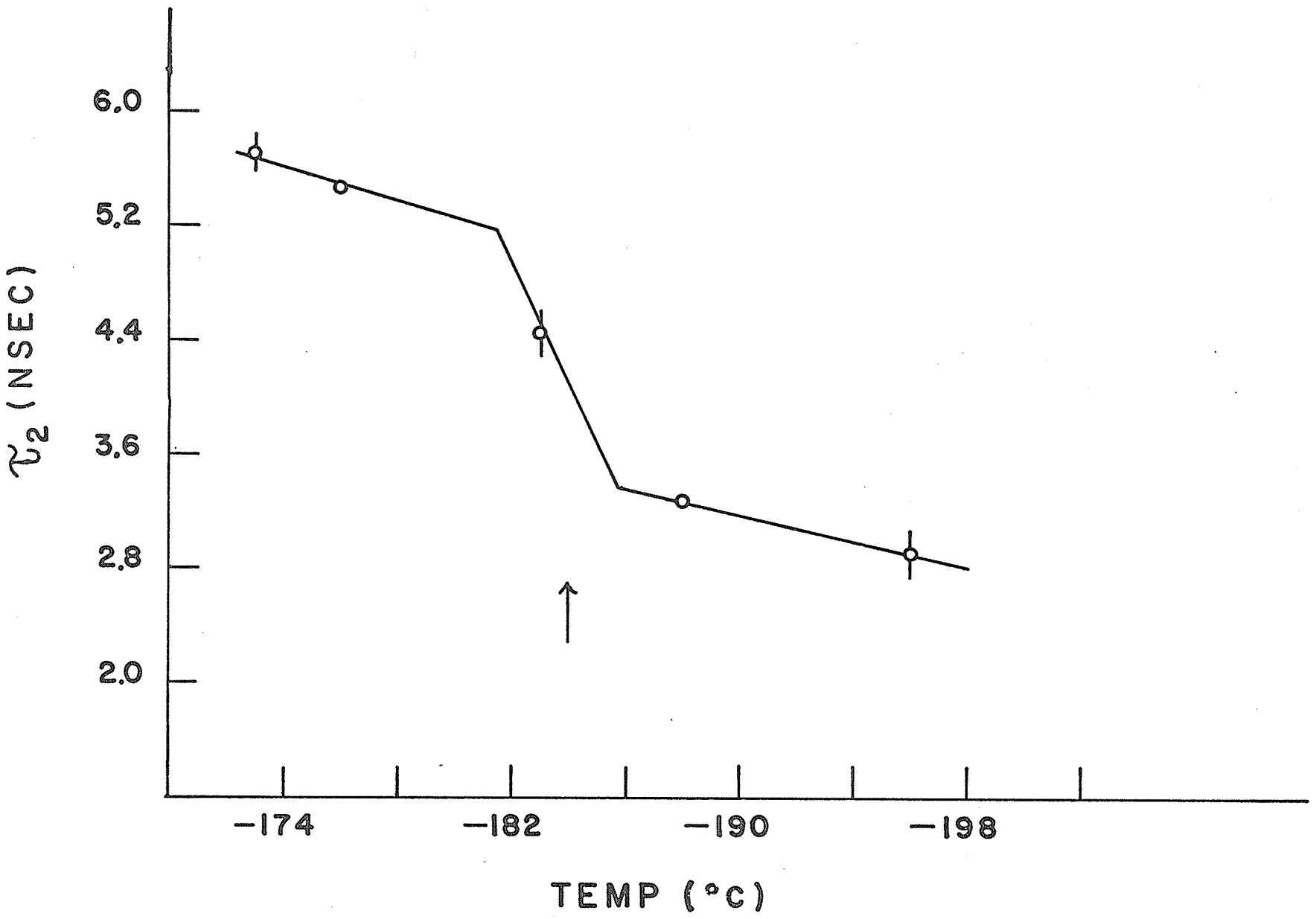
6.0
5.2
4.4
3.6
2.8
2.0
τ_2 (NSEC)
−174
−182
−190
−198
TEMP (°C)

Figure 5-12

Temperature Dependence of τ_1 for Methane

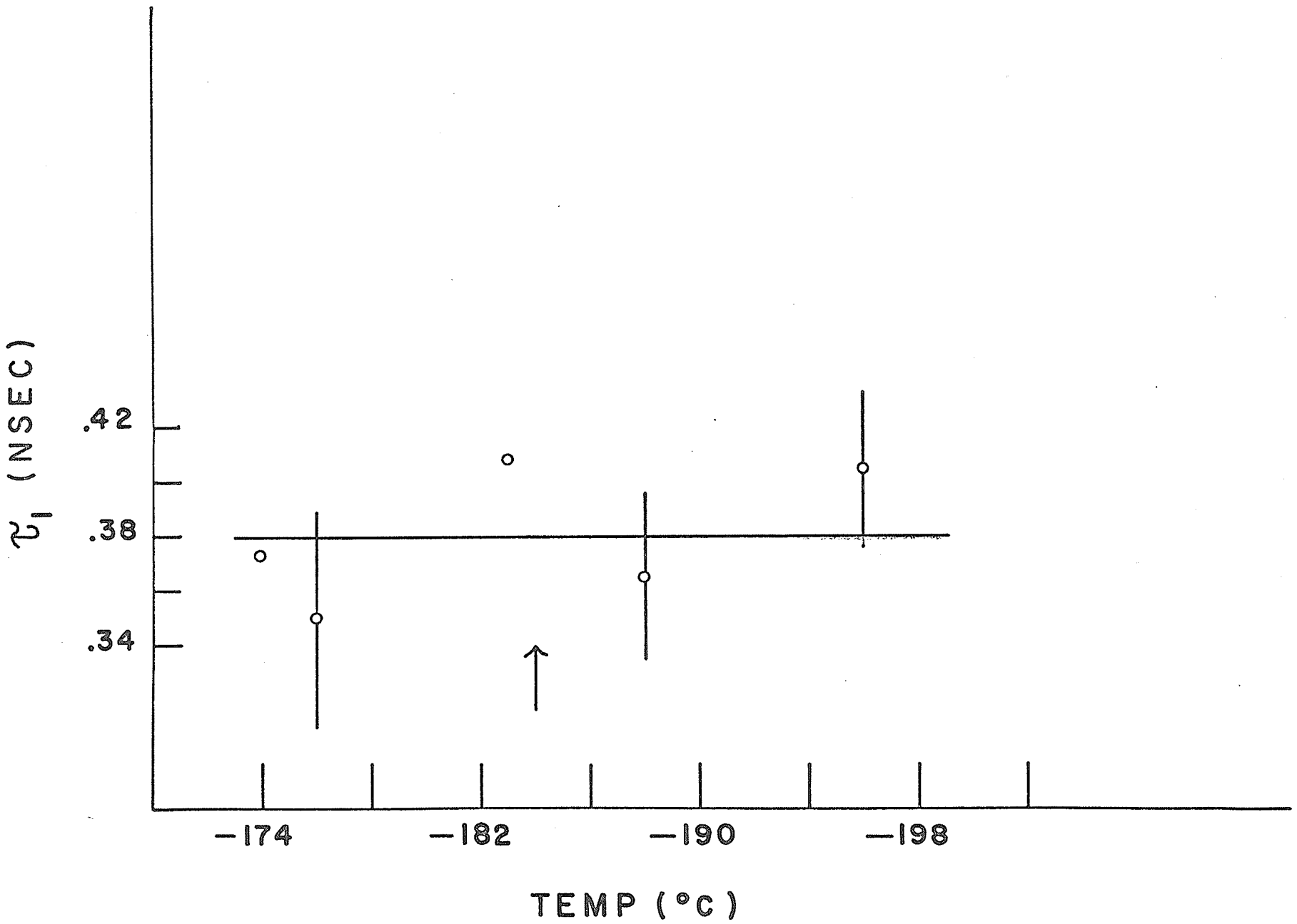
τ_1 (NSEC)
.42
.38
.34
−174
−182
−190
−198
TEMP (°C)

Figure 5-13

Temperature Dependence of I_2 for Methane

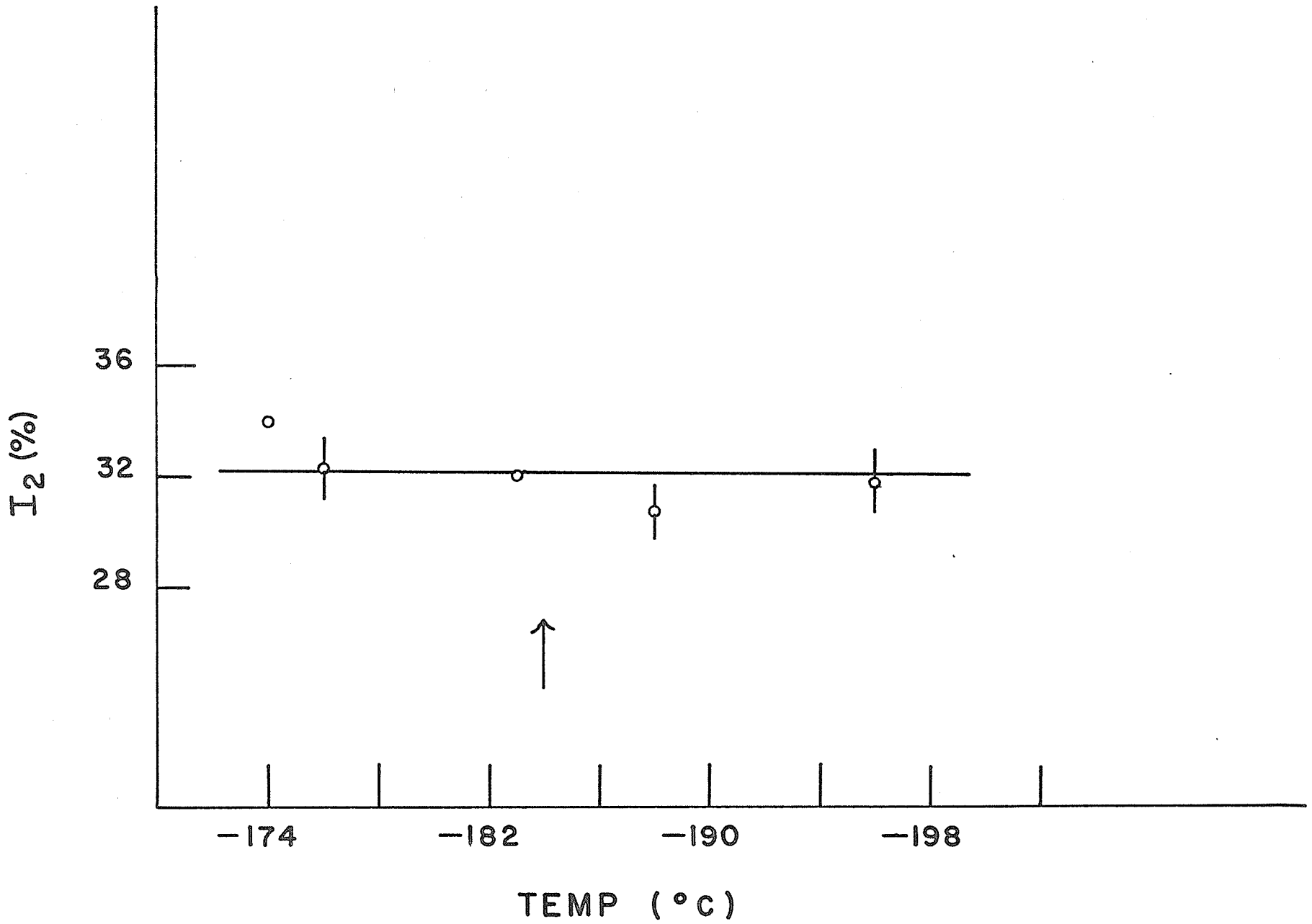
36
32
28
I_2 (%)
−174
−182
−190
−198
TEMP (°C)

Figure 5-14

Temperature Dependence of I_1 for Methane

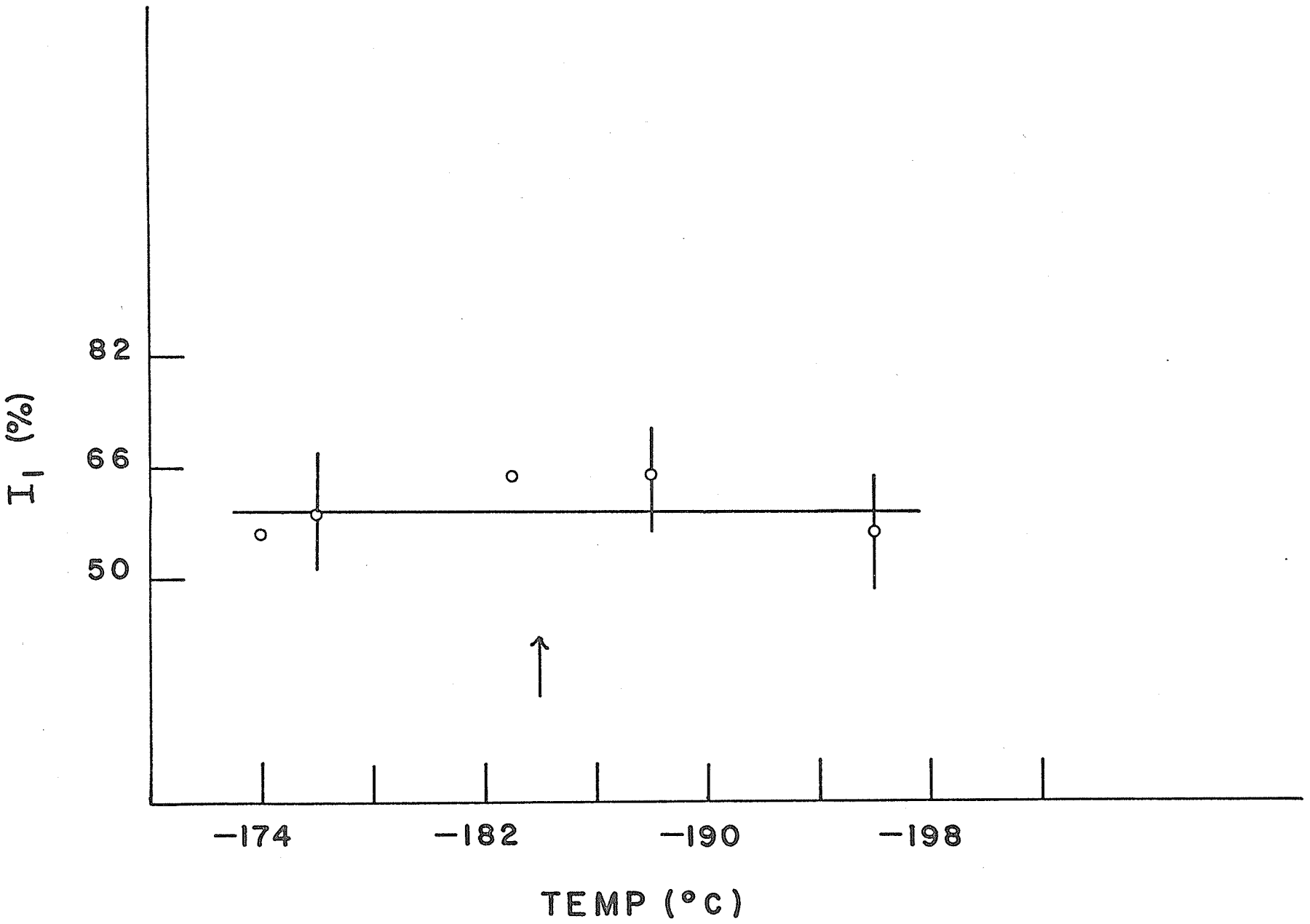
82
66
50
I_1 (%)
−174
−182
−190
−198
TEMP (°C)

TABLE 5-4

Butane

Temp (^{o}C)	τ_2 (nsec)	τ_1 (nsec)	I_2 (%)	I_1 (%)
-196	1.27 ± .03	.34 ± .02	12 ± 1	86 ± 2
-144	1.46 ± .04	.34 ± .02	14 ± 2	84 ± 7
-138	1.48 ± .04	.34 ± .02	17 ± 1	85 ± 8
-137	1.53 ± .05	.34 ± .02	14 ± 2	81 ± 8
-136	1.51 ± .04	.34 ± .02	12 ± 1	80 ± 7
-135	1.45 ± .03	.33 ± .01	12 ± 1	79 ± 5
-130	1.79 ± .03	.36 ± .03	13 ± 1	82 ± 7
-123	2.35 ± .04	.37 ± .02	17 ± 1	79 ± 11
- 88	3.23 ± .03	.43 ± .02	17 ± 1	71 ± 8
- 77	3.02 ± .03	.38 ± .02	17 ± 1	78 ± 7
- 75	3.10 ± .03	.42 ± .03	18 ± 1	74 ± 9

Figure 5-15

Temperature Dependence of τ_2 for Butane

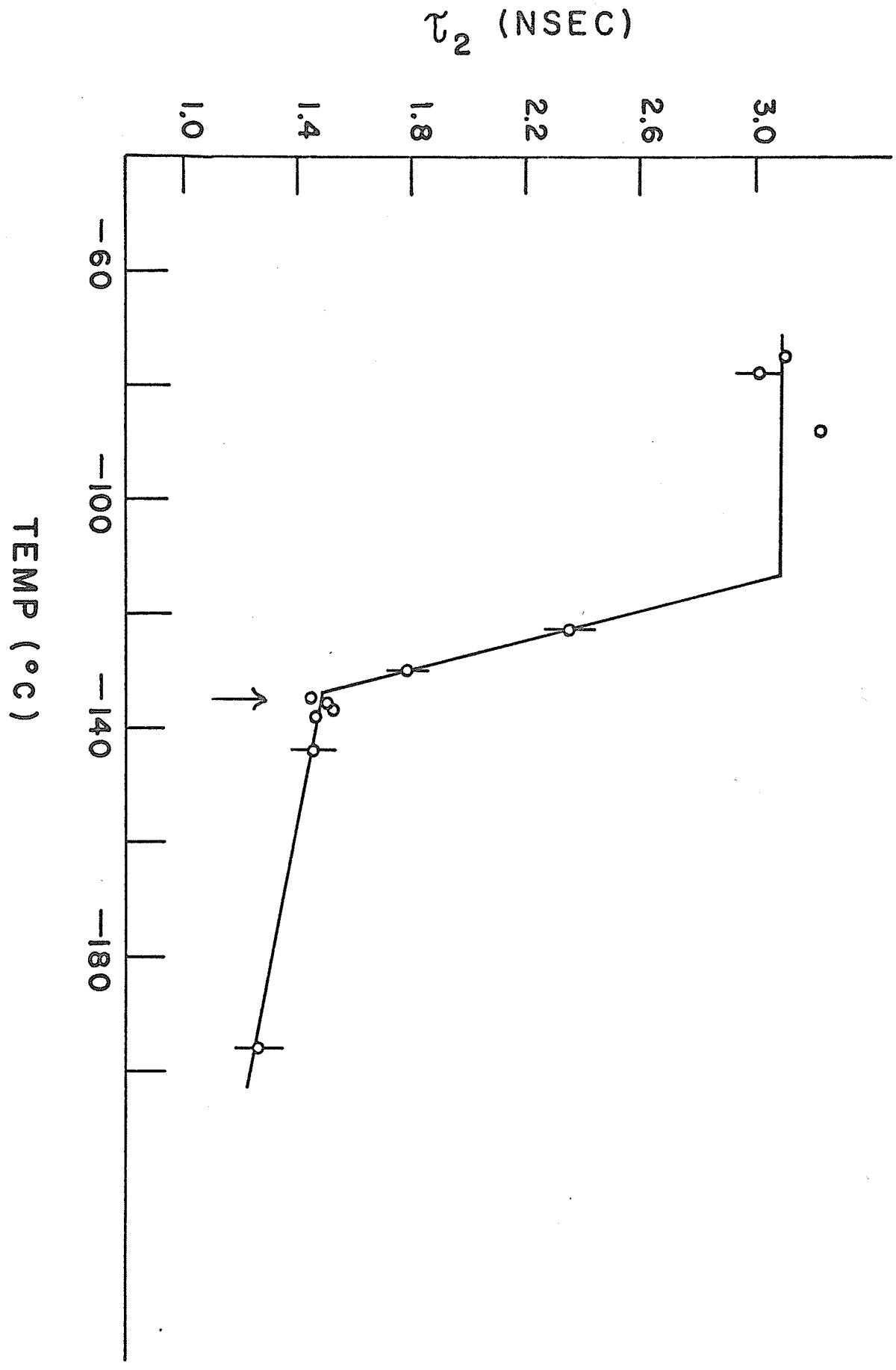
τ_2 (NSEC)
1.0
1.4
1.8
2.2
2.6
3.0
-60
-100
-140
-180
TEMP (°C)

Figure 5-16

Temperature Dependence of τ_1 for Butane

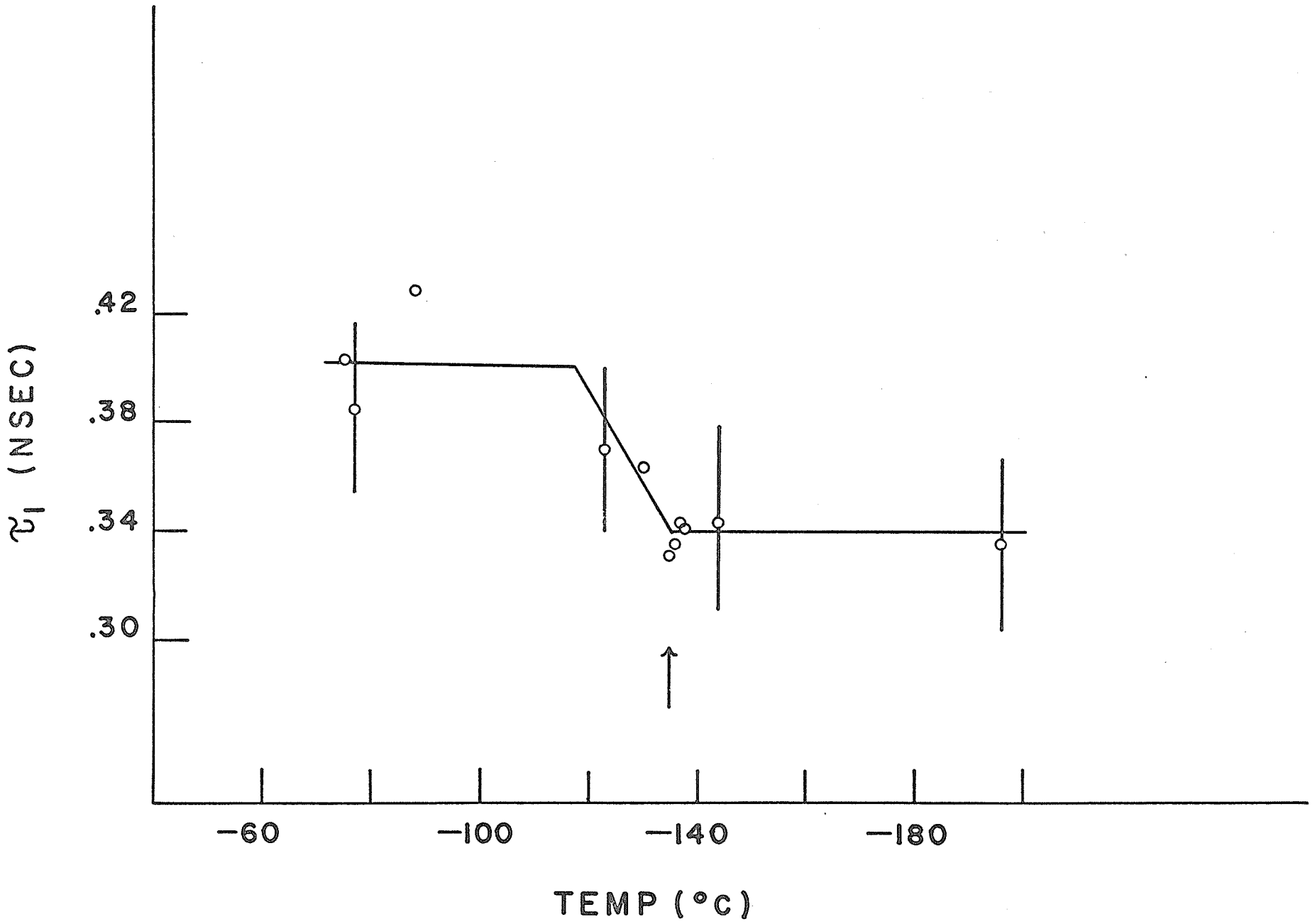
.42
.38
.34
.30
τ_1 (NSEC)
-60
-100
-140
-180
TEMP (°C)

Figure 5-17

Temperature Dependence of I_2 for Butane

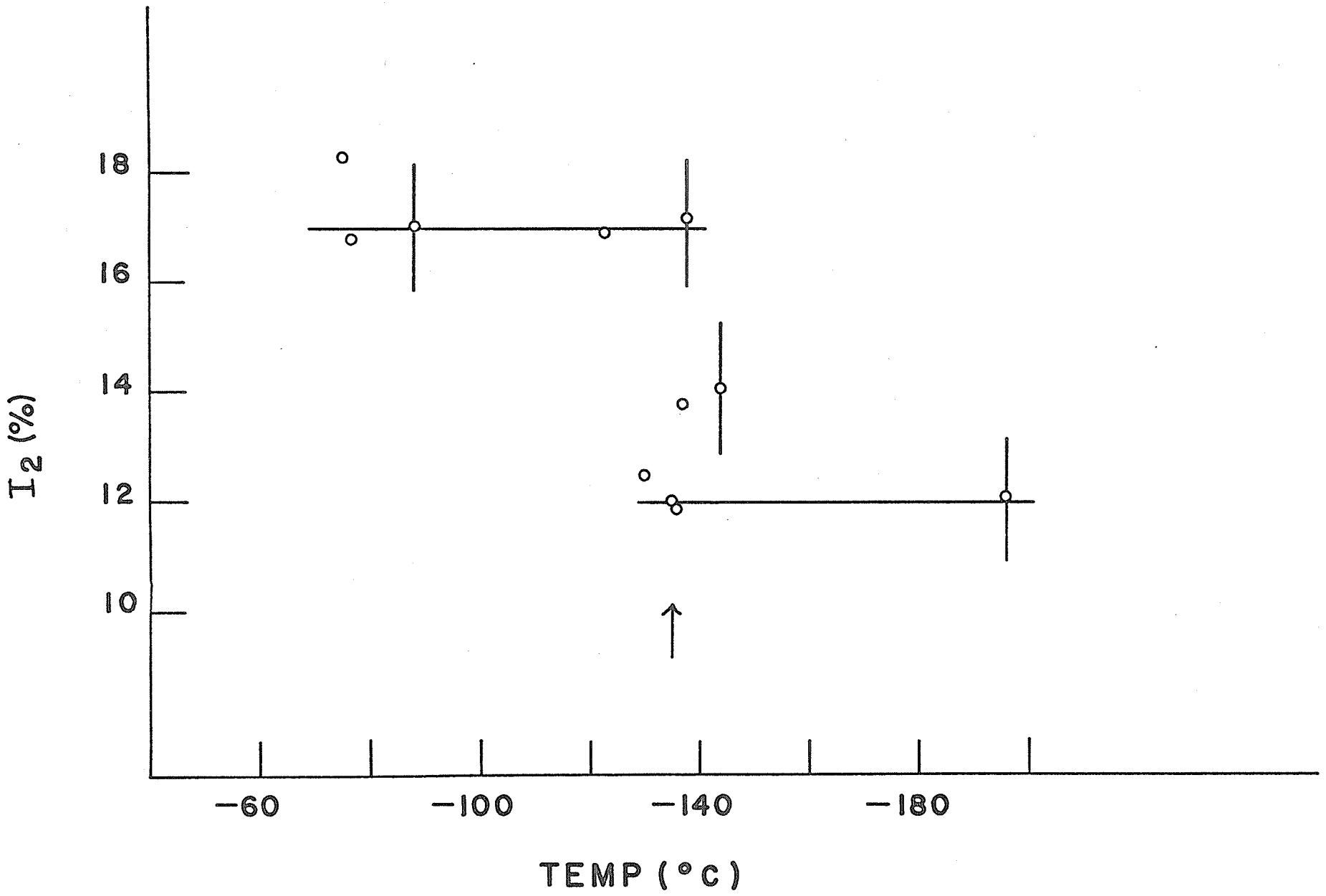
18
16
14
12
10
I_2 (%)
−60
−100
−140
−180
TEMP (°C)

Figure 5-18

Temperature Dependence of I_1 for Butane

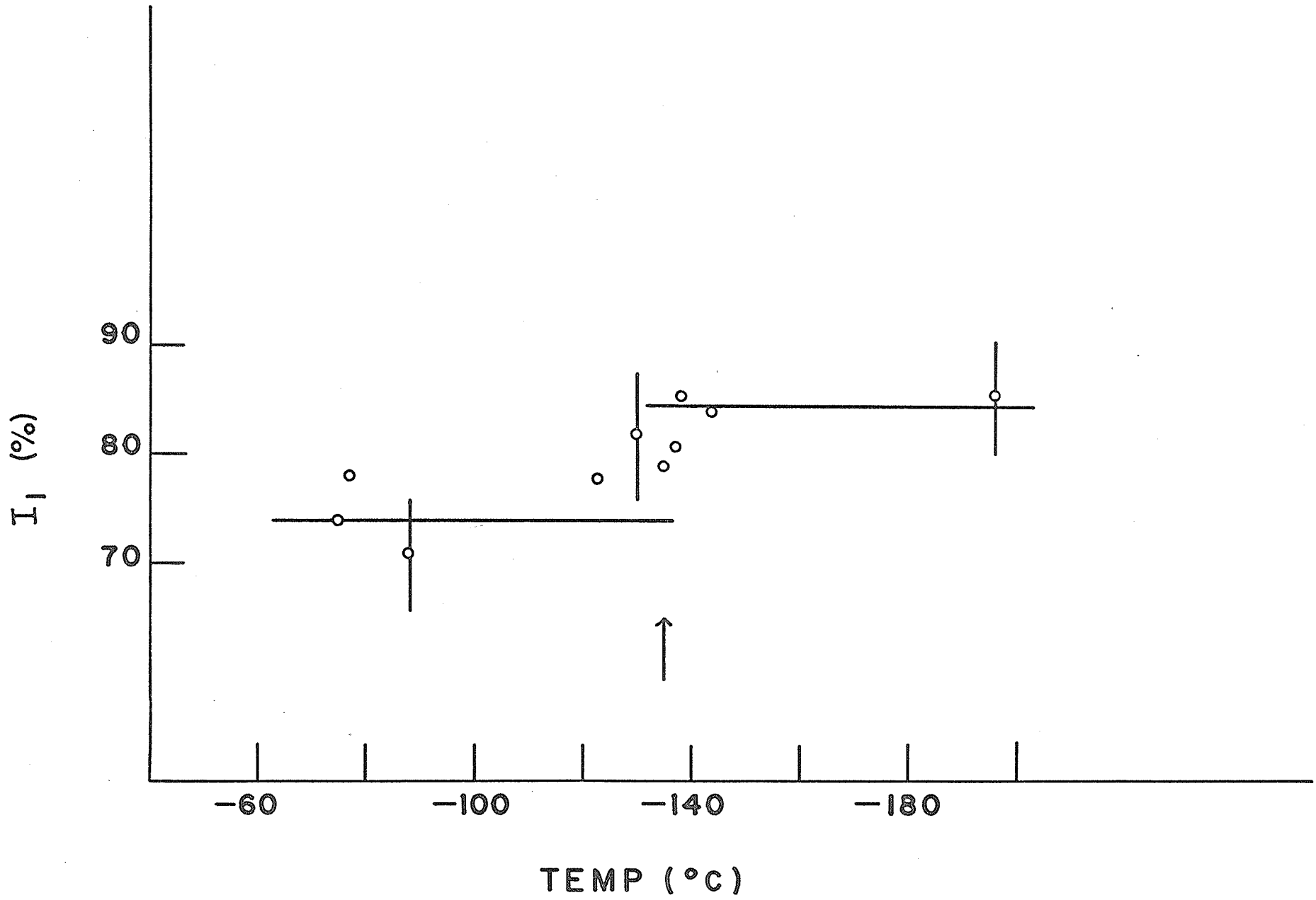
90
80
70
I_1 (%)
−60
−100
−140
−180
TEMP (°C)

TABLE 5-5

Benzene

Temp. (^{o}C)	τ_2 (nsec)	τ_1 (nsec)	I_2 (%)
-100	1.34 ± .10	.40 ± .06	20.4 ± 1
+ 20	2.39 ± .05	.20 ± .06	34.8 ± 1

5.3 Angular Correlation Results - Cyclohexane

The angular correlation work was done using a sample of degassed cyclohexane. In this substance the liquid-solid phase transition occurs at $+6.5^{o}C$, while a solid-solid transition exists at $-87^{o}C$. Angular correlation measurements were made in each of the three phases; the first at $+20^{o}C$, the second at $-70^{o}C$, and the final measurement at $-120^{o}C$.

Figure 5-19 illustrates the angular distribution of the annihilation photons in the three separate phases of cyclohexane. The curves have been normalized to equal areas to illustrate more effectively the feature that the distribution is more peaked in the liquid form.

A computer analysis was carried out to determine the momentum distributions N(p). This form lends itself more easily to interpretation than do the original angular distributions. Figure 5-20 illustrates the N(p) vs p curves for cyclohexane at $+20^{o}C$, $-70^{o}C$, and $-120^{o}C$. Since the constant B in the momentum distribution relation is not known, the term $\frac{dC(\theta)}{d\theta}$ is simply multiplied by a normalizing factor. In these experiments the curves are normalized to a peak of 10 to facilitate comparison.

Figure 5-19

Angular Distributions for Cyclohexane

The solid circles indicate experimental data for liquid cyclohexane (+20°C).

The open circles indicate experimental data for solid cyclohexane (-70°C).

The x's indicate experimental data for solid cyclohexane (-120°C).

The dashed curve indicates the distribution for liquid cyclohexane corrected for finite angular resolution.

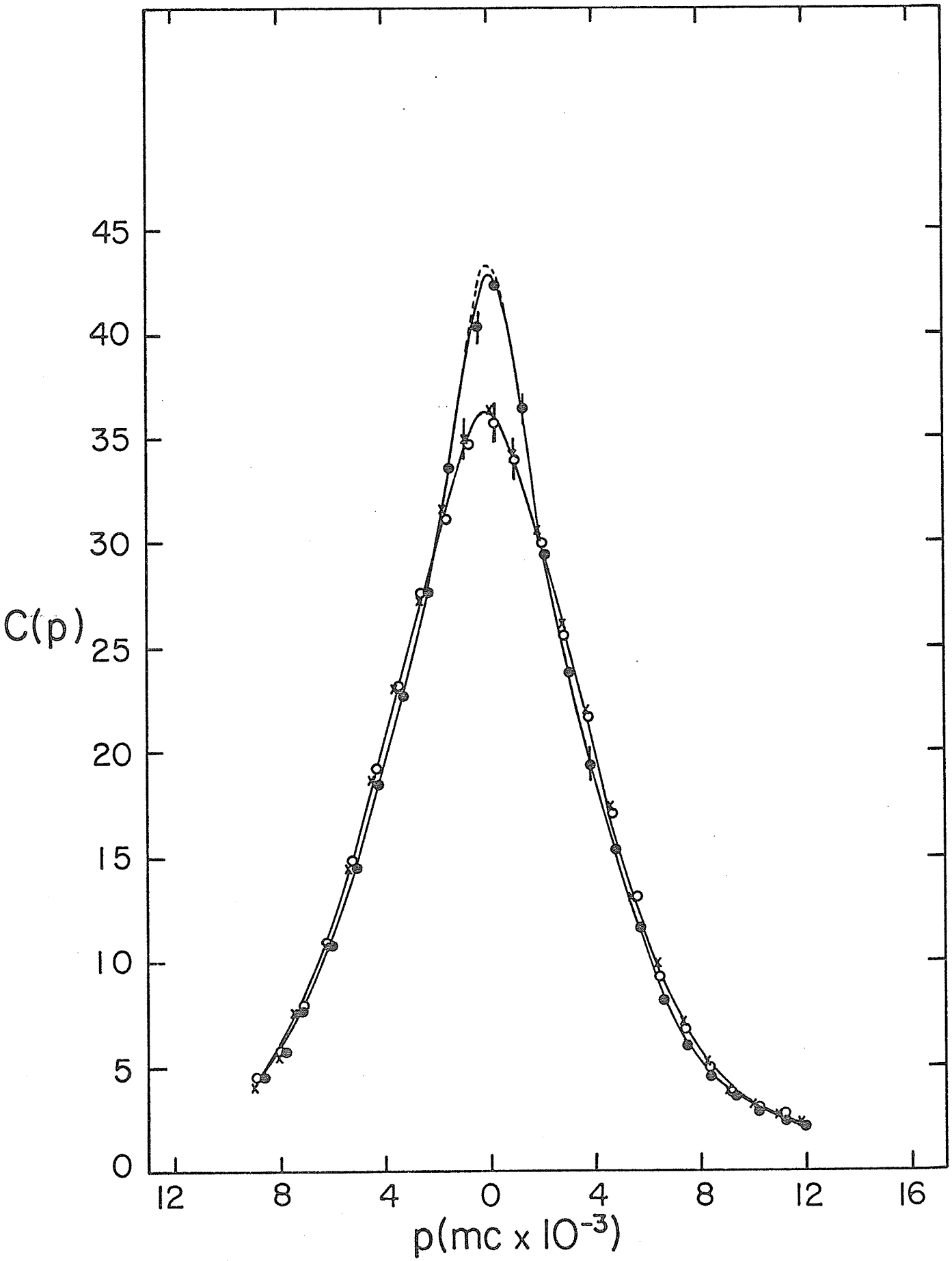
45
40
35
30
C(p)
25
20
15
10
5
0
12
8
4
0
4
8
12
16
p(mc x 10^-3)

Figure 5-20

The Momentum Distributions for Cyclohexane

Closed circles - liquid cyclohexane (+20^{o}C).

Open circles - solid cyclohexane (-70^{o}C).

x's - solid cyclohexane (-120^{o}C).

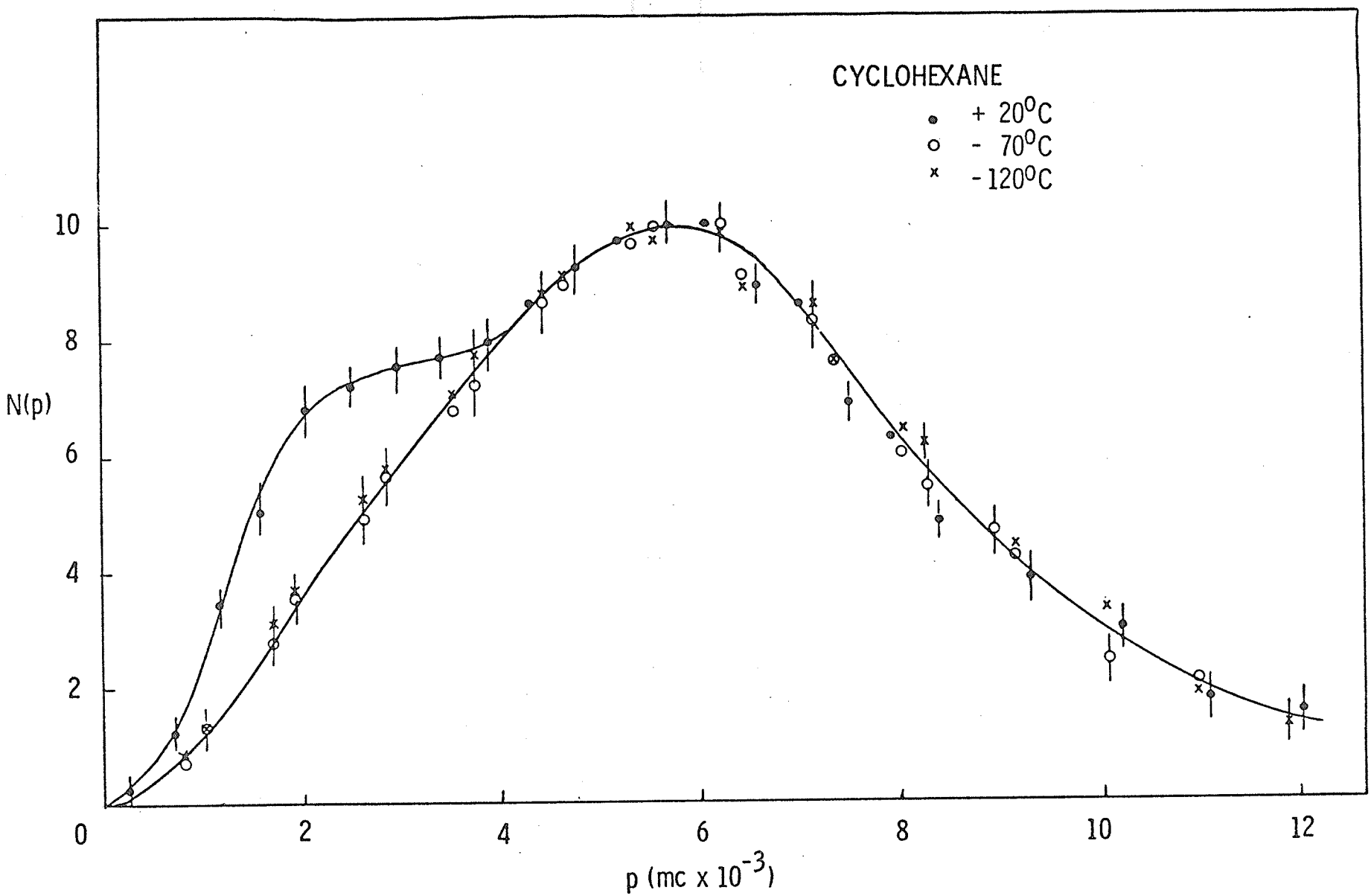
CYCLOHEXANE
+ 20°C
- 70°C
- 120°C
N(p)
0
2
4
6
8
10
12
p (mc x 10^-3)

5.4 Angular Correlation Results - Benzene

Angular correlation results on benzene were obtained using a degassed sample. The melting point of benzene is $+5.5^{o}C$. Measurements were made in both the liquid and solid phases; at $+20^{o}C$ in the liquid and at $-10^{o}C$ in the solid phase.

In Figure 5-21 the angular distributions $C(\theta)$ vs p for liquid and solid benzene are shown. As before the curves have been normalized to equal areas.

Figure 5-22 illustrates the momentum distributions for benzene at $+20^{o}C$ and at $-10^{o}C$. These curves have been normalized to a peak of 10.

Figure 5-21

Angular Distributions for Benzene

The open circles indicate experimental data for liquid benzene ($+20^{o}C$)

The x's indicate experimental data for solid benzene ($-10^{o}C$)

The dashed curve indicates the distribution for liquid benzene corrected for finite angular resolution.

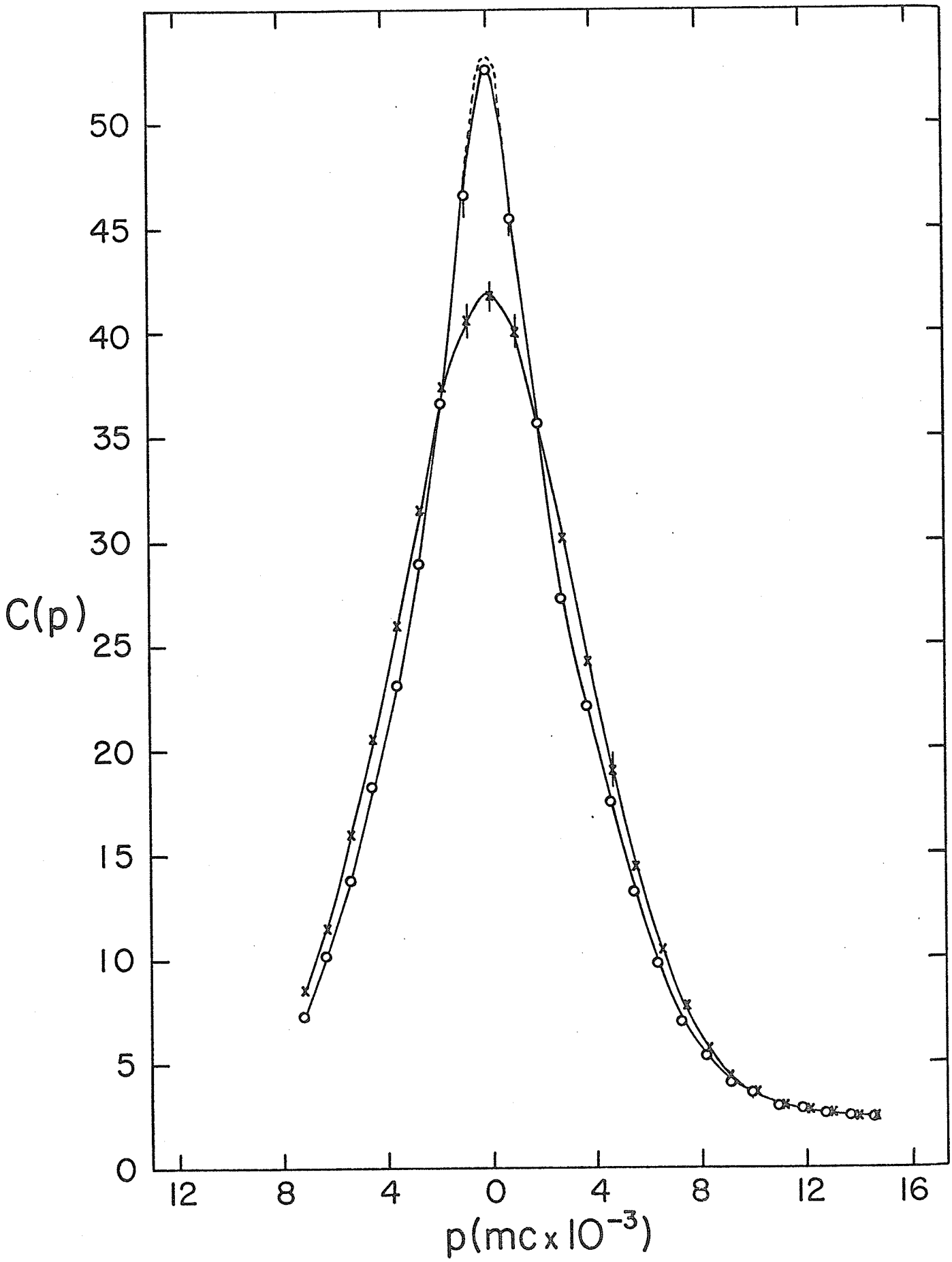
C(p)
50
45
40
35
30
25
20
15
10
5
0
12
8
4
0
4
8
12
16
p(mc x 10^-3)

Figure 5-22

The Momentum Distributions for Benzene

Closed Circles - liquid benzene ($+20^{o}C$)

Open Circles - solid benzene ($-10^{o}C$)

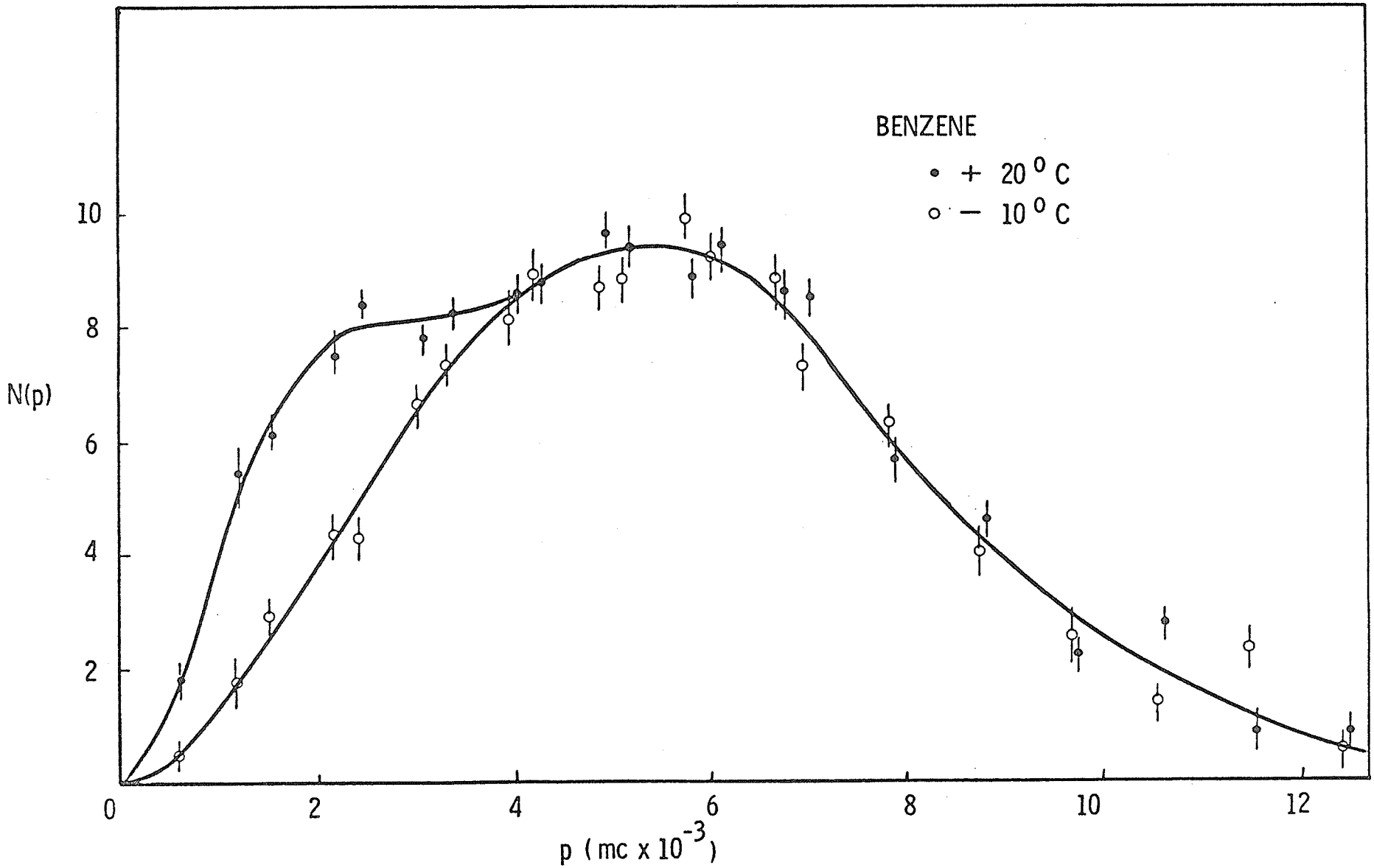
BENZENE
+ 20 °C
— 10 °C
N(p)
10
8
6
4
2
0
2
4
6
8
10
12
p (mc x 10^-3)

5.5 Angular Correlation Results - Methane and Butane

Angular correlation data on methane were obtained by Chuang (1968). During the experiment, the liquid methane sample was maintained at -177°C and the solid sample at -187°C. The temperature deviation was less than 1°C. The momentum distributions that were obtained are shown in Figure 5-23.

The angular correlation experimental work using a butane sample was done by Gould (1969). In Figure 5-24 are illustrated the momentum distributions for both solid and liquid samples.

As before all N(p) curves have been normalized to a peak of 10.

Figure 5-23

The Momentum Distributions for Methane

Closed Circles - liquid methane ($-177^{o}C$)

Open Circles - solid methane ($-187^{o}C$)

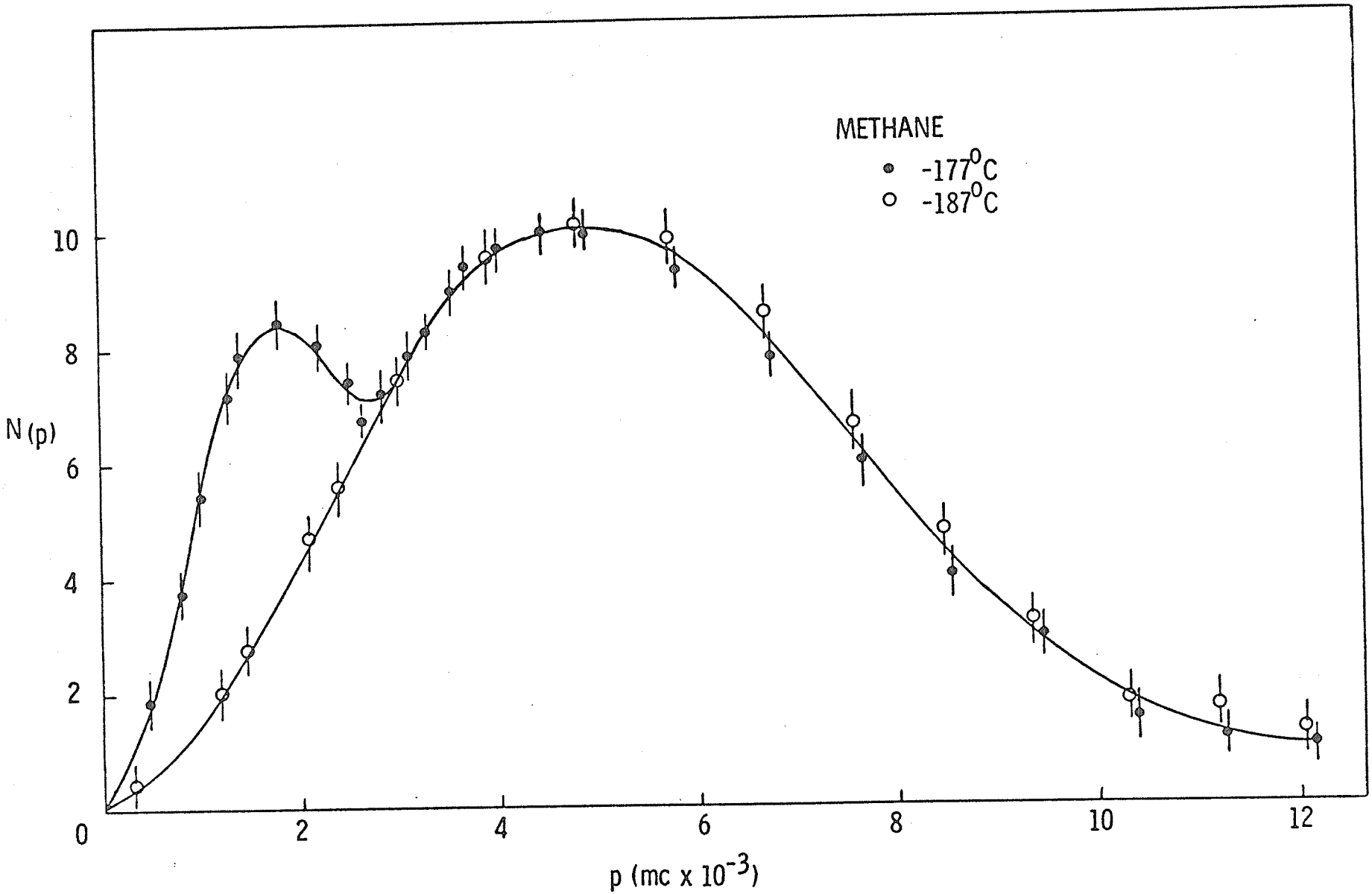
METHANE
-177°C
-187°C
N(p)
0
2
4
6
8
10
12
p (mc x 10^-3)

Figure 5-24

The Momentum Distributions for Butane

Closed Circles - liquid butane

Open Circles - solid butane

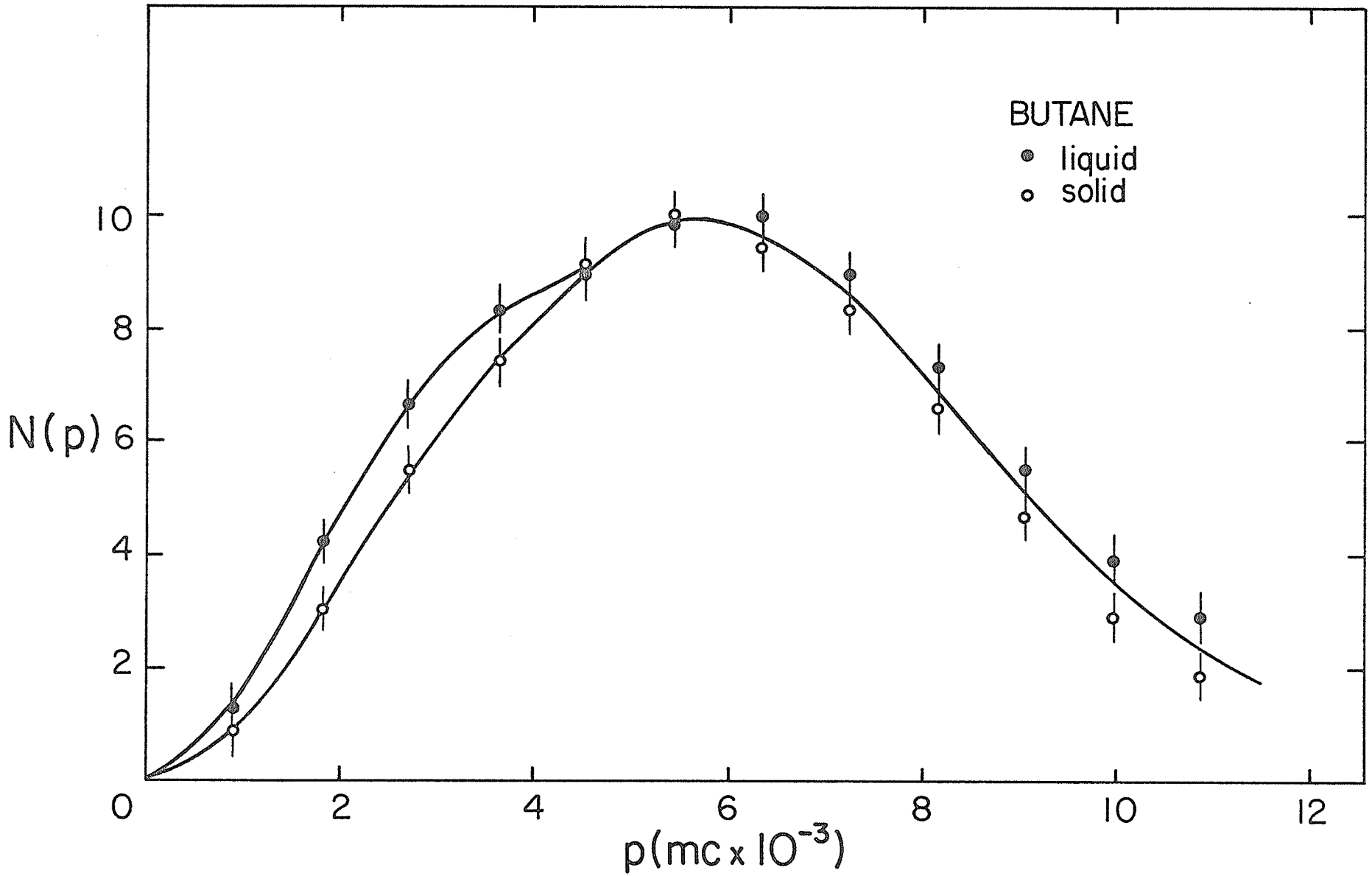
BUTANE
liquid
solid
N(p)
0
2
4
6
8
10
12
p(mc x 10^-3)

5.6 Three-Photon Coincidence Results

Three gamma coincidence results were obtained using liquid and solid samples of methane at temperatures of approximately -175^{o}C and -190^{o}C respectively. Table 5-6 lists the experimental three-photon count rates found for these samples. A lifetime measurement was taken concurrently with each triple coincidence measurement to ensure that the methane was in the correct phase, with the expected value for the long lifetime.

Experimental three gamma data are also tabulated in Table 5-6 for degassed samples of liquid and solid cyclohexane. Measurements in the liquid were conducted at room temperature and in the solid phase at a temperature of -120^{o}C. Two independent trials with slightly varying geometries were carried out to further verify the validity of the experimental results.

TABLE 5-6

Three-Photon Coincidence Rates

Sample	3γ Count Rate counts/200 sec	3γ Background counts/200 sec	True 3γ Events counts/200 sec
Methane Liquid	58.0 ± .6	14.9 ± .1	43.1 ± .6
Methane Solid	31.0 ± .3	19.7 ± .3	11.3 ± .5
Trial I			
Cyclohexane Liquid	17.7 ± .6	7.85 ± .06	9.9 ± .6
Cyclohexane Solid	10.2 ± .2	6.76 ± .15	3.4 ± .25
Trial II			
Cyclohexane Liquid	17.7 ± .3	7.85 ± .06	9.9 ± .3
Cyclohexane Solid	9.8 ± .2	6.74 ± .15	3.1 ± .25

CHAPTER VI

DISCUSSION OF RESULTS

6.1 Introduction

The work presented in this thesis was carried out in order to test current models of positron annihilation in organic liquids and solids. Of special interest is the effect of phase transitions in these materials. For this reason cyclohexane was chosen since a solid-liquid change occurs at easily accessible temperatures as well as a solid-solid phase change. To gain further insight into the annihilation processes in cyclohexane, angular correlation data were obtained for this material in each of its three distinct phases. This technique was also applied to liquid and solid benzene and the results combined with already existing lifetime information obtained by other researchers. Finally, since these two research methods showed somewhat conflicting results, triple γ-coincidence experiments were performed in an attempt to gain sufficient information to satisfactorily explain all experimental data.

6.2 Lifetime Studies

After a positron enters a condensed medium it can essentially annihilate with an electron from the medium to form gamma rays in two distinct modes. The first is to annihilate directly with an electron from the medium while the second way consists of the formation of a bound positronium atom before annihilation. The factors which effect the formation of positronium in a given substance have been studied by a number of workers (A. T. Stewart 1955, H. S. Landes, S. Berko, and A. J. Zuchelli 1956, C. R. Hatcher, W. E. Millet and L. Brown 1958, R. L. deZafra and W. T. Joyner 1958, C. R. Hatcher 1961, D. P. Kerr

and B. G. Hogg 1962, W. A. Falk and G. Jones 1964, R. K. Wilson, P. O. Johnson and R. Stump 1963, C. Y. Leung and D. A. L. Paul 1967) and from these and other investigations various models concerning the probability of positronium formation have been advanced.

Any detailed computation of the probability of positronium formation during the slowing down of positrons in a molecular medium, M, necessarily involves the cross-sections of many elementary processes and a knowledge of their energy dependence. These processes include ionization and excitation of M due to positrons, elastic e^+M scattering, electron capture by the positron, elastic and inelastic Ps-M scattering, and dissociation of Ps in collisions with M. In these respects appropriate data for the condensed phase are almost entirely lacking. However, in spite of these limitations, an experimental determination of the fraction of positrons which form positronium, and a comparison of this fraction with the predictions of theory, is bound to be of value. A scheme of representation based on the concept of the "Ore Gap", first postulated by A. Ore (1949), has proved to be the most useful as an approximate theoretical model.

In the Ore model the high energy positrons which enter a medium are rapidly slowed to energies approximating the first ionization potential, V_i, of the medium by non-elastic ionizing collisions. During this time the annihilation probability will be less than a few percent (J. Green and J. Lee 1964). Since the binding energy of a positronium atom is 6.8 eV and since V_i is generally greater than 6.8 eV only positrons with a kinetic energy greater than $(V_i - 6.8)$ eV will be capable of forming positronium. On the other hand, if positron energies are greater than V_i positronium formation will be negligible compared

with ionization; electron removal to the continuous spectrum region is naturally much more probable than the formation of a discrete bound state such as the positron-electron system. Moreover, as long as the kinetic energy of the positronium atoms formed exceeds their binding energy, these atoms are most likely to disintegrate in subsequent collisions. Therefore, when the energy of the positrons rises above the ionization potential V_i, the probability of positronium formation decreases rapidly. Along with ionization, excitation of the electron levels of the molecules of the medium can be one of the main competitors of positronium formation, and in this case the decrease in the probability of positronium formation manifests itself earlier - when the energy of the positrons begins to exceed the excitation energy of the first electron level E_1 (as a rule $E_1 < V_i$). After the positron's energy drops below E_1 positronium formation is considered to be the dominant process until such time that the positron loses sufficient energy such that positronium formation is no longer energetically possible. Below this point positrons will lose energy by elastic collisions until they annihilate freely with the electrons of the medium.

Using this model predictions can be made concerning the probability of positronium formation. Only positrons having an energy within the bounds of the "Ore gap" are capable of forming positronium. The upper limit of this gap has been designated as E_1 and the lower bound as V_i - 6.8 eV. If one now makes the assumptions that all positron energies from zero to V_i are equally probable, that all excitation collisions between E_1 and V_i degrade the positron's energy below the Ore gap, and that all positrons within the Ore gap form positronium, then the probability of the formation of a positronium atom will be given by

$$P = \frac{E_1 - (V_i - 6.8)}{V_i}$$

Since statistically three-quarters of the positronium atoms formed exist in the triplet state the intensity of the long lived component will be given by

$$I_2 = \frac{3}{4}\left[\frac{E_1 - (V_i - 6.8)}{V_i}\right]$$

This simple theory gave reasonable agreement in the case of a number of gases (M. Deutsch 1953, T. A. Pond 1952, B. Gittelman and M. Deutsch 1956). Also in 1961 Hatcher showed that the intensity of the long lived component in Halogen derivatives could be explained on the basis of the Ore model by assuming the upper bound of the Ore gap to be equal to the dissociation potential of the Carbon - Halogen bond.

Table 6-1 shows intensities as calculated by the Ore theory compared to our experimental results. The upper bound of the Ore gap has been taken to be the dissociation potential of the carbon - hydrogen bond and in the case of ammonia the nitrogen - hydrogen bond. It can be seen that there are large discrepancies between experimental data and the theoretical values. One of the most serious difficulties is that the Ore theory does not differentiate among the various physical states of a given system while experimentally large changes may be found in going from one state to another. Various modifications to the Ore model have been attempted and we are interested in those which attempt to explain the formation probability as affected by physical changes to the system.

As has been mentioned previously it is not only the basic parameters of the Ore gap which influence positronium formation.

TABLE 6-1

Substance	V_i* (eV)	E_1* (eV)	Calculated I_2 (%)	Experimental I_2 (%) Liquid	Solid
Cyclohexane	10.0	4.1	7	31±2	21±2, 18±2
Benzene	9.2	4.4	16	35±2	20±2
Methane	13.0	4.4	0	32±2	32±2
Butane	10.8	4.1	.7	17±2	11±2
Ammonia	10.3	4.5	7	25±2	25±2

Many processes are present which lower the upper boundary of the Ore gap or bring positrons rapidly beneath the gap and these depend not only on the chemical composition of the material but also on intermolecular interactions. These interactions could have a marked effect on positronium formation especially when related to phase transitions. A further influence which can affect formation probabilities, again especially at phase transitions, is related to the position of the lower boundary of the Ore gap. It is associated therefore with positronium affinity or, to put it another way, with the presence of a free volume which the positronium atom can occupy. In an attempt to explain the varying lifetimes and intensities in substances due to the changing of such parameters as pressure, temperature, and phases, various modifications of what has come to be known as "The Free Volume Model" have been proposed.

In its simplest form the free volume model attributes any change in lifetime due to pressure and temperature as being due to a change in density. As the density of a substance increases the free volume decreases resulting in a reduction in the space available for positronium and hence a corresponding reduction in τ_2. Wallace (1955) proposed a simple model in which positronium atoms resided in rectangular wells formed by repulsions from the surrounding atoms. If the radius of the well (i.e. the free volume) is reduced, the overlap of the positronium wave function with the electron clouds of the surrounding molecules increases resulting in an increase in the rate of pick-off annihilation.

Brandt, Berko and Walker (1960) developed a more detailed treatment of positronium decay in molecular materials on the basis of the free volume model. They obtained a solution of the equation characterizing

the rate constant for pick-off annihilation (λ_p),

$$\lambda_p = \pi r_o^2 C \rho_o \int_{v_o} \psi_{ps} \psi_{ps}^* dv$$

by calculating positronium wave functions for various lattice configurations. Here r_o represents the radius of square lattice potentials, ρ_o the electron density and v_o the excluded volume. Solving this relationship requires a knowledge of the lattice geometry as well as density data across the temperature range studied. Cooper (1969) tested this model and obtained reasonable agreement using experimental values of τ_2 in the liquid and solid phases for ammonia and methane. Sharp changes in lifetimes at solid-liquid transitions were largely accounted for but actual lifetimes in the solid phases were not correct. Unfortunately density data are not available for cyclohexane in the solid state so these calculations could not be carried out for this substance.

Brandt and Spirn (1966) modified the free volume model to take into account thermal effects. Thermal fluctuations cause a smearing of the electron density distribution through the lattice, thereby increasing the electron density in regions of free volume and hence shortening the long lifetime. This is the opposite of the effect which occurs when the average density is reduced by heating. Brandt and Spirn found that with their modifications maxima were found to occur in the τ_2 versus temperature curve just before melting, for substances with high melting points. In the present work the τ_2 curves for cyclohexane show no evidence of this and we can conclude that the thermal motion effects are small and masked by free volume changes occuring with temperature variation.

Lagu et al(1969) proposed an empirical model in terms of free volume to explain the formation and decay of the long component in molecular materials. Free volume in the medium is considered as divided into a number of cavities, void-cells or sites where positronium atoms lodge themselves after thermalization and annihilate by pick-off with surrounding electrons. If the average volume of the site decreases the electron density leaking into the site will increase as will the overlap of the wave functions of the positron and the electrons, resulting in a decrease in τ_2. In the limiting situation when the volume of the site is approximately one angstrom, the positronium atom will begin to lose its identity due to the crowding in of the surrounding medium, and the limiting value of τ_2 will approach that observed for the decay of positronium molecular complexes (approximately 1 nsec.). On the other hand if the volume of the sites reaches values such that the interaction of the trapped positronium atoms with the surrounding electrons is negligibly small, the $\tau 2$ intensity will be vanishingly small, the triplet positronium decaying into three photons.

In this model certain assumptions are made concerning the formation of the long lived bound states in solids and liquids. These assumptions are that in the substance the bound state can only form in vacancies which are larger than the classical diameter of a positronium atom (1.06 angstroms) and that the fraction of positrons forming this state in a substance is controlled by the number of vacancies with diameters above this critical size. It is further assumed that in a solid the number of vacancies will remain reasonably constant, with a decrease in density of the material simply enlarging the existing vacancies without creating many new ones, while on passing through the liquid-solid phase transition more vacancies will be created as well as enlargement

of existing vacancies. Thus if we apply this model to our results for cyclohexane we see that on passing through the solid-solid phase transition very little change in intensity takes place, while on passing through the solid-liquid transition a large increase in the long lived component is found. The constant values of I_2 in the liquid or in either of the solid states indicates that while the material is in a particular phase the number of vacancies remains essentially unchanged. The gradual increase in τ_2 with temperature in each phase indicates an increase in the size of the vacancies. The abrupt variation in the lifetime values at the phase transitions is due chiefly to density properties of cyclohexane at these temperatures (Cooper 1969). However it is expected that a change in molecular interactions across the transitions and the change in crystal structure associated with the solid-solid transition would also influence the values of these life-times.

Experimental data presented for benzene and butane are also consistent with this model. Again there is the expected increase in intensity in passing from the solid to the liquid and also the gradual decrease in values of τ_2 with decreasing temperature. Thus in all these cases the model presented by Lagu et al (1969) empirically explains the results.

A final point to be considered is the effect of the dissolved oxygen on formation probabilities and lifetimes for the cyclohexane samples. As can be seen in Fig. 5-9 the intensity of the long component was not affected which is in agreement with earlier work (D.P. Kerr et al. 1965)[1]. Concerning lifetimes, previous work (J. Lee and G.J. Celitans 1965, A.M. Cooper, G. Laidlaw and B.G. Hogg 1967) has shown

that dissolved oxygen has a large quenching effect on the long lifetime τ_2. This effect is noted for cyclohexane in Figure 5-7. An observation of interest is that the quenching effect of the dissolved oxygen carries on into the solid phase of the material but disappears after the solid-solid phase transition. A possible explanation for this would be that in the high temperature solid phase the dissolved oxygen retained some mobility through the lattice and thus was able to quench the long lifetime component while in the low temperature solid phase the oxygen was trapped in the lattice and therefore was not able to have any quenching effect on the long lifetime.

6.3 Angular Correlation Studies

When a positron enters a condensed hydrocarbon compound it may annihilate with an electron in the C-H bond or in the C-C bond. From the measurement of the angular correlations of the annihilating photons, one is able to obtain information concerning the momentum distribution of electrons annihilating with positrons. Most of our knowledge of momentum distributions for molecular systems comes from a series of papers given by Coulson and Duncanson (1941-1943). The general method used to obtain the momentum wave function consists of transforming the space wave function to momentum coordinates according to the Dirac transformation theory. Chuang (1968) extended these theoretical calculations and obtained good agreement with experimental data gathered using organic liquids. Since then Gould (1969) applied this theory to solid as well as liquid organic materials.

The method used by Chuang (1967, 1968[1]) involves the calculation of positron wave functions followed by determinations of the momentum distributions of annihilating positron-electron pairs in the

C-H and C-C bonds. Modifications to Chuang's treatment were made only in the calculation of the positron wave function $\psi_+(r)$.

To determine the numerical values for the positron wave function we first consider the interaction between a positron and a carbon atom. $\psi_+(r)$ is the ground state solution of the Schrödinger equation, i.e.,

$$-\frac{1}{2}\nabla^2\psi_+(r) + V_c(r)\psi_+(r) = E\psi_+(r)$$

where the potential $V_c(r)$ is taken to be that of a neutral carbon atom calculated by Herman and Skillman (1963). $V_c(r)$ is shown in Figure 6-1. The eigenvalue E is chosen to satisfy the boundary condition that the slope of the wave function vanish on the boundary surface of the atom, i.e.,

$$\psi_+(r)' = 0 \text{ at } r = r_c,$$

in which r_c is taken to be the average radius of the carbon atom, i.e., $r_c = 1.54$ a.u. For all values of r greater than r_c, $\psi_+(r) = 1$ which constitutes a second boundary condition. The Schrödinger equation was solved by a familiar method (D. R. Hartree, 1958), and the resulting positron wave function is shown in Figure 6-1.

To determine the value of $\psi_+(r)$ near a hydrogen atom we must consider the potential of such an atom as seen by the positron. This potential has the form

$$V_h(r) = \frac{1}{r} - \frac{1}{r}\int_0^r |\psi(H)|^2\, 4\pi r^2\, dr - \int_r^\infty |\psi(H)|^2\, 4\pi r\, dr$$

where the first term is the Coulomb repulsion of the nucleus, and the second and third terms are due to the charge distribution of the 1s electron. Since $\psi_{1s}(H) = \pi^{-1/2}\exp(-r)$, the expression for $V_h(r)$ becomes

Figure 6-1

The Potential of the Carbon Atom and the Corresponding Positron Wave Function

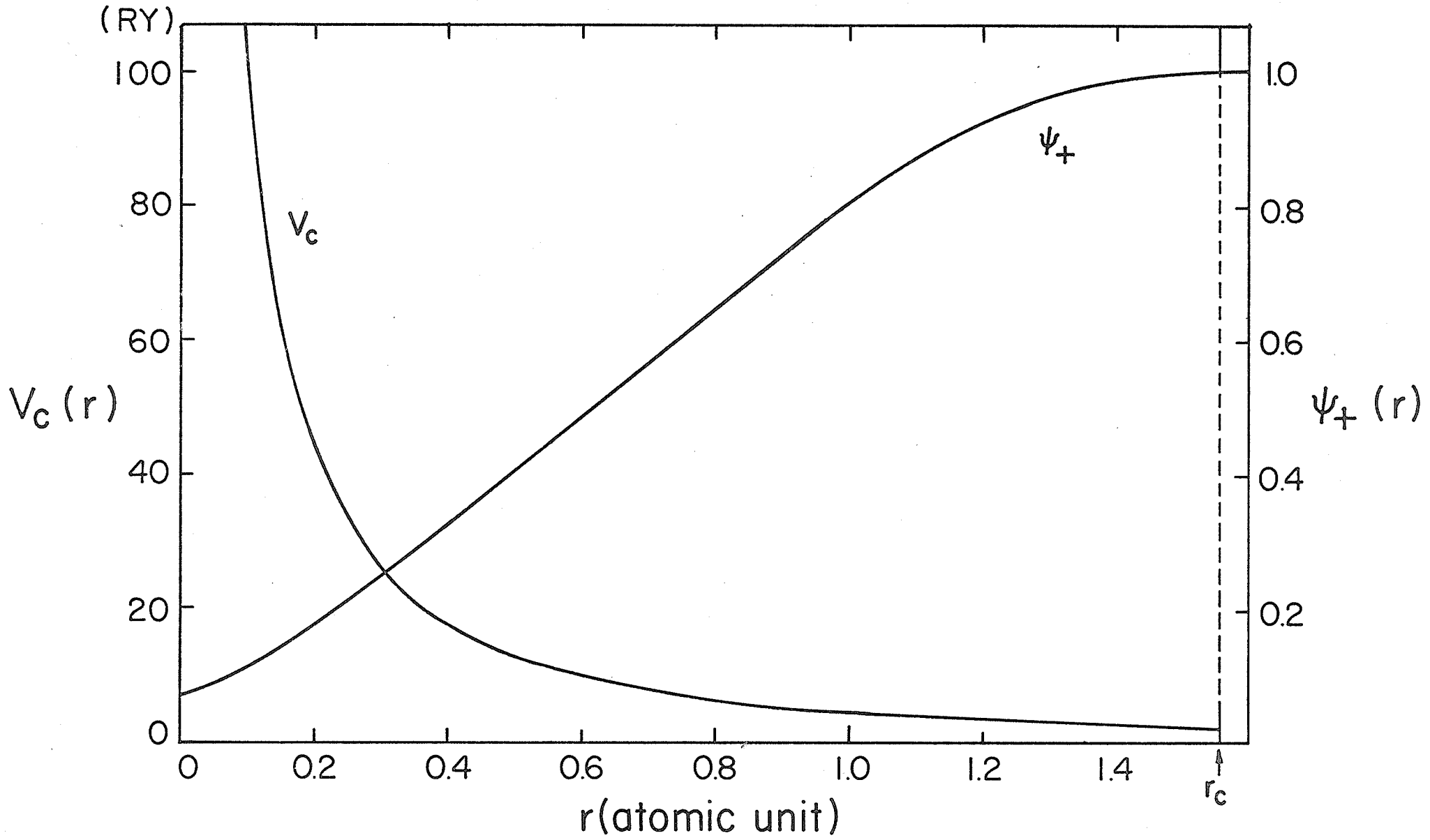
(RY)
100
80
60
40
20
0
V_c
$V_c(r)$
ψ_+
1.0
0.8
0.6
0.4
0.2
$\psi_+(r)$
0
0.2
0.4
0.6
0.8
1.0
1.2
1.4
r_c
r(atomic unit)

$$V_h(r) = \frac{1}{r} - \frac{4}{r}\int_0^r r^2 \exp(-2r)dr - 4\int_r^\infty r \exp(-2r)dr$$

$$= (1 + \frac{1}{r}) \exp(-2r)$$

which is as shown in Figure 6-2.

Using this value for the potential, the numerical values of the positron wave function are determined from a solution of the Schrödinger equation. Again the eigenvalue E is chosen to fit the boundary conditions $\psi_+(r)' = 0$ at $r = r_h$ and $\psi_+(r) = 1$ at $r > r_h$, where r_h is the average radius of hydrogen and has the value 1.50 a.u. In Figure 6-2 are shown the results of this calculation.

To calculate momentum distributions of annihilating positron-electron pairs a knowledge of the electronic wave functions in the carbon and hydrogen atoms as well as those in the C-H and C-C bonds is necessary. The hybrid orbitals of the carbon atom are described by the wave function

$$\psi(C) = \frac{\psi_{2s}(C) + \sigma\psi_{2p}(C)}{\sqrt{1 + \sigma^2}}$$

where $\psi_{2s}(C)$ and $\psi_{2p}(C)$ are the analytic SCF functions of 2s and 2p atomic carbon orbitals (Lowdin 1953) and σ is the coefficient of mixing. The momentum wave function for an annihilating pair is then

$$\chi_C(\underline{p}) = (2\pi)^{-3/2} \int \exp(-i\underline{p}\cdot\underline{r})\psi(C)\psi_+(r)d\underline{r}.$$

Using this the momentum distribution function $N_C(p)$ is found to be

$$N_C(p) = \frac{2p^2}{\pi(1+\sigma^2)} \{X_1(p)^2 + \sigma^2 X_2(p)^2\}$$

where $$X_1(p) = \int_0^\infty j_0(pr) R_{2s}(C)\psi_+(r)r^2 dr$$

$$X_2(p) = \int_0^\infty j_1(pr) R_{2p}(C)\psi_+(r)r^2 dr$$

Figure 6-2

The Potential of the Hydrogen Atom and the Corresponding Positron Wave Function

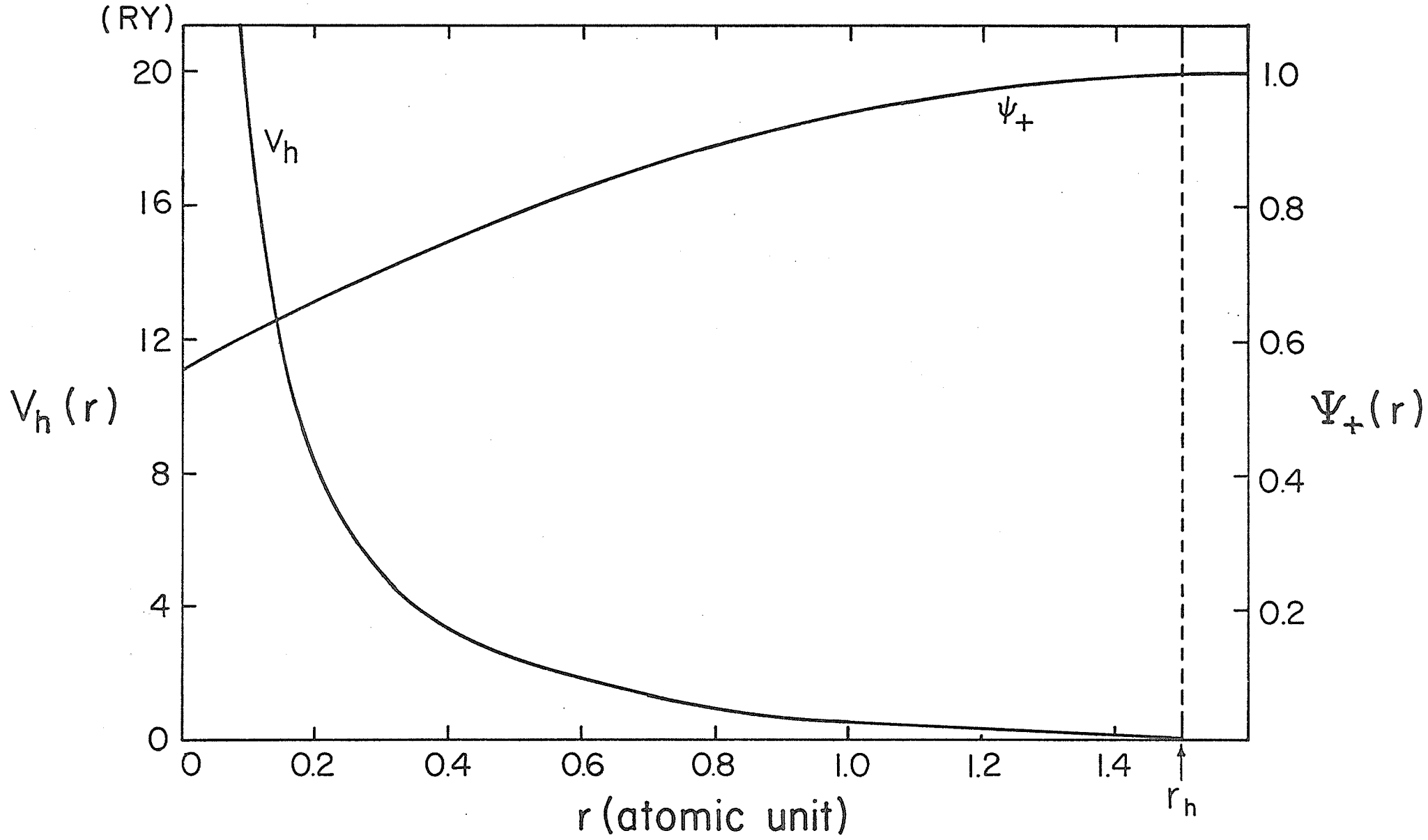
(RY)
20
16
12
8
4
0
V_h
ψ_+
1.0
0.8
0.6
0.4
0.2
$V_h(r)$
$\Psi_+(r)$
0
0.2
0.4
0.6
0.8
1.0
1.2
1.4
r_h
r (atomic unit)

In these equations $R_{2s}(C)$ and $R_{2p}(C)$ are 2s and 2p radial wave functions of carbon and $j_0(pr)$ and $j_1(pr)$ are spherical Bessel functions.

Similarly, the momentum distribution in the hydrogen 1s orbital becomes

$$N_H(p) = 4\pi p^2 |\chi_H(\underline{p})^2|$$

where

$$\chi_H(\underline{p}) = \frac{\sqrt{2}}{\pi} \int_0^\infty j_0(pr) \exp(-r)\psi_+(r)\, r^2\, dr.$$

The electrons in the C-H and C-C bonds are represented by Heitler-London wave functions which are known to be good approximations of the covalent bond. Numbering the electrons of the bond by 1 and 2, the wave function of the C-H bond, $\psi(C\text{-}H)$, is

$$\psi(C\text{-}H) = \frac{\psi(C:1)\psi(H:2) + \psi(C:2)\psi(H:1)}{\sqrt{2(1 + S_{CH}^2)}}$$

where S_{CH} is an overlap integral.

To calculate the momentum distribution of the photon pairs, we first transform the Fourier component of the positron wave function overlapping with electron 1

$$\chi(\underline{p}_1, \underline{r}_2) = (2\pi)^{-3/2} \int \exp(-i\underline{p}_1 \cdot \underline{r}_1)\psi(C\text{-}H)\psi_+(r_1)dr_1$$

and then average $\chi(\underline{p}_1, \underline{r}_2)^* \chi(\underline{p}_1, \underline{r}_2)$ over all positions of electron 2. The momentum distribution, N(C-H), obtained is

$$N(C\text{-}H) = \frac{1}{2(1+S_{CH}^2)} \{N_C(p) + N_H(p) + 2S_{CH}N_{ch}(p)\}$$

where
$$N_{ch}(p) = \frac{2\sqrt{2}\, p}{R_{CH}\sqrt{1+\sigma^2}} \chi_H(p) \{X_1(p) \sin(pR_{CH}) + \sqrt{3}\, \sigma\, X_2(p) [\frac{\sin(pR_{CH})}{pR_{CH}} - \cos(pR_{CH})]\}$$

in which R_{CH} is the length of the C-H bond.

The calculation of the momentum distribution in the C-C bond, N(C-C), is similar to that for N(C-H). The C-C bond is described by the wave function

$$\psi(C\text{-}C) = \frac{\psi_a(C:1)\psi_b(C:2)+\psi_a(C:2)\psi_b(C:1)}{\sqrt{2(1+S_{ab}{}^2)}}$$

where S_{ab} is the overlap integral. After the transformation to momentum coordinates and a considerable reduction, we have the momentum distribution in the C-C bond:

$$N(C\text{-}C) = \frac{1}{1+S_{ab}{}^2}\{N_C(p) + S_{ab}N_{ab}(p)\}$$

where
$$N_{ab}(p) = \frac{2p^2}{1+\sigma^2}\{X_1(p)^2\frac{\sin(pR_{CC})}{pR_{CC}} + 3\sigma^2X_2(p)^2 \cdot[\frac{\sin(pR_{CC})}{pR_{CC}} + \frac{2\cos(pR_{CC})}{(pR_{CC})^2} - \frac{2\sin(pR_{CC})}{(pR_{CC})^3}]\}$$

in which R_{CC} is the length of the C-C bond.

The momentum distribution for cyclohexane can be obtained by considering that only electrons from C-H and C-C bonds annihilate with the positrons and that annihilation is equally probable for an electron from either of these bonds. We will neglect the contribution due to carbon 1s electrons since the overlapping of wave functions of these core electrons with that of positrons is very small. The ratio of the number of electrons in the C-H and C-C bonds for cyclohexane is 24/12 and therefore

$$N(\text{cyclohexane}) = \frac{1}{36}[24N(C\text{-}H) + 12N(C\text{-}C)].$$

Since the positron wave functions are not analytic, the momentum distributions N(C-H) and N(C-C) were evaluated numerically by computer. The computed and experimental momentum distributions for cyclohexane are shown in Figure 6-3.

We assume that prior to annihilation, the positron acquires an energy of approximately 0.1 ev. Calculations have been made to estimate the thermalization time of positrons in metals (Lee-Whiting 1955; Carbotte and Arora 1967), but no rigorous calculation has been made to predict the thermalization time in non-metal solids or liquids. The calculations and experiments which have been described are based on the assumption that the energy of the positron is near thermal and that all the momentum assigned to the annihilating pair comes from the electron. This is consistent with the general overall agreement between the calculated N(p) curves and the experimental curves presented in this Chapter. A further indication that thermalization of the positron has occurred by the time the positron-electron pair annihilates, is that if we assume the contrary, then the experimental curve would be expected to lie above the calculated curve in the high momentum region. This is not the case and supports the view that the positron had a low momentum contribution to make to the pair.

6.4 Anomalous Annihilation

It is generally accepted that for positron annihilation in most organic substances, the lifetime, whose magnitude is usually 1 - 5 nanoseconds, represents events which occur by pickoff of an orbital electron by ortho-positronium. The measurement of positron lifetimes yields both the lifetime, τ_2, and the intensity, I_2, of the positrons which have formed ortho-positronium.

Figure 6-3

The Momentum Distribution for Cyclohexane

The solid line indicates the calculated momentum distribution.

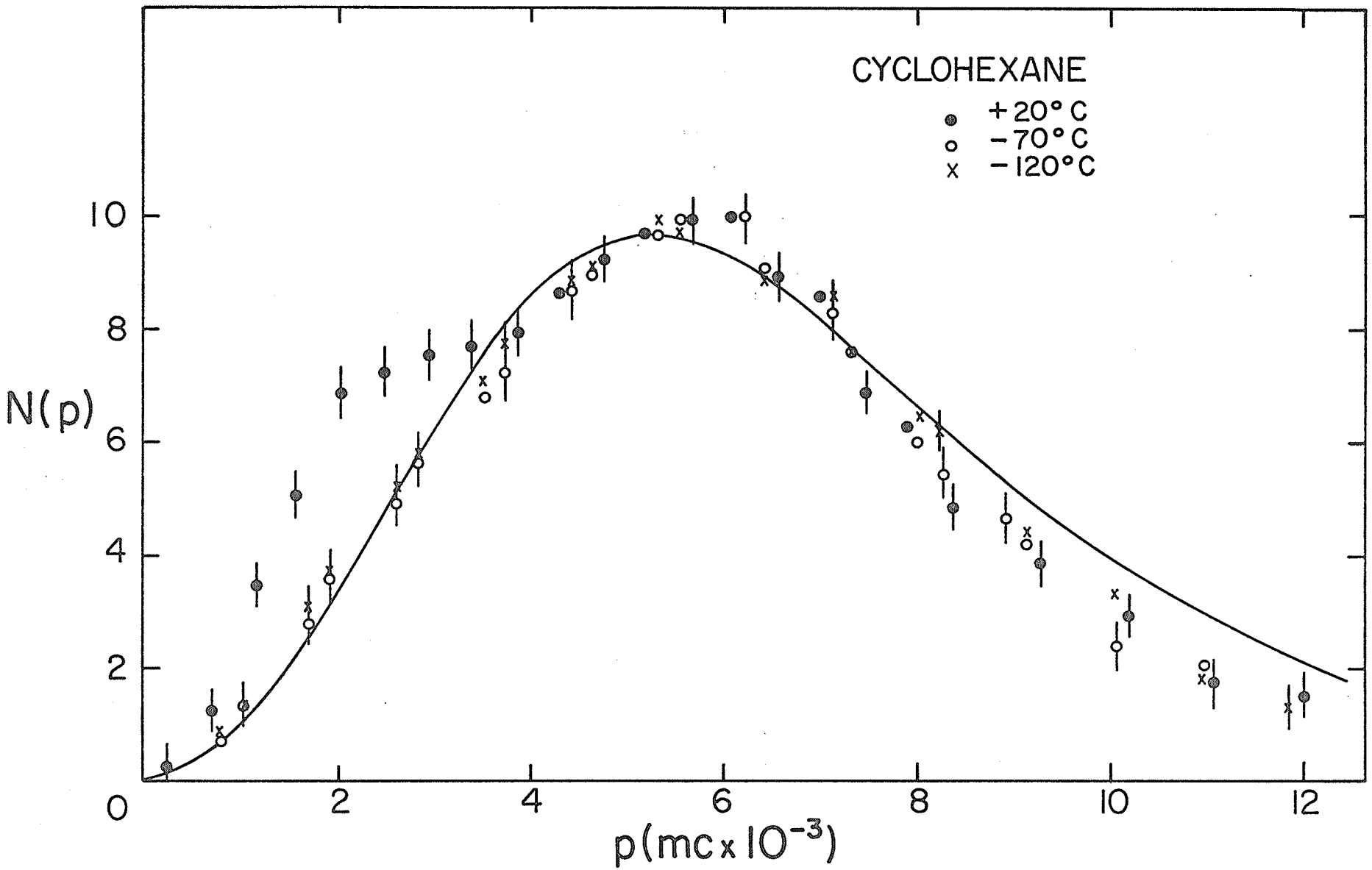
CYCLOHEXANE
+20° C
−70° C
−120° C
N(p)
0
2
4
6
8
10
12
p(mc x 10⁻³)

Angular correlations between the two photons produced in the annihilation process lead to momentum distributions of the annihilating positron-electron system. This momentum distribution generally shows a low and a high momentum peak when the experiments are performed in organic liquids. The low momentum peak has an intensity (I_N) which represents the annihilation of positrons in para-positronium. Positrons forming para-positronium annihilate with their own electrons and the momentum of such annihilating pairs is small. From statistical considerations alone one would expect $I_N = \frac{I_2}{3}$ unless there is appreciable conversion (e.g. by paramagnetic substance) from ortho-positronium to para-positronium. In this case $I_N > \frac{I_2}{3}$ would result.

In a number of organic liquids, verification of $I_N = \frac{I_2}{3}$ has been reported (Kerr et al. 1965). However, few workers use both time and angular correlation techniques in studying a given sample. In particular, only one investigation by both methods has been made on an organic substance undergoing a liquid-solid phase transition. This substance is napthalene where the lifetime measurements (Landes et al. 1956) and angular correlation measurements (deZafra 1958) may be compared. Unfortunately, the I_2 in the solid is only 9% and since I_N would then be approximately 3%, it is hard to verify that $I_N = \frac{I_2}{3}$ because errors of the order of 3% exist in I_N measurements. In this Chapter data is presented on four substances where direct comparisons can be made of I_2 and I_N in the liquid and solid phases.

Momentum distributions obtained from angular correlation measurements on liquid methane at -177 ± 1°C and on solid methane at -187 ± 1°C are shown in Figure 5-23. The values of I_N shown in Table 6-2 were obtained by subtracting a calculated high momentum distribution

(Chuang et al 1968) from the experimental distributions. Lifetime measurements carried out at -177°C and -187°C give the $\frac{I_2}{3}$ and τ_2 values also listed in Table 6-2. It is clear from the table that, in liquid methane, $I_N = \frac{I_2}{3}$ within the limit of experimental error, as expected. However, in solid methane, I_N is essentially zero, in marked disagreement with the value $\frac{I_2}{3} = 11\%$. In other words, the lifetime data indicate that 44% of the positrons form positronium in the solid phase, whereas the angular correlation data indicate that no positronium is formed.

In an attempt to resolve the discrepancy, triple coincidence rates, $R_{3\gamma}$, were measured for both phases using identical geometry. The measured rate, $R_{3\gamma}$, is proportional to $P_{3\gamma}$, the fraction of positrons undergoing 3γ annihilation, which is given approximately by

$$P_{3\gamma} = \frac{I_2\tau_2}{\tau_3} + \frac{1}{372}\left(1 - \frac{4}{3} I_2\right)$$

where τ_3 in the lifetime of ortho-positronium in free space.

Since the values of $R_{3\gamma}$ in the two phases are proportional to the corresponding values of $P_{3\gamma}$, one can check on the consistency of the results for the two phases by assuming, for example, that the measured values of I_2 and τ_2 in the liquid phase and τ_2 in the solid phase are correct and then solving the above equation for I_2 in the solid phase. The value of $\frac{I_2}{3}$ found in this manner is listed in the table under the heading $I_2(3\gamma)/3$. Unfortunately, the triple coincidence experiment is difficult in that the counting rate is low, typically 10 counts per minute, and the background counting rate comprises approximately 60% of the gross rate leading to large uncertainties in the values of $R_{3\gamma}$ and $I_2(3\gamma)/3$. Although the uncertainty in $I_2(3\gamma)/3$ for solid methane

is large, the value of $I_2(3\gamma)/3$, appears to be considerably less than the $I_2/3$ obtained from the lifetime measurements on solid methane. Thus, the three-photon annihilation measurements support the angular correlation measurements in indicating that there is an inconsistency in the assumption that I_2 is a measure of the amount of positronium formed in the case of solid methane.

The angular correlation and lifetime measurements performed on liquid cyclohexane at room temperature, on one solid phase at $-70^{o}C$ and on the second solid phase at $-120^{o}C$ yielded the results shown in Figure 5-20 and Table 6-2. The subtraction procedure to obtain I_N in cyclohexane was based on a calculated shape of the leading edge of the high momentum component. Three photon annihilation rates were measured for the liquid phase and the low temperature solid phase, the $I_2(3\gamma)/3$ for which is listed in the table. I_N is seen to agree with $I_2/3$ for the liquid phase; in the two solid phases a low momentum component is present but its intensity is considerably less than $I_2/3$. The triple coincidence results again yield an $I_2(3\gamma)/3$ smaller than the $I_2/3$ obtained from lifetime measurements.

Angular correlation and lifetime measurements were performed on liquid benzene at room temperature and on solid benzene at approximately $-10^{o}C$. The momentum distributions are shown in Figure 5-22 and the values of the various parameters are listed in Table 6-2. In the case of benzene no appropriate wave function was found to calculate the shape of the high momentum component and therefore the leading edge of the high momentum component was extrapolated smoothly to zero. Again, there is good agreement between I_N and $I_2/3$ in the liquid phase, but, in the solid phase, I_N is much less than $I_2/3$. No triple coincidence measure-

ments were made for benzene. The benzene results have been confirmed by O. Mogensen (1971) who found no I_N in solid benzene.

Table 6-2 also includes angular correlation and lifetime data for liquid and solid butane. As was the case for all other substances studied the values of $I_2/3$ and I_N agree in the liquid phase. Unfortunately, because of the small values of $I_2/3$ and I_N in the solid phase, conclusive evidence that I_N is in fact substantially less than $I_2/3$ is difficult to obtain. However, the results do indicate that this effect is present in butane as well.

Recently Mogensen (1971) discovered that the I_N component was not present in the solid phases of methanol, octanol, and eicosane. While no lifetime data is available for methane and octonal, solid eicosane has a reported value of 31% for I_2. All experimental evidence on solid organic materials has shown that the value of I_N is essentially zero suggesting that no positronium is formed; however the value of I_2 remains large.

TABLE 6-2

Comparison of Results from Lifetime, Angular Correlation and Triple Coincidence Measurements

Sample	Temperature (^{o}C)	τ_2 (nsec)	$I_2/3$ (%)	I_N (%)	$I_2(3\gamma)/3$ (%)
Methane	-177	5.5±.1	11±1	11±2	
Methane	-187	3.0±.1	11±1	0±2	2±2
Cyclohexane	+ 20	3.0±.1	10±1	11±1	
Cyclohexane	- 70	2.3±.1	7±1	1±1	
Cyclohexane	-120	1.1±.1	7±1	1±1	2±2
Benzene	+ 20	3.1±.1	12±1	13±2	
Benzene	- 10	1.1±.1	7±1	0±2	
Butane	- 80	3.1±.1	6±1	7±1	
Butane	-150	1.5±.1	4±1	2±1	

REFERENCES

R. E. Bell and M. H. Jorgensen, Can. J. Phys. 38, 652 (1960).

R. E. Bell, Coincidence Techniques and the Measurement of Short Mean Lives, IIα, β, γ-Ray Spectroscopy, Editor Kai Siegbahn, North Holland Publishing Company (1966).

M. Bertolaccini and L. Zappa, Nuovo Cim. 52B, 487 (1967).

A. Bisi, A. Fiorentini and L. Zappa, Phys. Rev. 131, 1023 (1963).

W. Brandt, S. Berko and W. W. Walker, Phys. Rev. 120, 1289 (1960).

W. Brandt, L. Eder and S. Lundquist, Phys. Rev. 142, 165 (1966).

W. Brandt and I. Spirn, Phys. Rev. 142, 231 (1966).

J. P. Carbotte and H. L. Arora, Can. J. Phys. 45, 387 (1967).

S. Y. Chuang and B. G. Hogg, Can. J. Phys. 45, 3895 (1967).

S. Y. Chuang, W. H. Holt and B. G. Hogg, Can. J. Phys. 46, 2309 (1968).[1]

S. Y. Chuang, Ph.D. Thesis, University of Manitoba (1968).

A. M. Cooper, G. J. Laidlaw and B. G. Hogg, J. Chem. Phys. 46, 2441 (1967).

A. M. Cooper, Ph.D. Thesis, University of Manitoba (1969).

C. A. Coulson, Proc. Cambridge Phil. Soc. 37, 55 (1941).

C. A. Coulson and W. E. Duncanson, Proc. Cambridge Phil. Soc. 37, 67 (1941).

C. A. Coulson, Proc. Cambridge Phil. Soc. 37, 74 (1941).

C. A. Coulson, Proc. Cambridge Phil. Soc. 38, 100 (1942).

S. deBenedetti, R. Siegel, Phys. Rev. 85, 371 (1952).

M. Deutsch, Phys. Rev. 82, 455 (1951).

M. Deutsch, Phys. Rev. 83, 866 (1951).

M. Deutsch, Prog. Nucl. Phys. 3, 131 (1953).

R. L. deZafra and W. T. Joyner, Phys. Rev. 112, 19 (1958).

W. E. Duncanson, Proc. Cambridge Phil. Soc. 37, 397 (1941).

W. E. Duncanson and C. A. Coulson, Proc. Cambridge Phil. Soc. 37, 406 (1941).

W. E. Duncanson, Proc. Cambridge Phil. Soc. 39, 180 (1943).

W. A. Falk and G. Jones, Can. J. Phys. 42, 1751 (1964).

E. Germagnoli, G. Poletti and G. Randone, Phys. Rev. 141, 419 (1966).

B. Gittelman and M. Deutsch, Ann. Prog. Report, Lab. Nuclear Science, M.I.T. (1956).

V. I. Goldanskii, A. V. Ivanova and E. P. Prokopev, Soviet Phys. - JEPT 20, 440 (1965).

V. I. Goldanskii and E. P. Prokopev, Soviet Phys. - Solid State 6, 2641 (1965).

V. I. Goldanskii, Atomic Energy Review, Vol. 6, No. 1 (1968).

A. G. Gould, Master's Thesis, University of Manitoba (1969).

R. L. Graham, J. S. Geiger, R. E. Bell and R. Barton, Nucl. Inst. and Meth. 15, 40 (1962).

J. Green and J. Lee, Positronium Chemistry, Academic Press 27 (1964).

D. R. Hartree, "Numerical Analysis" (Clarendon Press, Oxford, 1958), Chapter 7, Section 2.

C. R. Hatcher, W. E. Millet and L. Brown, Phys. Rev. 111, 12 (1958).

C. R. Hatcher, J. Chem. Phys. 35, 2266 (1961).

F. Herman and S. Skillman, "Atomic Structure Calculation" (Prentice-Hall, Inc., Englewood Cliffs, New Jersey, 1963).

D. P. Kerr and B. G. Hogg, J. Chem. Phys. 36, 2109 (1962).

D. P. Kerr, Ph.D. Thesis, University of Manitoba (1964).

D. P. Kerr, A. M. Cooper and B. G. Hogg, Can. J. Phys. 43, 963 (1965).[1]

D. P. Kerr, S. Y. Chuang and B. G. Hogg, Mol. Phys. 10, 13 (1965).

R. G. Lagu, V. G. Kulkarni, B. V. Thosar and G. Chandra, Proc. Indian Acad. Sci. LXIX, 48 (1969).

H. S. Landes, S. Berko and A. J. Zuchelli, Phys. Rev. 103, 828 (1956).

J. Lee and G. J. Celitans, J. Chem. Phys. 42, 437 (1965).

G. E. Lee-Whiting, Phys. Rev. 97, 1557 (1955).

C. Y. Leung and D. A. L. Paul, Positron Annihilation, edited by A. T. Stewart and L. O. Roellig, Academic Press 409 (1967).

P. O. Lowdin, Phys. Rev. 90, 120 (1953).

A. P. Mills and S. Berko, Phys. Rev. Letters 18, 420 (1967).

O. Mogensen, private communication (1971).

S. Mokorovicic, Astron. Nachr. 253, 94 (1934).

S. M. Neamtan, G. Darewych and G. Oczkowski, Phys. Rev. 126, 193 (1962).

S. M. Neamtan and R. I. Verrall, Phys. Rev. 134, A1254 (1964).

A. Ore and J. L. Powell, Phys. Rev. 75, 1696 (1949).

L. Pauling, Nature of the Chemical Bond, Cornell University Press (1948).

T. A. Pond, Phys. Rev. 85, 489 (1952).

J. A. Rich, Phys. Rev. 81, 140 (1951).

A. E. Ruark, Phys. Rev. 68, 278 (1945).

A. T. Stewart, Phys. Rev. 99, 594 (1955).

A. T. Stewart, Can. J. Phys. 35, 168 (1957).

A. T. Stewart and R. H. March, Phys. Rev. 122, 75 (1961).

V. I. Vedeneyev, L. V. Gurvich, V. N. Kondratyev, V. A. Medvedev and Y. L. Frankevich, Bond Energies, Ionization Potentials and Electron Affinities, Edward Arnold Publishers (1966).

W. R. Wall, Ph.D. Thesis, University of Manitoba (1968).

P. R. Wallace, Phys. Rev. 100, 738 (1955).

R. K. Wilson, P. O. Johnson and R. Stump, Phys. Rev. 129, 2091 (1963).

C. N. Yang, Phys. Rev. 77, 242 (1950).

PUBLICATIONS

Detection of the Polymorphic Transition at -86^{o}C in Cyclohexane by Positron Annihilation, A. M. Cooper, G. De Blonde and B. G. Hogg, Phys. Letters 29A, 275 (1969).

Anomalous Annihilation of Positrons in Several Solid Hydrocarbons, G. De Blonde, S. Y. Chuang, B. G. Hogg, D. P. Kerr and D. M. Miller, Canadian Journal of Physics 50, 1619 (1972).